Mechanistic Diversity in the Guest Binding with Cucurbit[7]uril or Octa Acid Complexes

by

Suma Susan Thomas
B.Sc, University of Kerala, 2008
M.Sc, Cochin University of Science and Technology, 2010

A Dissertation Submitted in Partial Fulfillment
of the Requirements for the Degree of

DOCTOR OF PHILOSOPHY

in the Department of Chemistry

Supervisory Committee

Mechanistic Diversity in the Guest Binding with Cucurbit[7]uril or Octa Acid Complexes

by

Suma Susan Thomas
B.Sc, University of Kerala, 2008
M.Sc, Cochin University of Science and Technology, 2010

Supervisory Committee

Dr. Cornelia Bohne (Department of Chemistry)
Supervisor

Dr. Frank C. J. M. van Veggel (Department of Chemistry)
Departmental Member

Dr. Dennis Hore (Department of Chemistry)
Departmental member

Dr. Stephen V. Evans (Department of Biochemistry and Microbiology)
Outside member

Abstract

Supervisory Committee
Dr. Cornelia Bohne (Department of Chemistry)
Supervisor
Dr. Frank C. J. M. van Veggel (Department of Chemistry)
Departmental Member
Dr. Dennis Hore (Department of Chemistry)
Departmental member
Dr. Stephen V. Evans (Department of Biochemistry and Microbiology)
Outside member

Supramolecular systems comprised of non-covalent interactions are reversible in nature. This intrinsic reversibility of these systems is essential in achieving several functions, making it crucial to understand the dynamics of supramolecular systems. However, studies on the dynamics of supramolecular systems have always lagged behind structural and thermodynamic characterization of innumerable supramolecular systems developed.

The first objective of this work was to understand the dynamics leading to a shift in the acidity constant (pK_a) for 2-aminoanthracenium cation (AH^+) upon binding with cucurbit[7]uril (CB[7]) host molecule. The adiabatic deprotonation of free AH^+ in water was found to be inhibited in the complex with CB[7]. Different spectral characteristics for the protonated and deprotonated form of the guest molecule were used to understand the mechanism of this pK_a shift associated with the binding to CB[7]. The results suggested that the pK_a shift upon binding with CB[7] is a result of the slowing down of the deprotonation step in the complex, whereas the association rate constant did not change very much.

The second objective of this work was to understand the role of cations on the binding dynamics of the N-phenyl-2-naphthyl amine (Ph-A-Np) binding to CB[7]. Ph-A-

Np has two binding sites, which can lead to 1:1 and 2:1 host-guest complexes. The results indicate a switch in the binding mechanism for Ph-A-Np at low and high concentration regimes of sodium ions. Sodium ion was found to reduce the binding affinity of the naphthyl group to CB[7] whereas the complex formed by the phenyl group with CB[7] bound to one sodium ion was found to be stabilized.

The final objective of this work was to study how structural changes to a guest molecule can affect the binding dynamics for the formation of a 2:1 "capsule" like complex with octa acid (OA). The dissociation for the OA capsule with pyrene (Py) as the encapsulated guest was shown to happen in 2.7 s previously. Two pyrene derivatives, 1-methylpyrene (MePy) and 1-pyrenemethanol (PyMeOH) were chosen as guest molecules to study the effect of these substituents on pyrene on the capsule dissociation dynamics. The results show that the residence time for the guests in the OA capsule depends on the substituents. For PyMeOH and MePy a shorter and longer residence time respectively in the capsule was observed when compared to Py.

Table of Contents

List of Tables

List of Figures

List of Schemes

List of Abbreviations

Å	Angstrom
A	2-aminoanthracene
AH^+	2-aminoanthracenium cation
A_i	pre-exponential factors for species *i*
β	Overall equilibrium binding constant
χ^2	reduced chi-squared parameter
C	host-guest complex
ºC	degree Celcius
CB[n]	cucurbit[n]uril
CB[5]	cucurbit[5]uril
CB[6]	cucurbit[6]uril
CB[7]	cucurbit[7]uril
CB[8]	cucurbit[8]uril
cm	centimeter
DCl	deuterium chloride
DNA	deoxyribonucleic acid
ESI-MS	Electrospray ionization mass spectrometry
Equiv	equivalent
g	gram
G	guest
H	hour
H	host
HCl	hydrochloric acid
Hg-Xe	mercury-xenon
I	fluorescence intensity
ΔI	change in fluorescence intensity
IRF	Instrument response function
k_+	association rate constant
k_-	dissociation rate constant

k_{obs}	observed rate constant
kV	kilovolts
K	equilibrium constant
L	litre
LFP	laser flash photolysis
LTJ	laser temperature jump
λ_{ex}	excitation wavelength
λ_{em}	emission wavelength
M	molar
min	minute
mL	millilitre
mm	millimetre
mM	millimolar
ms	millisecond
MΩ	megaohm
m/z	mass to charge ratio
μL	microlitre
μM	micromolar
μs	microsecond
MCP	micro channel plate
MePy	1-methylpyrene
MHz	megahertz
NaCl	sodium chloride
NaOH	sodium hydroxide
nm	nanometre
NMR	nuclear magnetic resonance
ns	nanosecond
OA	octa acid
Ph-A-Np	N-phenyl-2-naphthylamine
Ph-AH^+-Np	N-phenyl-2-naphthylammonium cation
pK_a	acid dissociation constant
pK_a*	Excited state acid dissociation constant

ppm	parts per million
Py	pyrene
PyMeOH	1-pyrenemethanol
s	second
SPR	surface plasmon resonance
τ	fluorescence lifetime
t	time
TOF	time of flight
UV-Vis	ultraviolet-visible
V	volts

Acknowledgements

I would like to express my deepest gratitude to my supervisor, Dr. Cornelia Bohne for her motivational support, generous help and expert guidance throughout my time at UVic. Without her incredible counsel, this study would have been an overwhelming pursuit. I am immensely grateful to Luis Netter, for his unequivocal support with the instruments and software and for all the invaluable lessons I learned, both on an academic and personal level over the past few years. I am hugely indebted to Mehraveh Seyedalikhani for being a great friend and co-worker from day one of my life at UVic.

I would like to thank Hao, Denis, Jason, Adam, Jessy, Kevin and all the other members of the Bohne research group and all the visiting researchers to the group during my research time for their support throughout my research. My appreciation and gratitude also extends to all the research groups with whom I have had a chance to collaborate with during my research. I would also like to thank Dr. Haridas Pal for giving me the opportunity to be a summer student in his lab during my Master's degree and introducing me to the world of supramolecular chemistry. I take this opportunity to also express my sincere thanks to my supervisory committee for their advice and feedback.

Thanks to my parents for their endless support, enduring love and unyielding confidence in me. They have, in countless ways, supported me to make all my dreams come true. I am also grateful to the rest of my family and friends for always being on my side and helping me grow as a person.

Finally, I would like to gratefully acknowledge NSERC and UVic for providing financial assistance for my research.

Dedication

To Daddy and Mummy

1 General Introduction

1.1 Supramolecular chemistry

Supramolecular chemistry deals with the science of molecular building blocks held together by non-covalent interactions. Whereas molecular chemistry is based on the covalently bonded atoms, supramolecular chemistry has its foundation on organized molecular assemblies formed from the relatively weaker intermolecular forces.[1] The interactions between the molecules in supramolecular systems ranges from weak hydrogen bonds, comparable to some weak enzyme-substrate interactions, to metal-ion coordination that is as strong as most antigen-antibody interactions. Other interactions in supramolecular systems can be π - π interactions, hydrophobic or solvophobic effects and dispersion interactions.[2-4] By bringing together two or more molecular entities in an organized fashion, several functions can be achieved which otherwise will be impossible with the individual units.[3,4]

Studies on supramolecular chemistry are inspired by biological systems in nature. For example, the double helical structure of DNA is stable due to the hydrogen bonding and π-π stacking interactions between the components of the two strands making up the DNA. Similarly antigen-antibody interactions that form part of the basis of our immune system operate essentially through non-covalent interactions. Protein folding is another example where supramolecular interactions play a vital role. Most of the biological recognitions operate through supramolecular interactions in one way or the other to achieve “flawless” functions in living systems.

Supramolecular systems can be broadly classified into two categories: host-guest systems and self-assemblies.[1] Host-guest systems comprise of a molecule large enough to encapsulate a smaller molecule by supramolecular interactions. The large molecule is called the "host" and the encapsulated small molecule is called the "guest". The three systems described in this thesis fall under the category of host-guest systems. In self-assemblies, two or more of the same or different units come together and form an aggregated structure spontaneously[5] where none of the subunits acts as a host for the other (Scheme 1.1).

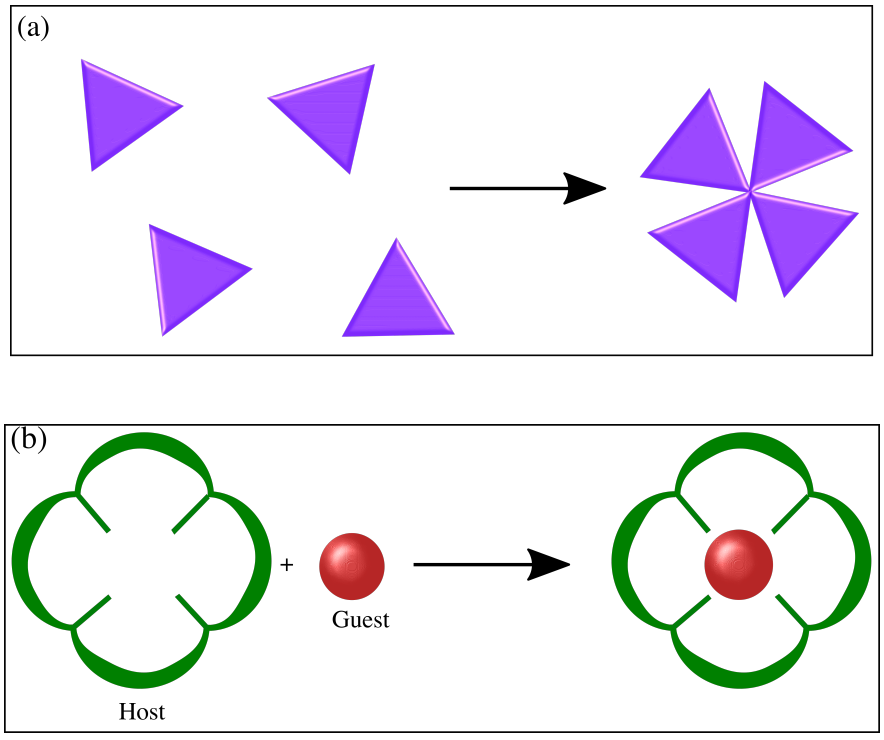

Scheme 1.1. Schematic representation of a self-assembly (a, top) and a host-guest system (b, bottom)

Host-guest systems where alkali and alkaline earth metal cations acted as guest molecules to certain crown ether hosts is one of the earliest studies of supramolecular chemistry. Charles J. Pederson in 1967 reported the "accidental" synthesis of dibenzo[18]crown-6 during the preparation of a bis(phenol) derivative.[6] This compound and several other polycyclic ethers were shown to have very high binding affinity for alkali and alkaline earth metal cations.[7-9] Soon after this discovery, Jean-Marie Lehn synthesized the three dimensional bicyclic "cryptand" type host molecules that could accommodate cations in their spheroidal cavity better than the two dimensional "flat" crown ether structures.[10-12] The crown ethers and the cryptands organize themselves around the cations during the complexation process owing to their flexible framework. Donald J. Cram in 1979 introduced a new type of host systems called spherands where oxygen atoms are rigidly preorganized in an octahedral manner to form a cavity that can accommodate cationic guests.[13,14] Pederson, Lehn and Cram shared the 1987 Nobel prize for these developments in supramolecular chemistry. Since then a large number of studies have been done in this field including synthesis of various synthetic hosts, studies on the interactions of cationic, anionic and neutral guest species to different hosts and the application of these systems in numerous functional materials. For example, supramolecular host-guest systems are widely used in biological systems including protein assembly,[15,16] protein recognition,[17,18] polyvalent interactions[19] and drug delivery.[20,21] Assembly of two peptides necessary for functional DNA binding was demonstrated to occur through cyclodextrin host-guest chemistry.[22] Supramolecular assemblies based on block-copolymer micelles were proposed to be active drug delivery systems for anti-tumor agents.[20] Supramolecular chemistry has also found applications in

several fields such as catalysis,[23,24] energy transfer devices,[25-27] sensors[28,29] and logic gates.[30-32]

A very important aspect of supramolecular systems is its reversibility. Due to the weak non-covalent nature of the interactions these systems are thermodynamically less stable and breaking and making of "bonds" is less difficult compared to covalently bonded systems. As a result supramolecular systems are generally very dynamic compared to covalently bonded molecules. This dynamic nature of supramolecular systems is crucial for the use of these systems in many functional applications. Also, during the design of supramolecular systems, this dynamic flexibility allows one to correct for any errors during formation of the system by disassembling the subunits that came together incorrectly and assembling them in the correct fashion.[33,34]

The design of a supramolecular system requires a detailed understanding of the system in order for the system to be used for any functional applications. Structural characterization, thermodynamic studies and the dynamics of the systems are the key features of supramolecular systems.[35] These three features are related to each other as shown in Scheme 1.2. The structure of a supramolecular system can be determined by conventional techniques such as NMR, mass spectrometry and X-ray diffraction. The structural characterization is often followed by thermodynamic studies. Thermodynamic studies help in understanding how strongly the subunits of the system are held together and also gives information on the stoichiometry of binding. Depending on the system under study techniques such as NMR, absorption, fluorescence and potentiometry can be used for thermodynamic characterization of supramolecular systems. Often the feature that is least understood for a supramolecular system is its dynamics and understanding

the dynamics of the system is essential in the use of the system for any practical purposes.[35-38] This lack of proper mechanistic understanding used to be mainly due to the unavailability of proper technique for dynamics characterization. The development in the techniques lagged behind the development and synthesis of supramolecular systems. Understanding the structure of a supramolecular system can give information about the thermodynamics of the system and vice versa. However, the dynamics of the system cannot be understood by studying either the structure or the thermodynamics of the system, but understanding the dynamics of the system sheds light on the other two key features of supramolecular systems. The studies on the dynamics of supramolecular systems are very few compared to the wealth of structural and thermodynamic information available for the various supramolecular systems.

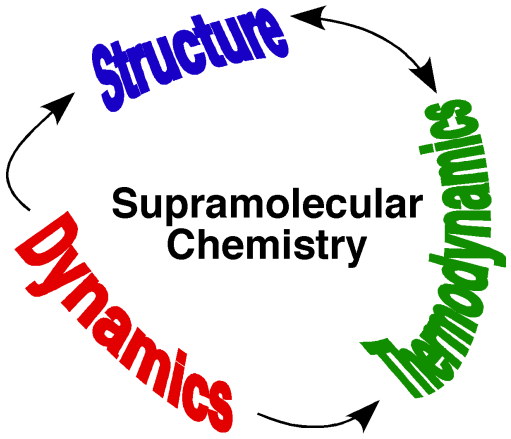

Scheme 1.2. Schematic representation for the relationship between structure, thermodynamics and dynamics for supramolecular systems. Reprinted with permission from Bohne's work.[35] Copyright (2006) American Chemical Society.

1.2 Supramolecular dynamics

The major challenge in determining the dynamics of a supramolecular system is the measurement of kinetics in real time. The conventional methods for the measurement of kinetics such as relative rates method does not work in the case of supramolecular systems. The method of relative rates presumes similar mechanisms for the reaction under study to a standard reaction whose rate constant is known. The rate constant for the unknown reaction is then obtained from the relationship of the ratio of the product concentrations and the rate constant. In the case of supramolecular systems, due to the diversity of kinetics observed and the lack of standard reactions to which a system under study could be compared, similar mechanisms cannot be assumed for different systems. The subunits in supramolecular systems typically measure sub nanometers to a few nanometers in length. At room temperature and water solutions, the diffusion of molecules over this length scales happens in the nanoseconds to microseconds time scale. Measurement of such short time scale processes in real time requires the creation of the species under study in a fast manner and fast detection techniques. Depending on the time scale of supramolecular dynamics different techniques can be used for its determination (Figure 1.1).

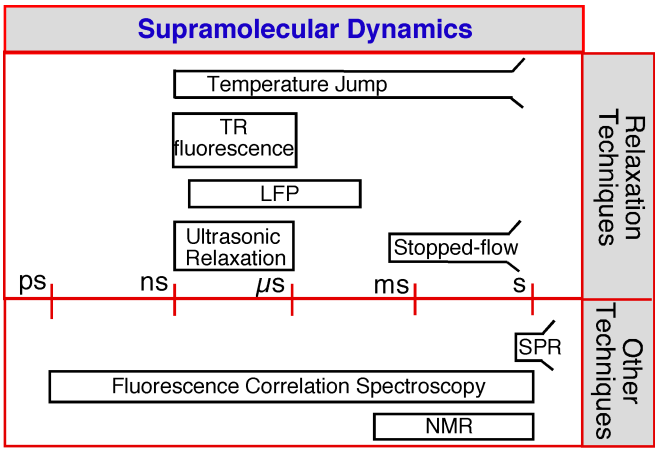

Figure 1.1. Measurable time regimes for different techniques used in the study of supramolecular systems. TR = Time resolved, LFP = Laser flash photolysis, SPR = Surface Plasmon Resonance, NMR = Nuclear Magnetic Resonance. Reprinted from the work of Pace and Bohne,[37] Copyright (2008), with permission from Elsevier.

1.2.1 Relaxation kinetics

The method of relaxation kinetics has been proven to be a useful tool to study the dynamics in supramolecular systems. The method of relaxation kinetics involves rapidly perturbing the equilibrium of a system and monitoring any observable property of the system while the perturbed system is relaxing to the new equilibrium.[39,40] In order to be able to measure kinetics by this method, the perturbation should be instantaneous compared to the time scale of the relaxation of the system. The perturbation from equilibrium is brought about by a sudden change in temperature, concentration, pressure, simultaneous changes in pressure and temperature, electric field or by making a new chemical species, for example, by generating excited state molecules by light.[39,41]

A simple host-guest system forming a 1:1 complex (*C*) from the host (*H*) and the guest (*G*) molecules can be represented by the following equation:

$$H + G \underset{k_-}{\overset{k_+}{\rightleftharpoons}} C \qquad \text{(Eq 1.1)}$$

The equilibrium constant (K_{11}) and the rate constants (k_+ and k_-) for the above process are related as (Eq 1.2):

$$K_{11} = \frac{k_+}{k_-} = \frac{[C]}{[H][G]} \qquad \text{(Eq 1.2)}$$

The relaxation kinetics following the perturbation of the system is given by the rate equation (Eq 1.3):

$$\frac{d[C]}{dt} = k_+[H][G] - k_-[C] \qquad \text{(Eq 1.3)}$$

When the reaction is carried out under pseudo-first order conditions where one reagent is in excess compared to the other (e.g. $[H] >> [G]$) and the perturbation is small, the kinetics can be expressed as an exponential function. The observed rate constant (k_{obs}) obtained from the exponential function is related to the association and dissociation rate constants for the complexation process as (Eq 1.4):

$$k_{obs} = k_+[H] + k_- \qquad \text{(Eq 1.4)}$$

For more complex systems involving more than one relaxation process the kinetic traces can be fitted to a sum of exponentials where each exponential term gives an observed rate constant associated with each relaxation process.[39] However, the observed rate constant for a relaxation process always has terms associated with the forward and reverse reaction of the equilibrium and these two processes cannot be decoupled during

the relaxation measurements. For systems as described by (Eq 1.1) the association process being concentration dependent can be manipulated by changing the concentration of the reactant species whereas the dissociation process is characteristic to the system and cannot be affected by concentration changes. In the latter case the time scale for the dissociation process determines the relaxation technique that is used and some of the relaxation techniques are described next.

1.2.1.1 Stopped-flow measurements

This technique involves the study of relaxation kinetics of a system by concentration jump. Typically, stopped-flow experiments can measure the kinetics of systems with relaxation times ranging from milliseconds to minutes. This technique was used to study the dynamics of the host-guest systems in this thesis. In stopped-flow experiments the solutions of reactant species in two different syringes are rapidly mixed using high pressure in a mixing chamber and the resultant mixture of the solutions is allowed to flow into an observation chamber where the flow is stopped suddenly[42,43] (Scheme 1.3). As the system relaxes back to equilibrium an observable property of the system is detected over time. Often, photophysical techniques like absorption or fluorescence are employed for detection in stopped-flow systems. Use of absorption or fluorescence detection requires a chromophore and/or a fluorophore to be present in the system. Moreover, the molar extinction coefficient and/or the fluorescence quantum yields for the unbound and the bound species should be sufficiently different at the monitoring wavelength to obtain a good amplitude and thus a good signal-to-noise ratio for the kinetic traces measured.

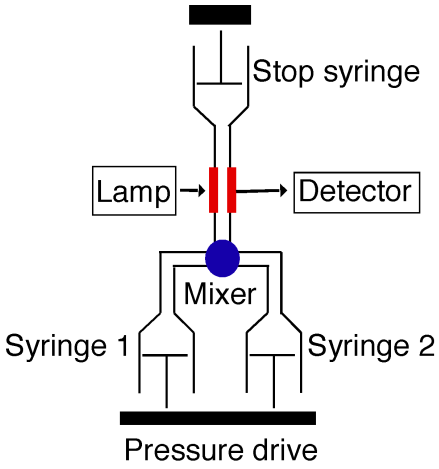

Scheme 1.3. Schematic diagram of a stopped-flow apparatus. Reprinted by permission of John Wiley & Sons, Inc from Bohne's work.[44]

The time resolution for stopped-flow experiments is limited by the mixing time of the solutions, typically 1-2 ms. Fluorescence detection enables the use of very low reagent concentrations,[45] which also helps in slowing down the kinetics for bimolecular reactions so that the measurement is possible by stopped-flow.

1.2.1.2 Temperature jump measurements

In temperature jump experiments the perturbation of a system at equilibrium is attained by a sudden change in the temperature of the system. This change in temperature can be attained in three different ways:[46] (i) Joule heating where an electric discharge from a capacitor through the solution containing electrolytes heats up the solution, (ii) Microwave heating where pulses of microwave radiation from a magnetron source is used for heating the solvent, (iii) Pulsed laser energy of suitable wavelength heats up the solvent, preferably, water. Depending upon the heating method used, temperature jump experiments can measure kinetics ranging from nanoseconds to seconds. The detection methods used in temperature jump experiments ranges from conductimetry to

photophysical techniques such as absorption, fluorescence and light scattering. Again, the choice of detection depends on the method of heating of the solution. For example, conductimetric detection is not possible with Joule heating due to the presence of high concentrations of electrolytes in the solution.

1.2.1.3 Ultrasonic relaxation measurements

Ultrasonic relaxation involves subjecting a system at equilibrium to sound waves, which induces a periodic oscillation of temperature and pressure in the system.[47,48] The energy from the sound wave is absorbed when the sound wave frequency matches the relaxation rate for a chemical equilibrium with non-zero value for the reaction enthalpy change (ΔH^o) or volume change (ΔV^o). This absorbed energy is utilized in providing heat to the system. The difference in energy for the emitted sound wave from the source and the resulting sound wave from the sample is measured by detector crystals and is related to the energy that is absorbed. The sound absorption coefficient along with the frequency ranges swept allows the determination of the relaxation time of the system. An advantage of this technique is that it does not require the presence of a chromophore in the system. This technique allows for the determination of relaxation times ranging from 1 ns to 1 μs.

1.2.1.4 Time-resolved fluorescence emission

This photophysical technique involves the perturbation of a system by generating excited singlet states of molecules of either the guest or the host in a host-guest system using an excitation light source. Molecules in their excited states are chemically different compared to their ground states owing to the differences in properties like bond lengths, geometries and dipole moments. Among several techniques[49-53] used to measure time-

resolved fluorescence, single photon counting is one of the popular methods.[54,55] In single photon counting measurements, the excited state of a fluorophore is created by an excitation source with high repetition rate. The time taken for the single photon detection is measured and a histogram of the number of photons detected as a function of time is constructed, allowing for the determination of the excited state lifetime of the fluorophore. When the binding dynamics of a host-guest system is slower compared to the fluorescence lifetime of the excited species, there is no relocation of the excited state species during the lifetime of the molecule. In such cases the lifetime measurements do not give any information on the association and dissociation process for the complexation. Thus the criterion for the use of time-resolved fluorescence in studying the dynamics of supramolecular systems is that the fluorescence lifetime of the excited species should be of the same order of magnitude as that of the relaxation process. Also, the excited state of the molecule should be non-reactive. Usually the fluorescence lifetime of organic molecules are in the nanoseconds timescale and thus the use of this technique is limited to studying the dynamics of supramolecular systems with fast association and dissociation rates. Kinetics ranging from nanoseconds to microseconds can be determined by these experiments.

In the case of host-guest systems where the free guest and the complex have similar spectral characteristics, the use of a quencher can be helpful in the determination of the dynamics of the system. Quenchers add competitive pathways for the deactivation of the excited state of the molecule. Usually the quenching efficiency for free guests in solution is much higher than that of the complex due to the protection offered by the host to the guest molecule from the quenchers.[54,56-58] Thus the high quenching efficiency for the free

guest molecule leads to the shortening of lifetime for the free guest making the dissociation of the complex the rate limiting step, thereby leading to the determination of the association and dissociation rate constants for the complex formation. Quenching studies are also used to determine the association rate constants for quencher-host encounters. In this case, the quenching rate constant for the excited state guest inside the host molecule gives information about the access of the quenchers to the host molecule.

In the studies reported in this thesis, the single photon counting technique was used to obtain the excited state lifetimes of the guest molecules in different environments. A guest molecule can have different lifetimes when it is free in water and inside a host molecule. The singlet excited state decay of a solution containing the host and the guest molecule in principle gives the lifetimes of the free guest and the complex if they are different. Analysis of the singlet excited state lifetime decay also gives information on the relative contribution of each of these species to the decay, which is a rough approximation of the relative concentrations of each species present in the system. The lifetimes and the relative contributions are key to understanding the dynamics of the system under study because they provide information on the distribution of the guest.

1.2.1.5 Laser flash photolysis

In this photophysical technique,[55,59] a pulsed laser generates the excited state of the molecule. This excited state species now present in the system absorbs light from a lamp set up in a perpendicular arrangement with respect to the laser. The detector measures the light intensity changes before and after the laser pulse thus allowing the measurement of the absorbance for the transient species formed in the system over time. The

measurement of changes in absorption of the transient species leads to the determination of the lifetime of the species formed. As is the case with time-resolved fluorescence emission measurements this technique also requires the generation of non-reactive and long-lived excited state species for the study of the dynamics of supramolecular systems. This method allows for the measurement of kinetics in the nanoseconds to microseconds time scale and is more useful than the single photon counting technique because of the longer lived transient species generated compared to the shorter lived singlet excited states. Introduction of a quencher molecule can modulate the lifetimes of the different transient species to different extents in solutions and quenchers are useful tools in the study of dynamics of supramolecular systems.[54,56-58]

1.2.2 Non-relaxation techniques

Some non-relaxation techniques are also used in the determination of the dynamics in supramolecular systems. These techniques do not involve a perturbation of the system at equilibrium. Fluorescence correlation spectroscopy, nuclear magnetic resonance (NMR) and surface plasmon resonance are some examples. Fluorescence correlation spectroscopy involves the measurement of fluorescence intensity changes for single molecules,[60-62] which allows for the use of very low concentrations of the species studied. This technique can be used for the study of dynamics ranging from picoseconds to seconds time range. In NMR measurements, the change in NMR signal for active nuclei in the free and bound species makes it possible to measure the kinetics of supramolecular system by line shape analysis.[63,64] The low sensitivity of NMR to concentration changes requires the use of high concentrations of reactants for these experiments and the

dynamics timescale that can be probed by NMR ranges from sub milliseconds to seconds. Surface plasmon resonance is a useful tool in the determination of the dynamics of supramolecular systems.[65,66] In this technique one of the reactant species is adhered to a metal surface and an excess of the second reactant is brought in contact with this metal surface. The interaction between the reactants at the metal surface brings about a change in the refractive index of the metal surface, which is measured and utilized in the determination of kinetics for the system. Kinetics in the sub seconds time range can be determined by surface plasmon resonance.

1.3 Different host systems

Many research groups all over the world have developed several hosts systems over the last few decades. These host molecules differ in size, shape, structure and complexity and exhibit different molecular recognition properties. Water soluble host molecules are more popular among the numerous host molecules synthesized. This is due to the reason that natural and biological systems are water based and applications of host-guest systems in natural and biological systems requires the ability of host-guest systems to function in aqueous solutions. For example, if a host-guest system needs to be used in drug delivery applications, the characterization of the host-guest system must be performed in aqueous solutions similar to body fluids.

Host molecules can be acyclic or cyclic. Acyclic host systems consist of linear or branched molecules with the binding site present in the chain. In cyclic or macrocyclic host systems the atoms are arranged in such a way that the binding site is located in a closed ring arrangement. The host molecules synthesized and studied have been

discussed in detail by several researchers.[67-69] Cyclophanes,[70,71] cyclodextrins,[72,73] calixerenes,[74,75] resorcarenes[76,77] and cryptophanes[78,79] are a few among them. Depending upon the functional groups and the structure of the host molecules, these host systems can selectively bind to cationic, anionic or neutral guest molecules leading to several practical applications. The host-guest systems presented in this thesis consist of marocyclic hosts and are described in detail below.

1.3.1 Cucurbit[n]uril host system

Cucurbit[n]urils (CB[n]s) are macrocyclic host molecules that are made up of glycoluril monomer units joined together by methylene bridges. Depending upon the number of glycoluril units joined to form the macrocycle, CB[n]s come as CB[5], CB[6], CB[7], CB[8] or CB[10]. From CB[5] to CB[10], CB[n]s differ in the cavity size and volume (Table 1.1). In 1905, Behrend synthesized CB[6] by the condensation reaction between formaldehyde and glycoluril,[80] however the molecule was characterized only decades later by Mock et. al in 1981.[81] Cucurbiturils were so named due to their likeness in shape to pumpkins that belongs to cucurbitaceae family. CB[n]s in general have a hydrophobic cavity and two identical portals lined by carbonyl groups, as shown in Scheme 1.4 for CB[7]. Due to the presence of two different binding sites in the molecule, these host molecules can stabilize complex formation through ion-dipole interactions at the portals and hydrophobic interactions in the cavity. CB[n]s can form either exclusion complexes where the guest molecules interact with the portals of CB[n]s through ion-dipole interactions or inclusion complexes where the guest is included in the hydrophobic cavity resulting in the release of high energy water molecules from the cavity.[82,83] As a

result, CB[n]s exhibit very high affinity binding with positively charged guest molecules with a hydrophobic moiety attached to it. For example, CB[7] was reported to have a very high equilibrium constant of 3×10^{15} M^{-1} with a dicationic ferrocene derivative[84] that matches the binding affinity for avidin-biotin pair, one of the strongest binding interaction in biological systems.[85] More recently, Isaacs and coworkers reported a binding constant of 7.2×10^{17} M^{-1} s^{-1} between CB[7] and diamantane diammonium ion, the highest ever measured for a host-guest binding process.[86] Host-guest systems involving CB[n]s find several applications, such as in the field of catalysis,[87-92] photocatalysis,[93] control of aggregation in guest molecules,[94,95] tandem enzyme assays,[96-98] drug delivery[99-102] and self-sorting systems.[103-106] CB[7] was chosen as host system for two of the three projects described in this thesis due to its superior water solubility and ideal cavity size (Table 1.1) to accommodate a wider variety of guest molecules compared to other CB[n] homologues. Among the different CB[n] homologues, CB[7] was shown to have the largest energy gain due to the release of high energy water from its cavity during guest binding.[82] This leads to equilibrium binding constants ranging from moderate to high for these systems.[107,108] The guest molecules reported in this thesis has moderate equilibrium binding constants of the order of 10^5 M^{-1} with CB[7]. Two different aspects of CB[n]-guest chemistry was studied in two different projects in this thesis. In the first project, the kinetics leading to the shift in acidity constant for a guest molecule with CB[7] was explored. In the second project, the role of sodium cation on the binding dynamics of a guest with two different binding sites was investigated.

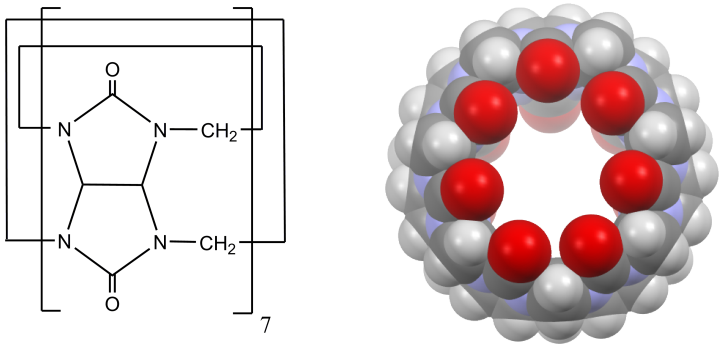

Scheme 1.4. Chemical structure (left) and space fill model of CB[7] molecule.

Table 1.1. Molecular dimensions and solubilities for different CB[n] homologues.

CB[n]	Diameter / Å		Height / Å	Cavity volume / Å^3	Solubility / mM
	Portal	Cavity[d]			
CB[5][a]	2.4	4.4	9.1	82	20-30[f]
CB[6][b]	3.9	5.8	9.1	164	0.013-0.020[g]
CB[7][a]	5.4	7.3	9.1	279	20-30[f]
CB[8][a]	6.9	8.8	9.1	479	<0.01[f]
CB[10]	9.0-11.0[c]	10.7-12.6[c]	9.1[c]	870[e]	<0.05[e]

[a,b]The values are taken from Kim's work.[109,110] [c]The values are taken from Day's work.[111] [d]The cavity diameter is measured at the equator of the molecule. [e]The values are taken from Isaacs's work where the solubility determination was done in D_2O.[112] [f]The values are taken from Kim's work.[113] [g]The values are taken from the work reported by Jekel's group[114] and Buschmann's group.[115]

1.3.1.1 pK_a shift for guest molecules upon binding with CB[n]s

The affinity of CB[n]s to positively charged guest molecules has an important consequence in the acidity constant of the guest molecule bound to CB[n]s. Weakly basic molecules in solution get protonated upon binding with CB[n]s, thus increasing the pK_a of the guest inside CB[n]s (Scheme 1.5). This observation was first reported by Mock et al. in 1990 for a triamine ligand with CB[6].[116] This system was reported to be a "molecular switch" where the pK_a shift for the molecule upon binding with CB[6] was responsible for the shuttling of CB[6] between the two binding sites of the guest molecule at different pH values. This property of the CB[n] hosts is useful in the design of host-guest systems that have applications in catalysis, drug delivery, sensing and logic gates. Different research groups have studied various CB[n]-guest systems where the shift in pK_a of the guest molecule upon binding with CB[n]s is key to the function of the system.[117] For example, Nau et al. showed that lansoprazole and omeraprazole, drugs used in the treatment of gastric and duodenal ulcers can be stabilized and activated by their pK_a shift upon complexation to CB[7].[118] Bhasikuttan et al. studied the pK_a shift of well known laser dyes coumarin 7 and coumarin 30 upon CB[7] binding which has potential applications in the development of stable aqueous dye laser systems.[119] The shift in pK_a on CB[7] binding for a fluorescent dye molecule was shown to switch between "on" and "off" fluorescence states of the dye molecule, making it possible for its use in logic gates.[120] A detailed understanding of the dynamics of CB[n]-guest systems is required for the effective design and improvement of any of the functional systems mentioned above. The first project described in this thesis studies the dynamics behind the pK_a shift for 2-aminoanthracenium cation inside CB[7] cavity.

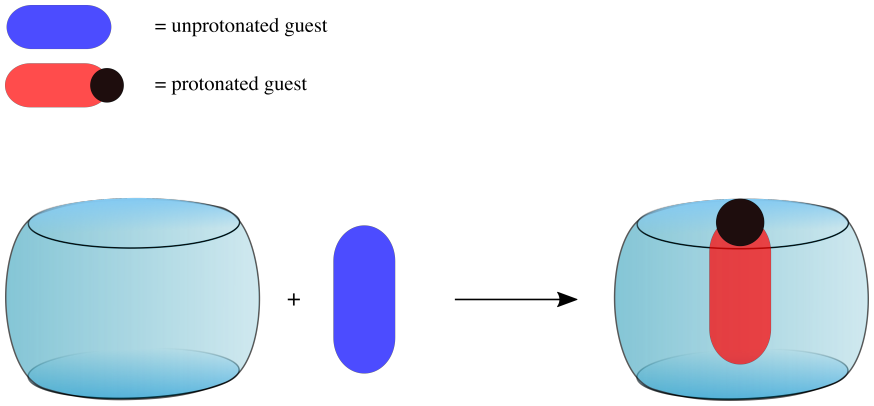

Scheme 1.5. Schematic representation for the protonation of a guest upon binding to CB[n].

1.3.1.2 Binding affinity of CB[n]s for other cations in the system

Another important aspect of CB[n] chemistry is its ability to bind metal cations, hydronium and ammonium ions at the carbonyl rim of the molecule. CB[n]s can bind one or two of these cations at its portals depending upon the magnitude of the equilibrium binding constant for the cations to CB[n]s (Scheme 1.6).[121-124] The presence of these cations in solution can offer competitive binding to other guest molecules present in the system.[124-130] The binding of these cations also increases the solubility of the CB[n]s in water.[109,115,122,131-133] The competitive binding affects both the thermodynamics and the dynamics of the CB[n]-guest system. Equilibrium binding constants have been shown to decrease for the complexation of guests to CB[n]s with increasing concentrations of other cations present in the system. This decrease in the magnitude of equilibrium binding constant in the presence of other cations can be orders of magnitude different from the equilibrium binding constant in the absence of other cations. For example, the equilibrium binding constant for acridine orange with CB[7] was determined to be 2.0×10^5 M^{-1} in the absence of sodium ions whereas the value decreased to 6.7×10^3 M^{-1} in the

presence of 1 M NaCl.[130] The strategy of using other cations in CB[n]-guest systems is also used to slow down the dynamics of the system so that the kinetics can be slowed down to the time resolution of the technique used.[123,124,134-136]

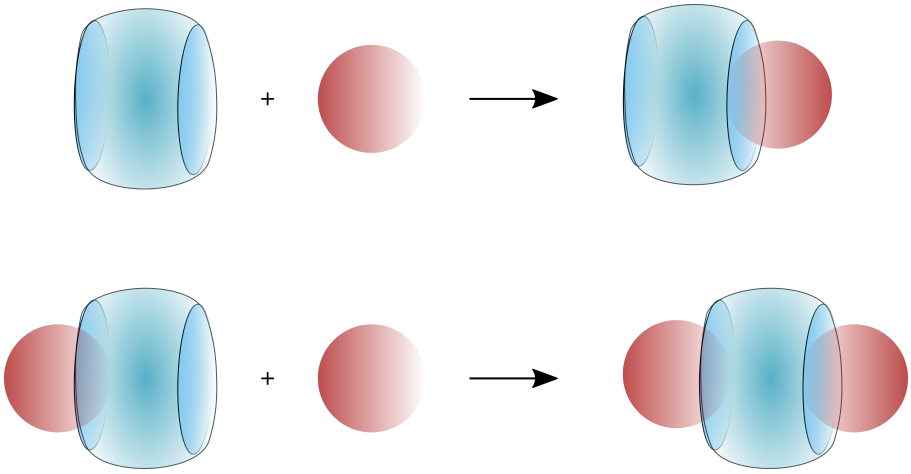

Scheme 1.6. Schematic representation of cations binding to one or both the portals of CB[n]s.

The effect of other cations in the system on the binding properties of CB[n]-guest complexation is underappreciated in the CB[n] literature. The binding constant for the other cations to CB[n]s must be known in order to evaluate the binding of the guest with CB[n]. This is especially important when designing CB[n]-guest systems for applications like drug delivery. Body fluids have high concentrations of metal ions like Na^+ and K^+.[137] While designing a drug delivery system involving CB[n] it should be ensured that the drug will be bound to CB[n] inside the body in the presence of all the cations in the body fluid and that the drug is delivered only at the target. Using berberine and 2-naphthyl-1-ethylammonium cation as guests Biczok's group and Bohne's group have individually determined the binding constants for the formation of CB[7]•Na^+ to be 120-130 M^{-1} and

Na^+•CB[7]•Na^+ to be 11-21 M^{-1}.[124,136] The equilibrium binding constant for the formation of CB[7]•K^+ and K^+•CB[7]•K^+ has been determined to be 600 M^{-1} and 53 M^{-1} respectively by EPR measurements.[138] The second project described in this thesis studies the effect of sodium ion on the binding properties of a CB[7]-guest system where the guest molecule has two different binding sites.

1.3.2 Octa acid host system

Octa acids (OAs) are a relatively new class of deep cavity compounds synthesized by the Gibb's group in 2004.[139] Prior to the synthesis of OA a series of water insoluble, hydrophobic deep cavity host molecules were synthesized by the same research group.[140-142] Due to the feasibility of studying host-guest systems in aqueous solutions OAs were synthesized. The name octa acid comes from the eight carboxylic acid groups present in the molecule, four at the upper and wider rim and four at the lower and narrower rim (Scheme 1.7). Unlike CB[n]s, OA do not have symmetrical rims. These host molecules are approximately 10 Å deep and 10 Å across the wider rim.[139] As a result the OA cavity is much bigger compared to the CB[7] cavity and was reported to have a hydrodynamic volume of 7200 $Å^3$.[143] OA has a hydrophobic cavity and also a hydrophobic wider rim that serves as the entrance site for the guest molecules. The narrow rim of OA is too narrow for the guests to enter the cavity.[144]

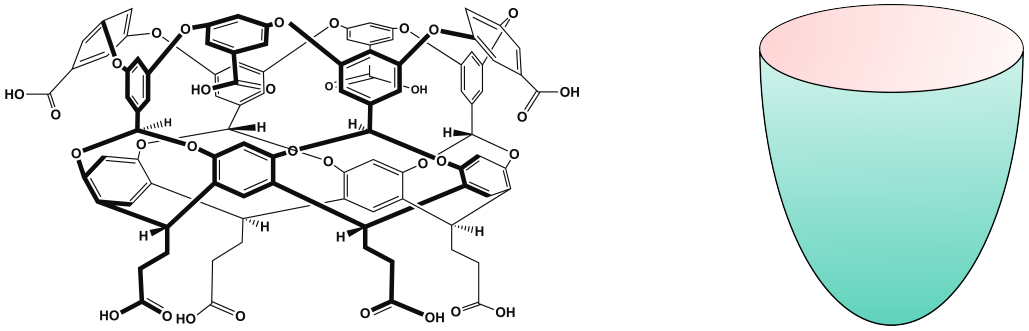

Scheme 1.7. Chemical structure (left) and schematic representation (right) of octa acid.

Depending upon the structure of the guest molecules OA can form a 1:1, 2:1 or a 2:2 host-guest complex (Scheme 1.8).[145] During the formation of 2:1 and 2:2 complexes, two OA molecules come together joined at the wider rim to form a capsule like structure around the guest molecule.[139,146] The desolvation of the hydrophobic rim during the capsule formation strongly favors the formation of higher order complexes in the case of OA. However, the stoichiometry of the complex is determined by the size, structure and the charge on the guest molecule. For example, adamantane, a neutral molecule was shown to form both 2:1 and 2:2 host-guest complex with OA whereas cationic and anionic derivatives of adamantane were found to form 1:1 complexes with OA.[145] In these 1:1 complexes formed by OA with ionic head groups, the hydrophiobic moiety is included in the cavity whereas the ionic head groups positioned at the wider rim are exposed to water.[144,145] Among the cationic and anionic derivatives of adamantane, the cationic derivative was found to be buried deep in the cavity of OA compared to the anionic derivative.[145] This difference was attributed to the favorable interaction of the positively charged group with the carboxylate groups at the wider rim. In the case of neutral molecules, size is a major factor that decides the number of guest molecules encapsulated in the capsule. Studies done on a series of aromatic guest molecules show

that naphthalene and anthracene form 2:2 complexes with OA whereas tetracene and pyrene form 2:1 host-guest complexes with OA.[147,148] In the capsules, the guest molecules are fully protected from water in aqueous solutions.

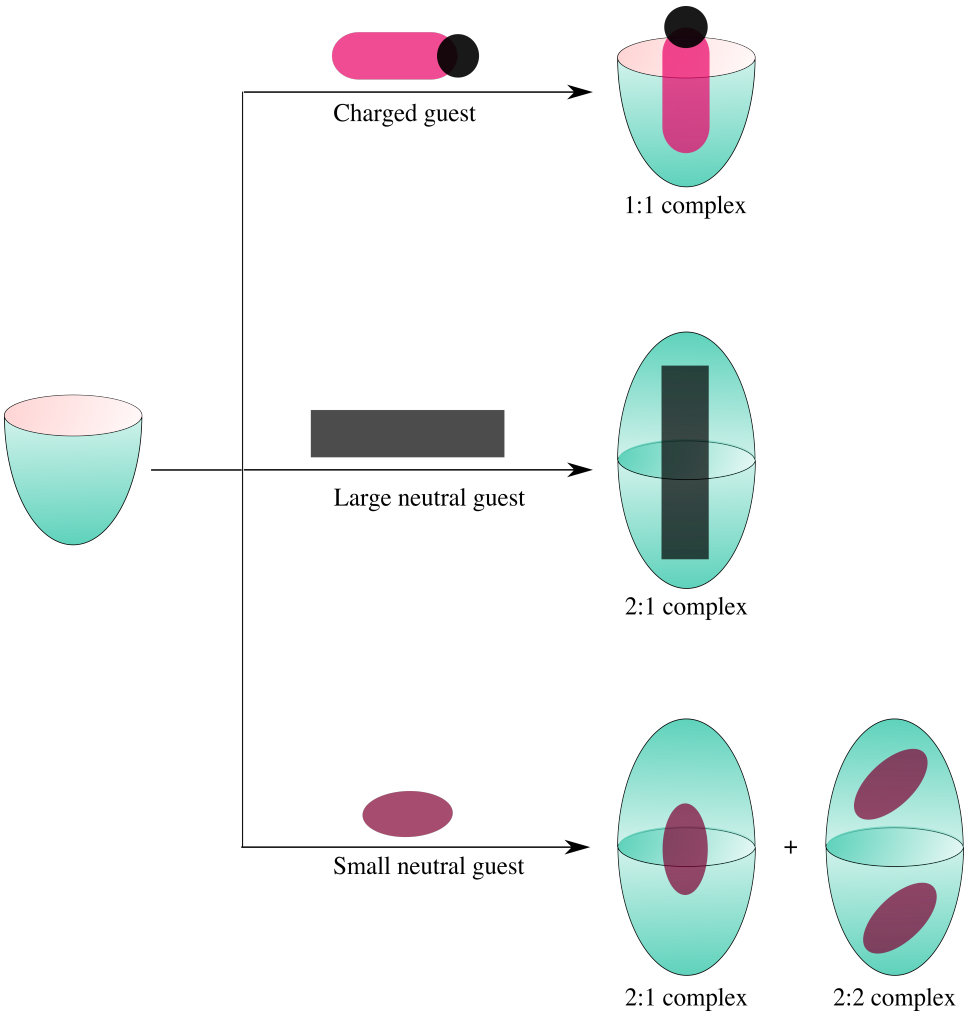

Scheme 1.8. Schematic representation for the formation of complexes with different stoichiometries between OA and guest molecules. © 2008 Canadian Science Publishing or its licensors. Adapted with permission from the work of Jayaraj et al.[149]

Another interesting feature of the host-guest complex formed by OA is the conformation of the guest molecules inside the OA cavity. Phenyl substituted alkyl

guests, with chain length exceeding the size of the octa acid capsule were shown to fold the alkyl chain inside the cavity to maximize the interactions of the guest molecules with OA.[145,150] The folded conformations for these molecules are otherwise highly unstable in solvent media. Interesting chemistry can be done with these capsules if the host molecule can stabilize a particular conformation of the guest which otherwise is unstable in other solvent media.[147,151,152] For example, trans-4,4'-dimethylstilbene undergoes fast photoisomerization in hexane to its cis form with 76% yield, which upon further irradiation gives phenanthrene derivative as the photoproduct. In the presence of OA, irradiation of both the cis and trans form of 4, 4'-dimethylstilbene yielded 80:20 trans-cis mixture which yielded less than 5% of phenanthrene derivative as the photoproduct (Scheme 1.9). The methyl groups on the phenyl ring of trans-4,4'-dimethylstilbene were found to be buried deep in the narrow rim of the OA molecule, which prevented the photoisomerization of the molecule to the cis form inside the octa acid capsule, thus stabilizing the trans form of the molecule inside the capsule.[151,153,154] This positioning of the methyl group was proposed to be due to CH_3-π interactions and van der Waals interactions possible for that particular orientation of the molecule with the narrow rim of OA.

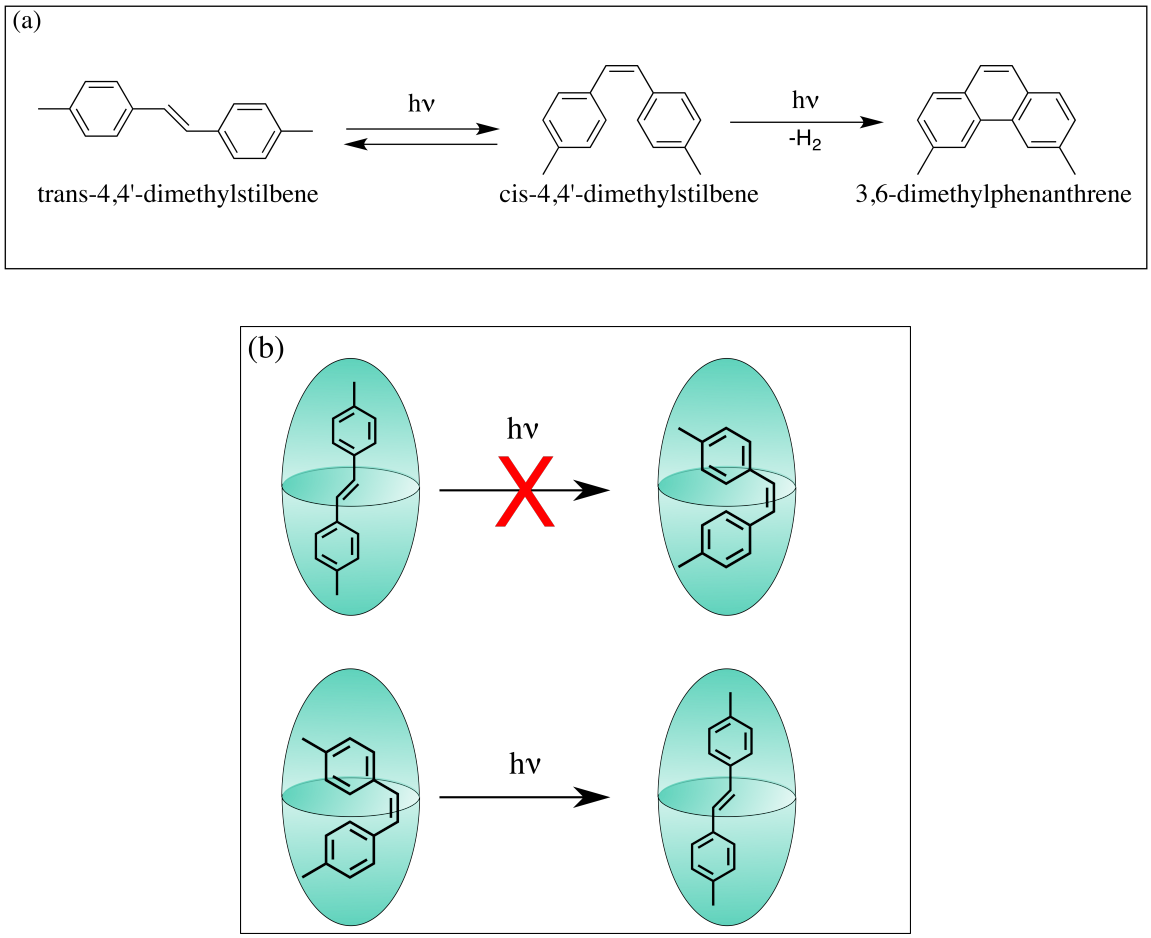

Scheme 1.9. Photochemical reaction of cis and trans 4,4'-dimethylstilbene in hexane (a, top) and in OA (b, bottom).

The encapsulation of two guest molecules by OA has been shown to catalyze several photodimerization reactions due to the increase in "effective concentration" of the guest molecules inside the capsule.[151,152] The dynamics for the formation and dissociation of the capsule is an important aspect that needs to be known when OA is to be used in applications where the release of the guest molecule is important. Ramamurthy et al., in 2011 reported that the OA capsule undergoes a "breathing" movement, which partially opens and closes the octa acid capsules.[149] This movement occurs in the microseconds time scale and during this process, small molecules like oxygen can enter or exit the

capsule. However, the complete dissociation of the capsule was shown to occur at a much longer time scale (2.7 s) by Bohne's group using pyrene as a guest molecule in the octa acid capsule.[155] The third project in this thesis studies the effect of structure of the guest molecule on the dynamics of the capsule formation and dissociation.

1.4 Objectives

The objective of the projects presented in this thesis is to explore the dynamics related to three different aspects of supramolecular host-guest systems. In chapter 2, the dynamics leading to the pK_a shift in guest molecules upon binding with CB[7] is explored. This study lays the ground work for the better understanding of the acid-base catalysis applications of CB[7] system. In chapter 3, the role of sodium ion in the binding dynamics of a guest molecule with two binding sites to CB[7] was investigated. This study will have impact on applications such as drug delivery, where the binding dynamics of a host-guest system need to be very well understood in an environment rich in ions. In the final chapter, the relationship of the structure of a guest molecule to the dynamics of the OA capsule formation was studied. With the increase in number of studies where the OA finds application as containers catalyzing different photochemical reactions, it is important to understand how structural changes for the guest molecule affect the OA capsule formation dynamics. In all the three projects a combination of different techniques was used to understand the mechanisms associated with each host-guest system.

2 Binding Dynamics Study Of 2-Aminoanthracenium Cation That Undergoes pK_a Shift Upon Complexation With Cucurbit[7]uril

The results reported in this chapter have been published in *Faraday Discussions*[156] in 2015.

2.1 Introduction

2.1.1 Shift in acidity constant (pK_a) for guests upon cucurbit[n]uril binding

Cucurbit[n]urils (CB[n]s) are very widely studied host molecules due to their high binding affinity for a wide variety of guest molecules.[107,108] The increase in the acidity constant (pK_a) upon binding with cucurbituril for a guest molecule was first reported by Mock et al. in 1990 for a triamine ligand.[116] This increase in pK_a for the guest molecule is due to the stabilization of the positive charge on the molecule by the carbonyl portals of CB[n]s through ion-dipole interaction. The shift in pK_a for the guests upon complexation with cucurbit[n]urils can be used in several applications such as acid catalysis,[157,158] drug delivery,[118,159-161] enzyme assays,[96] dye lasers[119,162] and logic gates.[120] Proper understanding of the mechanism leading to this pK_a shift is necessary for the efficient design of such functional supramolecular systems.

2.1.2 Objectives

As mentioned in the previous sections, CB[n]s increase the pK_a of the guests upon complexation. The stabilization of the protonated guest molecule inside CB[7] is an indication of the changes in protonation and/or deprotonation rates of the molecule inside

CB[7] compared to the same reactivity in water. The objective of this work is to study the kinetics of complexation for 2-aminoanthracenium cation (Scheme 2.1), which undergoes a pK_a shift upon binding with CB[7] to determine if the kinetics for protonation and deprotonation of the guest inside CB[7] could be obtained. Studying the kinetics underlying this effect is important in designing functional supramolecular systems with application in acid or base catalysis. For example, CB[7] has been shown to catalyze the acid hydrolysis of encapsulated guests.[157,158]

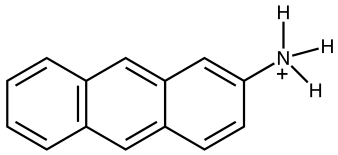

Scheme 2.1. Chemical structure of 2-aminoanthracenium cation (AH^+)

2.1.3 Criterion for choosing the guest molecule

The increase in the hydronium ion concentration at pH values where the guest is protonated led to slower kinetics due to the competitive binding of hydronium ions to CB[n] portals.[129,136,163] The protonation state of the guest affects its binding dynamics with CB[n]s. For example, the association and dissociation rate constants of the cyclohexylmethylammonium cation with CB[6] are lower than the same rate constants for cyclohexylmethylamine because, in the case of the cation, an exclusion complex is formed before the guest is included within the cavity.[129,164] An exclusion complex is formed through the interaction of the guest with only the portals of CB[7] whereas an inclusion complex is formed when the molecule is encapsulated in the hydrophobic cavity of CB[7]. For pH values between the pK_a values of the guest in water and in the

complex, the association process corresponds to the binding of the neutral amine followed by fast protonation of the amine@CB[6] complex, whereas dissociation corresponds to the exit of the ammonium cation from CB[6].[129] The kinetics for the cyclohexylmethylamine-CB[6] system occur on hour to day time scales, depending on the pH. Therefore, the acid-base equilibria for the guest in water or within the complex were fast compared with the complexation dynamics with CB[6]. On the other hand, no evidence for the formation of an exclusion complex was observed for the binding of the 2-naphthyl-1-ethylammonium cation with CB[7].[136]

In order to study the kinetics of protonation and deprotonation of a guest inside CB[7], the guest molecule should be chosen with care. First of all the guest should show a change in pK_a upon complexation with CB[7]. Secondly, it should be possible to monitor the concentration of the protonated and the neutral form of the molecule separately. Finally, the pK_a changes with inclusion in the CB[7] cavity should be in a reasonable range which is not too high or low to be measured in aqueous solutions. 2-aminoanthracene was a good choice because it meets all the mentioned criteria as explained in section 2.1.4.

2.1.4 2-aminoanthracenium cation

The 2-aminoanthracenium cation (AH^+) is reported to form a 1:1 complex with CB[7] by Macartney et al. in 2005.[165] AH^+ is a molecule with interesting fluorescence properties both in the absence and presence of CB[7]. The neutral form of the molecule (A) has a broad emission centered around 510 nm ("green" region) whereas the protonated form of the molecule emits around 400 nm ("blue" region). The ground state of AH^+ has a pK_a

value[166] of 4.0 while the excited state of the molecule has a pK_a* of -5.4 (in 1:1 water:ethanol).[167,168] Due to its very low excited state pK_a, excited AH^+ deprotonates adiabatically resulting in emission in the "green" region from excited A (Scheme 2.2).

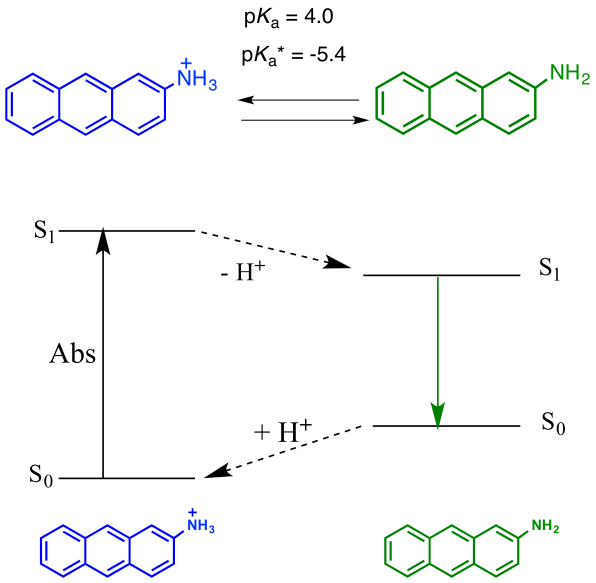

Scheme 2.2. Schematic representation for the excited state deprotonation and emission for AH^+.

In the presence of CB[7], the ground state and excited state pK_a for AH^+ increases to 7.1 and between 4.7 and 5.2 respectively.[165] As a result when CB[7] is present in the solution, at pH values less than these two pK_a values for the complex, the emission happens from the excited state of AH^+. In other words AH^+ is stabilized inside CB[7] and there is no deprotonation of AH^+ in the excited state (Scheme 2.3).

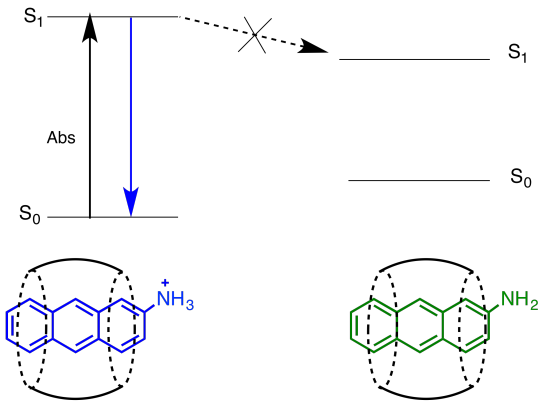

Scheme 2.3. Schematic representation for the emission of AH^+ encapsulated in CB[7] cavity.

AH^+ forms a stronger complex with CB[7] due to the presence of the positive charge in the molecule that can interact with the carbonyl portals of CB[7] compared to complexed A. However depending upon the pH, all the equilibria present in the system containing AH^+/A and CB[7] in the solution can be represented by Scheme 2.4

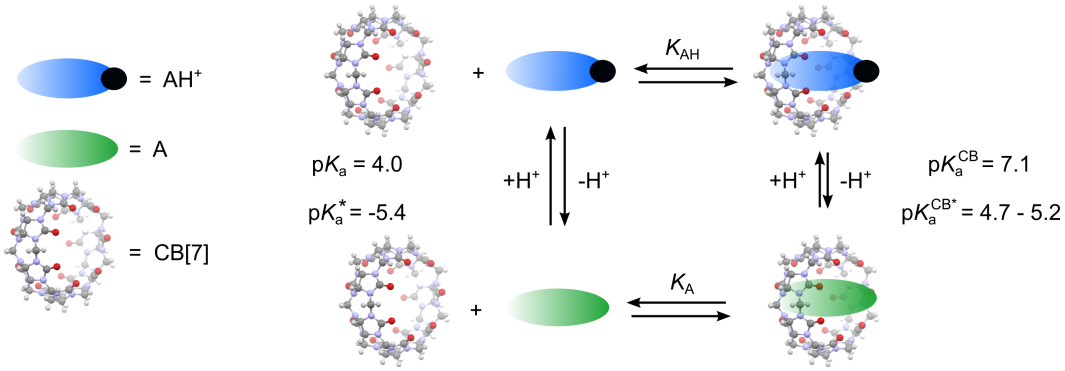

Scheme 2.4. Equilibria between protonated AH^+, neutral A, and CB[7], and pK_a values for the ground (pK_a, pK_a^{CB}) and singlet excited state (pK_a^*, pK_a^{CB*}) of AH^+ in the absence[166-168] and presence of CB[7].[165]

2.2 Experimental section

2.2.1 Materials

2-aminoanthracene purchased from Aldrich (96%) was recrystallized once from ethanol. Hydrochloric acid (2.0 M, Anachemia, ACS reagent grade), sodium hydroxide (2.0 M, Anachemia, ACS reagent grade), glacial acetic acid (ACP, ACS reagent grade) and methanol (Fisher, spectral grade, >99.9%) were used as received. Cucurbit[7]uril was synthesized by following a modified procedure based on previous literature[169-171] and purified as discussed in section 2.2.7. All the aqueous samples were prepared in deionized water (Barnstead NANOpure deionizing systems ≥ 17.8 MΩ cm)

2.2.2 Sample preparation

A stock solution of 2-aminoanthracene of 1 mM concentration was prepared in methanol. Appropriate quantities of NaCl and HCl were added to water to prepare solutions of pH 2.0, 3.8 and 4.3 containing 20 mM NaCl. Buffer solutions were prepared at pH 5.0 and 5.5 by adding sufficient amount of NaOH to water to attain a 20 mM concentration of sodium ions and then adding glacial acetic acid to this solution until the required pH was attained. Solutions of AH^+ or A for the experiment were prepared by diluting the stock solution into the aqueous solutions of required pH. CB[7] stock solutions (≈ 850 μM) were prepared by dissolving appropriate quantities of solid CB[7] in the aqueous solutions of required pH and sodium ion concentration. Solid CB[7] absorbs water over time and the percentage purity of CB[7] was calculated at different days of experiment by the procedure described in section 2.2.9 based on a literature report.[172] For the stopped-flow experiments a set of CB[7] solutions were prepared from

the stock solution by dilution. For binding isotherm experiments and time-resolved fluorescence measurements small volumes of the stock CB[7] solutions were injected into 3 mL of AH^+/A solution in a 10 × 10 mm quartz cell using a gas tight syringe. Control solutions containing all the chemicals except the fluorophore were also prepared for all the experiments.

2.2.3 Equipment

Absorbance measurements were performed on a Cary 100 UV-Vis spectrophotometer. Steady-state fluorescence measurements were recorded with a PTI QM-40 spectrofluorimeter. The emission spectra were recorded by exciting the samples at 365 nm and collecting the emission between 380-650 nm. The bandwidths for the excitation and emission monochromators were set to 2 nm. A step size of 0.5 nm and an integration time of 0.5 s were used during the collection of spectra. The sample was kept at 20 ºC throughout the experiment and it was equilibrated at 20 ºC for 10 min before a spectrum was taken. The fluorescence spectra obtained were corrected by subtracting a baseline spectrum for a solution containing all the chemicals except the fluorophore from the sample spectra.

Time-resolved fluorescence decays were recorded with an Edinburgh Instruments OB920 single photon counting system. The samples were excited with a light emitting diode (EPLED-360, λ_{ex} = 365 nm). The emission from the sample was recorded at 405 or 510 nm using a monochromator whose bandwidth was set to 16 nm. The maximum intensity channel had 2000 counts. The emission from a Ludox solution was collected at the excitation wavelength to record the instrument response function (IRF).

Binding dynamics experiments were performed on an Applied Photophysics SX20 stopped-flow system. The excitation source was a Hg-Xe vapor lamp. The samples were excited at 365 nm where the Hg-Xe lamp has a peak and the excitation monochromator bandwidths were set to 2 nm. This excitation wavelength led to a better signal on the stopped-flow owing to a higher excitation efficiency of the sample. In order to correct for any offset in the excitation monochromator position scattering from water was recorded on the stopped-flow and the maximum intensity peak position from the scattering was compared to the maximum intensity peak for the Hg-Xe lamp provided by the manufacturer. The emission from the samples were collected using an interference filter (385-423 nm) with a maximum transmission at 405 nm and a cut-off filter with transmittance above 515 nm for the measurements in the "blue" and "green" region respectively. The guest and the host solutions were mixed in a 1:1 ratio in the mixing chamber. The samples were equilibrated at 20 ºC for 10 min before a measurement was done. For each experiment the stopped-flow trace was obtained by averaging at least 25 traces. The stopped-flow traces obtained were corrected for baseline by subtracting the fluorescence intensity on the stopped-flow for a solution containing all the components except the fluorophore and CB[7].

2.2.4 Fitting of binding isotherms for 1:1 complexes

The area under the emission spectra was integrated from 380-456 nm and 456-650 nm to construct binding isotherms for the "blue" and "green" regions respectively. The integrated intensities were then normalized by dividing all the intensities by the intensity for the spectra in the absence of CB[7]. Numerical analysis was employed to fit the

binding isotherms using Scientist 3 software from Micromath. The model used for the fitting of the binding isotherms assumed a 1:1 complexation for AH^+/A with CB[7] and yielded an overall equilibrium binding constant for the complexation process. The model was defined as follows. $[CB[7]]_T$ denotes the total concentration of CB[7] and $[G]_T$ denotes the total concentration of guest, which is the sum of protonated (AH^+) and deprotonated forms (A) of the guest. Both $[CB[7]]_T$ and $[G]_T$ are defined as independent variables. The equilibrium concentrations of free CB[7] ($[CB[7]]_{eq}$), free guest ($[G]_{eq}$), the 1:1 complex ($[G@CB[7]]_{eq}$), and the fluorescence intensity (I) are defined as dependent variables. R corresponds to the ratio of the fluorescence intensity of the guest in the absence of CB[7] (I_0) to the total guest concentration, while C_{11} is the ratio of the emission efficiencies of the guest in the complex and in water, and β_{11} is the overall equilibrium binding constant for the 1:1 complex. R, C_{11}, and β_{11} were set as parameters.

$$\left[G@CB[7]\right]_{eq} = \beta_{11} \times [G]_{eq} \times \left[CB[7]\right]_{eq} \quad \text{(Eq 2.1)}$$

$$\left[CB[7]\right]_{eq} = \left[CB[7]\right]_{T} - \left[G@CB[7]\right]_{eq} \quad \text{(Eq 2.2)}$$

$$[G]_{eq} = [G]_{T} - \left[G@CB[7]\right]_{eq} \quad \text{(Eq 2.3)}$$

$$I = R \times \left([G]_{eq} + C_{11} \times \left[G@CB[7]\right]_{eq}\right) \quad \text{(Eq 2.4)}$$

where

$$R = \frac{I_0}{[G]_T} \quad \text{(Eq 2.5)}$$

The concentration constraints for the dependent variables are as follows:

$$0 < \left[CB[7]\right]_{eq} < \left[CB[7]\right]_{T} \quad \text{(Eq 2.6)}$$

$$0 < [G]_{eq} < [G]_{T} \quad \text{(Eq 2.7)}$$

$$0 < \left[G@CB[7]\right]_{eq} < [G]_{T} \quad \text{(Eq 2.8)}$$

2.2.5 Analysis of time-resolved fluorescence decays

Time-resolved fluorescence decays were analyzed using FAST software from Edinburgh Instruments. Fits were performed by reconvoluting the IRF with the decays. A fit was considered good if the residuals were random and the χ^2 values from the fits were close to unity (0.9-1.2).[55] The decays were fit to either a monoexponential function or sum of two exponentials depending upon the number of species in the solution contributing to the decay as per the following equation.

$$\mathrm{I(t)} = \mathrm{I_0} \sum_{1}^{i} A_{\mathrm{i}}\ e^{-t/\tau_{\mathrm{i}}} \quad \text{(Eq 2.9)}$$

In the above equation τ_i represents the lifetime of species i, and the pre-exponential factor A_i denotes the contribution of species i to the fluorescence decay.

2.2.6 Data analysis for stopped-flow experiments

The stopped-flow traces were analyzed by fitting the averaged traces for an experiment to a sum of exponential functions (Eq 2.10) or by using a global analysis method where all traces were simultaneously fit to a defined model. The fit to a sum of

exponentials is defined by an offset (a_0) and the sum of exponentials terms, each of which has a corresponding observed rate constant (k_{obsi}) and an amplitude of a_i.

$$\Delta I = a_0 + a_1 e^{-k_{obs1}\, t} + a_2 e^{-k_{obs2}\, t} \qquad \text{(Eq 2.10)}$$

The analysis of the individual stopped-flow traces at pH 2.0 and 3.8 was done as follows: To obtain the rate constant for the slow relaxation time, the traces were fit to a mono-exponential function by starting the fit at incrementally longer times until the residuals became random and the observed rate constant was constant (Figure 2.1). The rate constant for the fast relaxation time was then obtained by fitting the traces to a sum of two exponentials and fixing the rate constant for the slow relaxation process. The stopped-flow traces at pH 5.0 and 5.5 were fit to a mono-exponential function to yield one relaxation time. In the global analysis method, all the kinetic traces for a particular experiment were fit simultaneously to a model defined in the Prokineticist II software from Applied Photophysics. The goodness of the fit was judged by the randomness of the residuals.

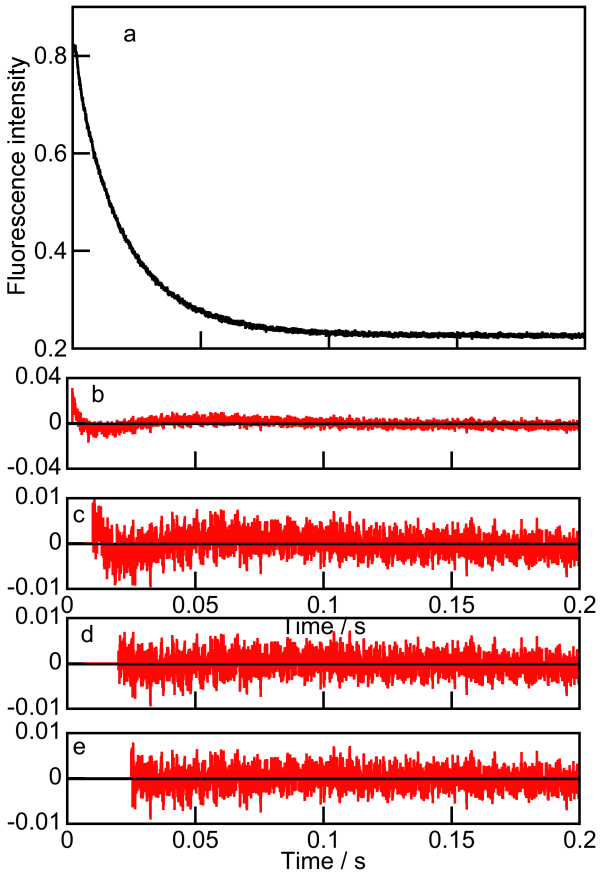

Figure 2.1. Kinetic trace (a) for the mixing of 1 μM AH^+ with 9 μM CB[7] at pH 2.0, and the residuals between the trace and the calculated fit of the trace to a mono-exponential function when the fit was started incrementally at 2 (b, k_{obs} = 51 s^{-1}), 10 (c, k_{obs} = 49 s^{-1}), 20 (d, k_{obs} = 47 s^{-1}), and 25 ms (e, k_{obs} = 47 s^{-1}).

2.2.7 Synthesis and purification of CB[7]

The synthesis of CB[7] was adapted from previous procedures.[169-171] Reagent grade chemicals were used in all steps of the synthesis and purification, except for the spectral grade methanol that was used in the final purification steps. Glycoluril (10.0 g, 1 equiv) and powdered formaldehyde (4.0 g, 1.9 equiv) were magnetically stirred to ensure homogeneous mixing in a two-necked 100 mL round bottom flask attached to a condenser and a $CaCl_2$ guard tube. After heating the solid at 50 ºC for 5-10 min, 20 mL of an acid mixture of 20% H_2SO_4 in HCl was added dropwise to the solid while stirring. The

reaction mixture formed a hard solid upon vigorous stirring. After the addition of acid, the temperature was raised to 80 ºC, and the hard solid dissolved slowly to give a clear solution after about 15 min of heating. After heating the reaction mixture at 80 ºC for 3 h, the temperature was raised again to 95–105 ºC, and the reaction mixture was heated for another 5 h. The homogeneous reaction mixture was cooled down to room temperature using a water bath and was then poured slowly into 150 mL of cold methanol (in an ice bath) with vigorous stirring. This suspension was left standing for 30 min to completely precipitate the CB[n]s. This heterogeneous suspension was then filtered, and the solid from the filtration was mixed with 120 mL of water in a beaker. This water suspension was stirred vigorously at 40 ºC for 4 h and then filtered while hot. Care was taken not to exceed a temperature of 60 ºC while heating the solution, as this resulted in a waxy hard solid after filtration. The solid from the filtration was stirred with water twice more at 40 ºC for 4 h to extract more CB[n]s. The filtrate contained the desired CB[7]. The three fractions of the filtrates, saved separately, were cooled down to room temperature and 150 mL of methanol was added to each of these fractions to precipitate the CB[n]s. This methanol-water suspension was kept in the fridge overnight (minimum 12 h) for the complete precipitation of CB[n]s and was then vacuum filtered. The residue that contains CB[n]s was washed very well with at least 100 mL of methanol. Of the three residue fractions, the second and third ones had a higher percentage of CB[7], determined through titration[172] as explained in section 2.2.9. The air-dried solid obtained from the second and third fractions (2.0 g) was characterized by electrospray ionization mass spectrometry (ESI-MS).[173]

The solid containing 60–75% CB[7] obtained from the second and third fractions as described above was further purified as follows: The solid (2.0 g) was stirred with 50 mL of water for 1 h. This water suspension was vacuum filtered, and the residue was stirred with another 30 mL of water for 1 h and filtered again. The filtrate fractions were combined, added to 120 mL of methanol, and refrigerated overnight for complete precipitation of CB[n]s. This water–methanol suspension was filtered, and the residue was washed with plenty of methanol to remove mineral acids. The reprecipitation of CB[7] from water using methanol was repeated to remove CB[5] from CB[7]. The solid from the filtration (1.0 g) was dissolved in the minimum required amount of water with heating (45–50 ºC). Methanol was added dropwise to this hot solution until the solution turned slightly turbid. The turbid solution was filtered while hot, and the insoluble solid (mainly CB[6]) was discarded. The filtrate was cooled to room temperature and methanol (1:1.5 water–methanol volume ratio) was added to reprecipitate CB[7]. This suspension was filtered after overnight refrigeration. The solid from the filtration (700 mg) was refluxed in 50 mL of a methanol–water mixture (1.3:1 by volume) for 10 h. The resultant suspension was cooled to room temperature, filtered, and washed with methanol. The solid obtained was vacuum dried at 80 ºC for 12 h. The resultant solid (500 mg) was characterized by ESI-MS, ^{13}C NMR, and ^{1}H NMR.[170,173,174] The mass spectrometry data did not show the presence of any CB[6], but showed traces of CB[5]. The ^{13}C NMR results showed the presence of less than 3% CB[5]. Immediately after vacuum drying, a titration with cobaltacenium cation[172] showed that the sample contained 90% CB[7].

2.2.8 Characterization of CB[7] by ESI-MS and NMR

Mass spectra were recorded on a Micromass Q-TOF II mass spectrometer. The major impurity present in CB[7] samples after synthesis are the other CB[n] homologues, mainly CB[5] and CB[6]. ESI-MS in the positive ion mode was employed for the characterization of CB[7] samples after synthesis. The samples were sprayed using a syringe pump operating at 10 μL/min and the spectrum was collected over an m/z range of 200-2000. The desolvation and the cone gas flow rates were set to 200 and 50 L h^{-1} respectively. The voltage parameters used during mass spectrometric analysis were: cone voltage = 120 V, capillary = 3 kV, MCP = 2150 V, pusher = 980 V, TOF = 9.2 kV. The source and desolvation temperatures were kept at 100 and 200 ºC respectively. A standard solution containing 100 μM each of CB[5], CB[6] and CB[7] were prepared in 20% formic acid solution. Approximately 100 μM solution of sample CB[7] from synthesis was also prepared in 20% formic acid solution. The standard solution was used to optimize the mass spectrometer where maximum signal for the impurity (CB[5] and CB[6]) was obtained. The CB[7] sample solution was then injected into the mass spectrometer and the ratio of the intensity for the impurity to that of CB[7] signal was compared between the standard solution and the CB[7] sample to obtain an estimation of the amount of impurity present in CB[7] sample.

^{1}H NMR spectra were recorded with a Bruker Avance I 500 MHz NMR spectrometer operating at 500.27 MHz frequency using a BBO probe. A standard solution containing 30 mM each of CB[5], CB[6] and CB[7] was prepared in DCl. Approximately 30 mM CB[7] sample from synthesis was also prepared by dissolving the solid in DCl. The spectra were acquired using 30º pulse angle and a 10 s relaxation delay. The T_1 was

estimated to be ≤ 1.3 s via the T_1 null in the inversion recovery sequence for the peaks of interest. The number of data points collected was 32,000. The spectrum was referenced to the methanol solvent CH_3 peak at 3.30 ppm. The lower frequency resonance of the geminal pairs of the methylene signals were obtained at 4.85, 4.70 and 4.46 ppm for CB[5], CB[7] and CB[6] respectively. The spectral width was 9 ppm centered at 5.5 ppm. The quantitation was obtained by the integration of signals. Quantitative comparison of the peaks of the spectrum for the CB[7] sample from synthesis to that of the standard solution led to the determination of the percentage of impurities of CB[5] to be less than 3% in the CB[7] sample.

2.2.9 Titration of CB[7] solutions

A 1 mM stock solution of Bis(cyclopentadienyl)cobalt(III)hexafluorophosphate (Cob^+) was prepared in methanol. A 15 μM solution of Cob^+ was prepared by diluting the stock solution in 2 mM sodium chloride solution. Molar absorption coefficient for Cob^+ in water[172] at 261 nm is 34200 M^{-1} cm^{-1}. Around 1 mM CB[7] solution (whose purity needs to be determined) was prepared in 2 mM sodium chloride solution.

A 3 mL volume of the 15 μM solution of Cob^+ was transferred to an absorption cell. The titration was performed by adding 8 μL aliquots of 1 mM CB[7] (assuming 100% purity for CB[7]) into the Cob^+ solution using a 10 μL gastight syringe and recording the absorption spectrum after each addition of CB[7]. The absorbance of Cob^+ at 261 nm is depressed by the addition of CB[7] as shown in Figure 2.2. The titration was continued until there was no change in the absorbance spectrum for Cob^+ with the addition of CB[7]. At least 3 more spectra were collected after saturation was attained for the spectra.

A blank spectrum was also recorded for 2 mM sodium chloride solution and the absorbance for the blank was subtracted from each Cob^+ spectrum. The absorbance values were corrected for dilution before the equivalence point for titration was determined. The equivalence point was determined from the titration plot as shown in Figure 2.3. The percentage purity of CB[7] can be calculated by the Eq 2.11 where C_{cob^+} is the molar concentration of Cob^+ solution used, $C_{CB[7]}$ is the molar concentration of CB[7] stock solution prepared assuming 100% purity for CB[7], V_i is the initial volume of Cob^+ solution taken in the cell and V_e is the volume of CB[7] stock solution added corresponding to the equivalence point from the titration curve.

$$\%p = \frac{C_{cob^+} \times V_i}{C_{CB[7]} \times V_e} \qquad \text{(Eq 2.11)}$$

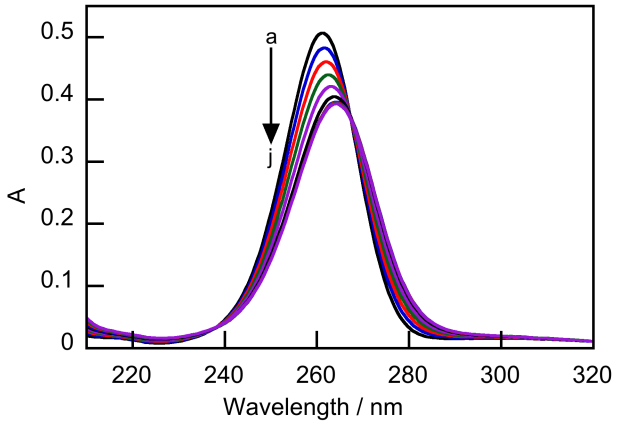

Figure 2.2. Absorption spectrum for 15 μM Cob^+ in the absence (a) and presence of increasing concentrations of CB[7] (b to j).

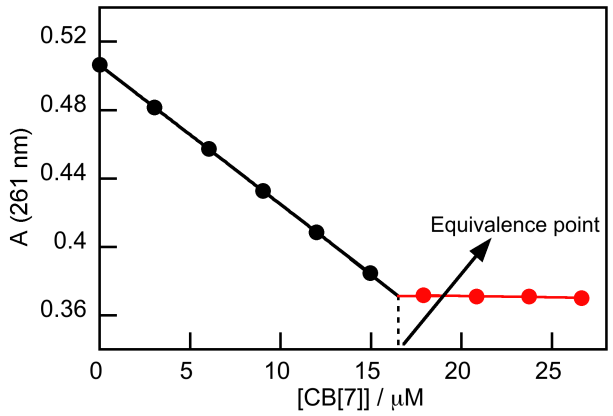

Figure 2.3. Plot for the dependence of absorbance at 261 nm for Cob^+ with CB[7] concentration. The percentage purity obtained for this CB[7] sample was 90%.

2.3 Results

2.3.1 Absorption and steady-state fluorescence

The absorption and emission spectra for AH^+/A are dependent on the pH of the solution. The absorption spectrum at pH 2.0 (Figure 2.4a), where all the molecules are protonated shows sharp peaks which undergo a red shift in the presence of 25 μM CB[7] indicating the formation of a complex. At pH 5.5 (Figure 2.4c), where most of the molecules are in the neutral form there is a broad absorption band centered around 400 nm corresponding to the presence of A.[166] The absorption spectrum at pH 5.5 showed smaller changes in the presence of CB[7]. At intermediate pH of 3.8 (Figure 2.4b), where approximately 3:2 mixture of AH^+/A is present in water, the broad band around 400 nm decreased in the presence of CB[7], and the sharp peaks shifted to the same wavelengths observed at pH 2.0 in the presence of this host. These absorption spectra show that the equilibrium shifts toward AH^+ when the guest is bound to CB[7] and these results are consistent with the stabilization of AH^+ when bound to CB[7]. For fluorescence emission

spectra at pH 2.0, a small emission intensity is observed from AH^+ around 400 nm in addition to the predominant emission centered at 510 nm from A formed adiabatically from excited AH^+ (Figure 2.4d). The emission from AH^+ is absent at pH 6.0, which is two pH units higher than the pK_a of AH^+/A. At pH 6.0, only A is present in solution.

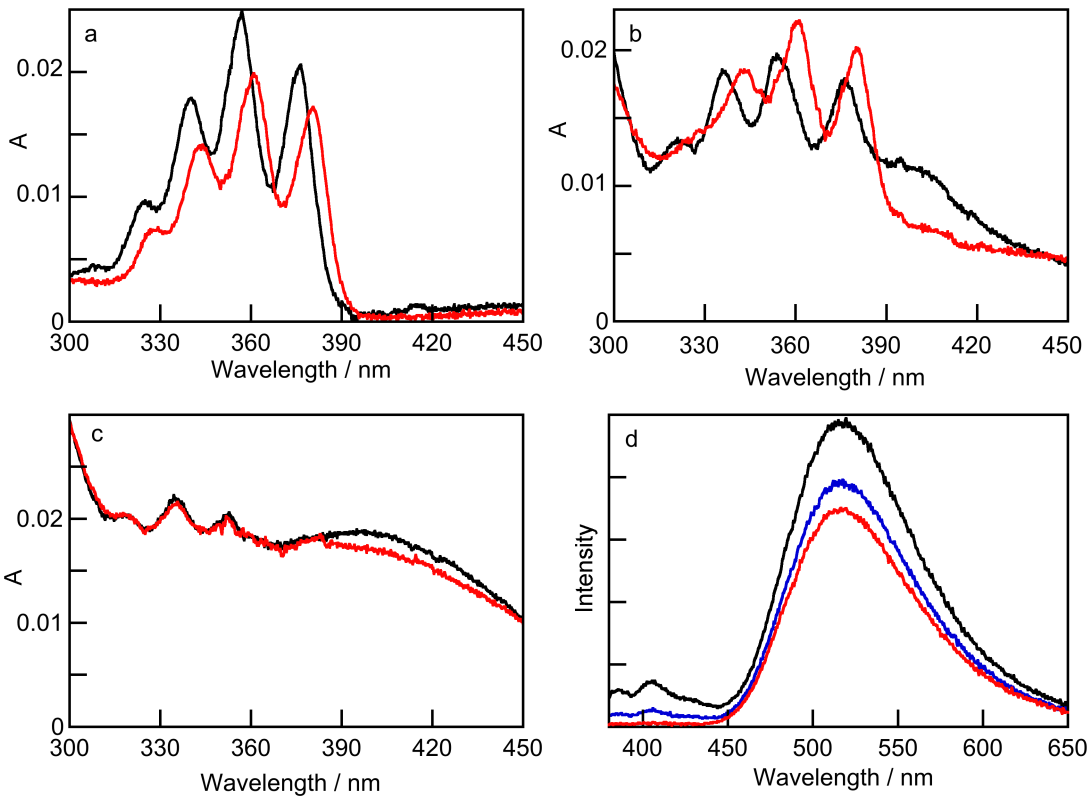

Figure 2.4. Absorption spectra of AH^+/A (5 μM) at pH 2.0 (a), 3.8 (b), and 5.5 (c) in the absence (black) and presence of 25 μM CB[7] (red). (d) Emission spectra for AH^+/A (1 μM) in water at different pH values: 2.0 (black), 4.0 (blue), and 6.0 (red).

2.3.2 Optimization of the NaCl concentration

The solubility of CB[7] is enhanced by the presence of Na^+ ions. This is due to the binding of Na^+ to the carbonyl portals of CB[7]. Moreover, the presence of Na^+ was

required to achieve a stable pH for the samples. For a solution containing Na^+, AH^+ and CB[7] the equilibria of the system can be described by Scheme 2.5.

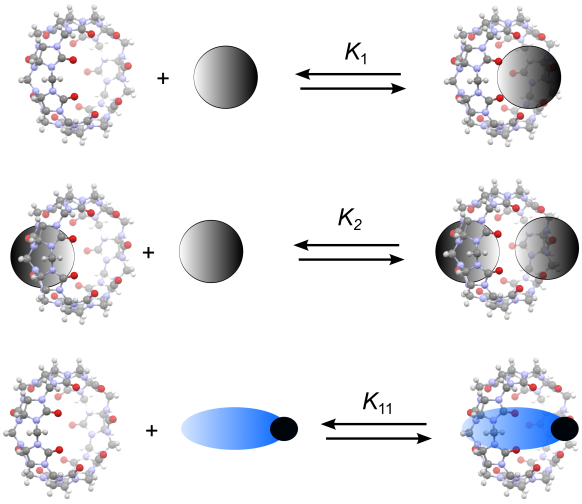

Scheme 2.5. Equilibria for CB[7] binding to Na^+ cations (black circles) and AH^+.

The overall equilibrium binding constant (β_{11}) for the formation of 1:1 complex for AH^+ with CB[7] can be defined as follows.

$$CB[7]_{GF} + AH^+ \underset{}{\overset{\beta_{11}}{\rightleftharpoons}} AH^+@CB[7]_{GF} \qquad \text{(Eq 2.12)}$$

$$CB[7]_{GF} = CB[7] + CB[7]\bullet Na^+ + Na^+\bullet CB[7]\bullet Na^+ \qquad \text{(Eq 2.13)}$$

The competitive binding of Na^+ to CB[7] was shown to slow down the kinetics of AH^+ binding with CB[7] and to decrease the amplitude of the kinetics (Figure 2.5). This observation is consistent with previous literature for 2-naphthyl-1-ethylammonium cation binding to CB[7].[136] The decrease in amplitude is due to the formation of less amount of complex as less amount of free CB[7] is available for binding. The slowing down of the

relaxation kinetics is a consequence of a slower bimolecular association process because of the lower effective concentration of free CB[7] in the presence of Na^+ cations, while the dissociation is unaffected as it is a unimolecular reaction. Stopped-flow experiments were performed to determine the ideal Na^+ ion concentration for the kinetic studies. The kinetics was followed in the "blue" region where AH^+ emits because its excited state does not deprotonate owing to the higher pK_a^* for AH^+@CB[7]. A concentration of 20 mM Na^+ was chosen for all experiments because the kinetics was sufficiently slow to be detected in stopped-flow experiments with reasonable amplitude.

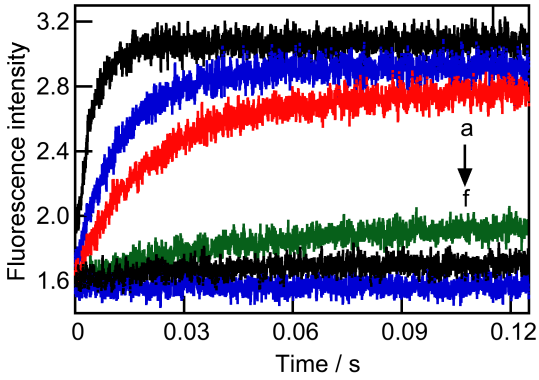

Figure 2.5. Kinetics for the formation of the AH^+@CB[7] complex ([AH^+] = 2 μM, [CB[7]] = 7 μM) at pH 2.0 in the presence of increasing Na^+ cation concentrations: 2 (a), 10 (b), 20 (c), 100 (d), 200 (e) mM. Trace "f" corresponds to the baseline measurement in the absence of CB[7].

Any parameter that is dependent on the concentration of CB[7] is an overall or apparent parameter because a fraction of the CB[7] molecules was non-reactive owing to the formation of CB[7] complexes with Na^+ cations (Scheme 2.5). The binding isotherms led to the determination of overall binding constants (β), while the bimolecular rate constants for the reactions involving CB[7] are apparent rate constants and are denoted k'.

The individual equilibrium constants (K) or bimolecular rate constants (k) can be obtained following the procedure previously described.[136] I chose to present the β and k' values in the results section as these are the values derived directly from the experiments.

2.3.3 Binding constants for complexation

The overall equilibrium binding constants for the complexation of AH^+ with CB[7] at pH values of 2.0, 3.8, 5.0 and 5.0 were determined by steady-state fluorescence measurements. The addition of increasing concentrations of CB[7] to AH^+ (1.0 μM) at pH 2.0, where 99 % of AH^+ is present in the solution, led to a decrease of the "green" emission of A around 510 nm and an increase of the AH^+ "blue" emission below 450 nm (Figure 2.6). As the pH was raised to 5.5 the increase in emission intensity in the blue region was suppressed due to the presence of more A in solution (Figure 2.7). The intermediate pH values of 3.8 and 5.0 showed emission properties intermediate to that of pH 2.0 and 5.5. The increase and decrease in fluorescence intensities for the "blue" and the "green" regions respectively with CB[7] concentrations were fit numerically to determine the overall equilibrium constant as explained in section 2.2.4. The fits were good and the residuals between the experimental data and the calculated intensities were random. The recovered average β_{11} values for the experiments at pH 2.0 from two independent experiments were $(4.92 \pm 0.09) \times 10^5$ M^{-1} when the emission intensity for A was followed and $(4.8 \pm 0.2) \times 10^5$ M^{-1} when the intensity changes for AH^+ were measured, leading to an overall average β_{11} value of $(4.9 \pm 0.1) \times 10^5$ M^{-1}. At pH 5.5 the average overall equilibrium binding constant values recovered from the fits were $(1.52 \pm 0.04) \times 10^4$ M^{-1}. At intermediate pH values of 3.8 and 5.0 the binding constant values

were (2.83 ± 0.03) × 10^5 and (3.49 ± 0.09) × 10^4 M^{-1} respectively. At pH values of 3.8, 5.0, and 5.5, the percentage of AH^+ is 61, 9, and 3%, while the percentage of A is 39, 91, and 97%. The decrease in binding constant values with the increase in pH is due to the weaker binding of A compared to AH^+ with CB[7]. Table 2.1 shows the equilibrium binding constants obtained for the "blue" and "green" regions for experiments performed at all pH values.

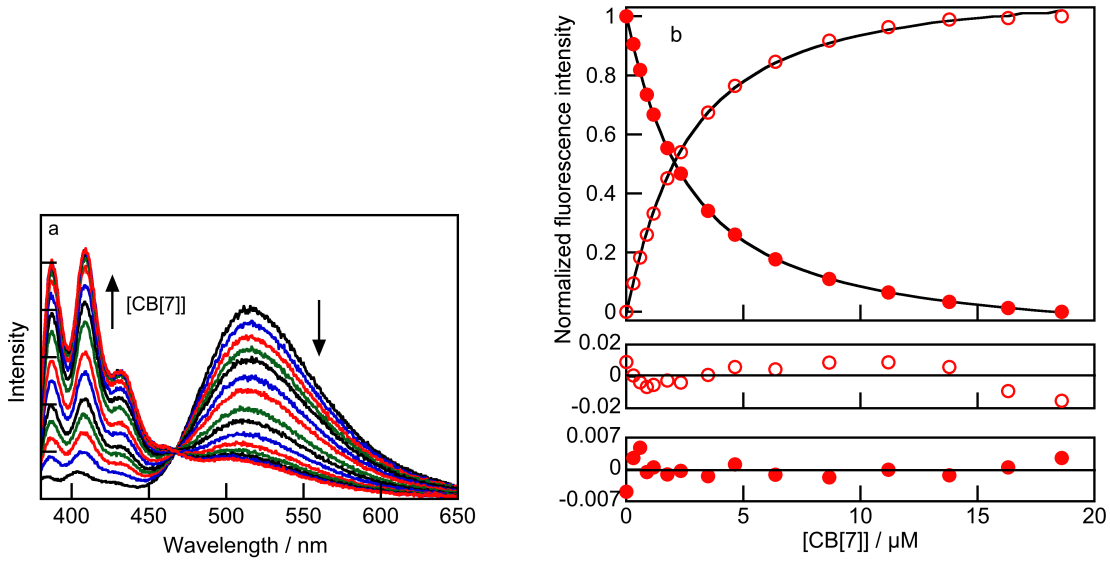

Figure 2.6. (a) Fluorescence spectra for AH^+ at pH 2.0 (a) in the presence of increasing CB[7] concentrations from 0 to 19 μM. (b) Binding isotherms (top panel) for the intensity changes for the "blue" (integration from 380 to 456 nm, open circles) and "green" (integration from 456 to 650 nm, solid circles) emission. The black lines correspond to the numerical fits of the data. The residuals between the experimental data and calculated values are shown in the middle panel ("blue" emission) and lower panel ("green" emission).

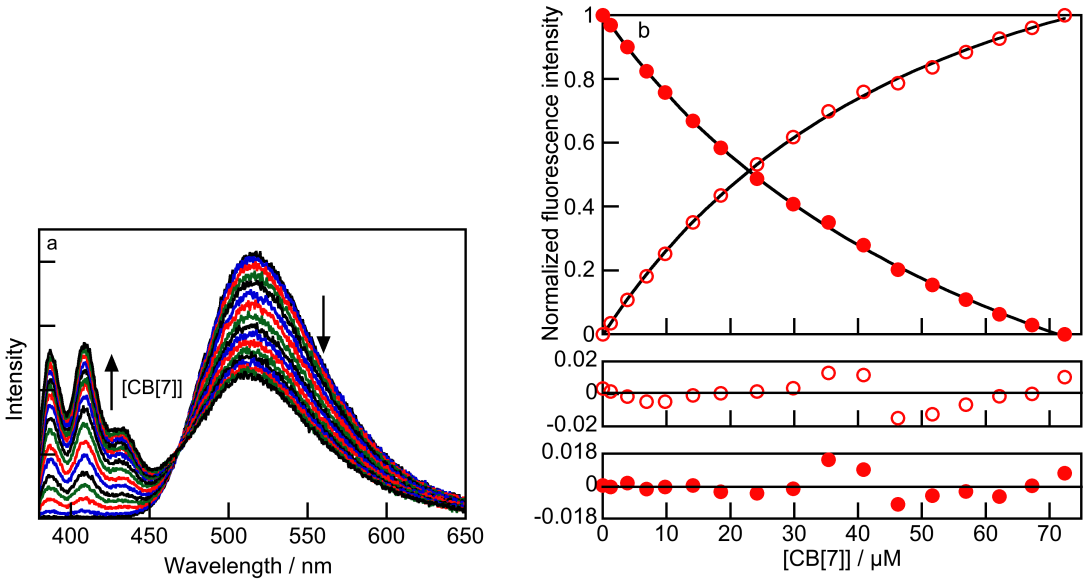

Figure 2.7. (a) Fluorescence spectra for AH^+ at pH 5.0 (a) in the presence of increasing CB[7] concentrations from 0 to 72 μM. (b) Binding isotherms (top panel) for the intensity changes for the "blue" (integration from 380 to 456 nm, open circles) and "green" (integration from 456 to 650 nm, solid circles) emission. The black lines correspond to the numerical fits of the data. The residuals between the experimental data and calculated values are shown in the middle panel ("blue" emission) and lower panel ("green" emission).

Table 2.1. Overall equilibrium constants for the binding of A/AH^+ with CB[7] determined from the changes in the "blue" and "green" emission intensities at different pH values.[a]

pH	**β_{11} / 10^5 M^{-1} ("green")**	**β_{11} / 10^5 M^{-1} ("blue")**
2.0	4.92 ± 0.09	4.8 ± 0.2
3.8	2.86 ± 0.03	2.80 ± 0.06
5.0	0.36 ± 0.01	0.340 ± 0.004
5.5	0.155 ± 0.006	0.148 ± 0.006

[a], errors correspond to those recovered from the numerical fit of the data.

The equilibrium binding constant for A with CB[7] was calculated from the thermodynamic cycle (Scheme 2.4) since three of the other equilibrium constants were known. The thermodynamic cycle is valid for overall equilibrium constants and the binding constant value for AH^+ (β_{11}^{AH}) is the one determined at pH 2.0. The equilibrium constants in a thermodynamic cycle are related by equations 2.14 to 2.17 and the binding constant for A (β_{11}^{A}) was determined from equation 2.18, to be 390 ± 10 M^{-1}, where the error is related to the measurement of β_{11}^{AH}.

$$K_a = \frac{[A][H^+]}{[AH^+]} \qquad \text{(Eq 2.14)}$$

$$K_a^{CB} = \frac{[A@CB[7]][H^+]}{[AH^+@CB[7]]} \quad \text{(Eq 2.15)}$$

$$\beta_{11}^{AH} = \frac{[AH^+@CB[7]]}{[AH^+]\,[CB[7]]} \quad \text{(Eq 2.16)}$$

$$\beta_{11}^{A} = \frac{[A@CB[7]]}{[A][CB[7]]} \quad \text{(Eq 2.17)}$$

Combining equations 2.14, 2.15, 2.16, and 2.17 and expressing the acid dissociation constants as pK_a values leads to the following equation:

$$\frac{10^{-\mathrm{p}K_a^{CB}}}{10^{-\mathrm{p}K_a}} = \frac{\beta_{11}^{\mathrm{A}}}{\beta_{11}^{\mathrm{AH}}} \quad \text{(Eq 2.18)}$$

Experimental determination of β_{11}^{A} under conditions where only A was present was difficult due to very small changes in fluorescence intensity with the addition of CB[7]. However, an experiment was performed at pH 12 where it was found that no saturation could be attained for the binding isotherm (Figure 2.8). The value of β_{11}^{A} and the quantum yield of A in A@CB[7] are correlated, and for this reason, no accurate value for β_{11}^{A} could be obtained. Adequate fits were observed for β_{11}^{A} values fixed between 100 and 700 M^{-1} (Figure 2.9), which are of the same order of magnitude as the value calculated from the thermodynamic cycle. This proved that the equilibrium binding constant obtained from the thermodynamic cycle is valid.

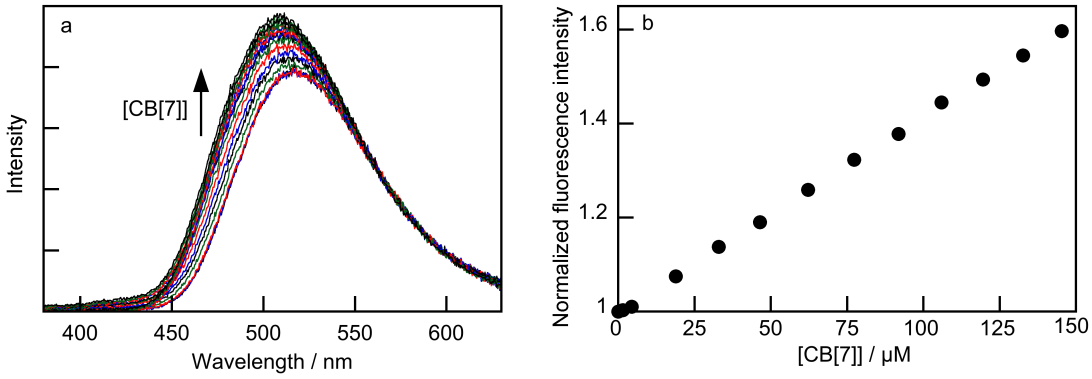

Figure 2.8. (a) Emission spectra for A at pH 12 in the presence of increasing concentrations of CB[7] from 0 to 145 μM. (b) Dependence of the emission intensity of A with the CB[7] concentration.

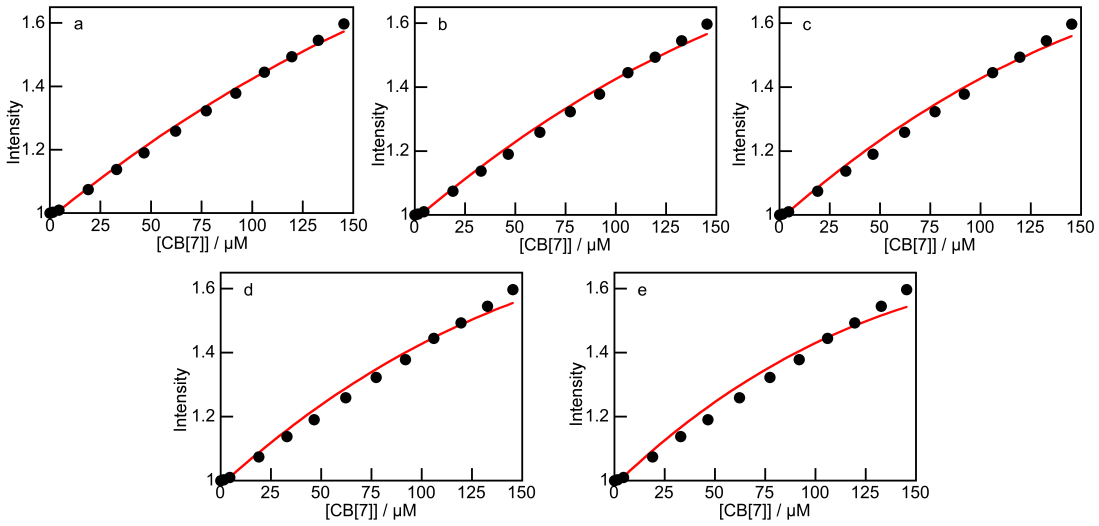

Figure 2.9. Fitting of the binding isotherm for A with CB[7] determined at pH 12 by fixing the β_{11}^{A} value to 100 (a), 400 (b), 700 (c), 900 (d), and 1500 M^{-1} (e).

2.3.4 Time resolved fluorescence

Time-resolved fluorescence experiments give information on fluorophores with different lifetimes. In supramolecular systems, the same fluorophore can have different lifetimes depending upon the environment in which the fluorophore is present. Fitting the

fluorescence lifetime decays for such systems to equation 2.9 gives the associated lifetime (τ_i) and the pre-exponential factor A_i for these species. The A_i values are related to the abundance of each species; a positive value indicates the disappearance of the fluorophore, while a negative value indicates the formation of the fluorophore.

The excited state of A yielded a lifetime of 24.8 ± 0.1 ns when measured at 510 nm at pH 6.0. This value is of the same order of magnitude as the lifetimes previously determined for A in water-ethanol (14 ns)[167] or cyclohexane (25–33 ns)[175] At pH 2.0, the kinetics at 510 nm for the emission of A showed a growth kinetics with a lifetime 1.0 ± 0.2 ns followed by a decay with a lifetime of 24.6 ± 0.1 ns (Figure 2.10 and Table 2.2). The growth corresponds to the adiabatic deprotonation of excited state of AH^+ to form excited state of A, which decays with the same lifetime as excited A at the higher pH. The absolute values for the pre-exponential factors for these lifetimes at pH 2 were the same (≈ 0.50, Table 2.2), supporting the assignment of lifetimes. The equal pre-exponential factors indicated that all the excited states of A were formed from AH^+, as would be expected at a pH where the fluorophore is in the protonated form.

In the presence of 16 μM CB[7] at pH 2.0, where all AH^+ is bound, the fluorescence decay could only be measured at 410 nm because AH^+ is stabilized in the complex and is the predominant species in the system. The decay was mono-exponential with a lifetime of 7.6 ± 0.1 ns, which corresponds to the emission of excited state of AH^+ complexed with CB[7]. Since pH 2.0 is lower than the pK_a^{CB} and pK_a^{CB*} values, this lifetime is not limited by the deprotonation of AH^+@CB[7]. In the presence of 2.6 μM CB[7], 50% of AH^+ is bound to CB[7] and the remainder is free in water. This allowed the fluorescence kinetics to be measured at 410 nm for the emission of AH^+ and 510 nm for the emission

of excited A. The emission decay for AH^+ at 410 nm gave two lifetimes of 0.9 ± 0.1 and 7.7 ± 0.1 ns, which corresponds to the deprotonation of AH^+ in water and the emission of AH^+ in the AH^+@CB[7] complex respectively. At 510 nm, where the excited state of A emits, a growth with a 1.1 ± 0.1 ns lifetime was observed followed by a decay with a 24.5 ± 0.1 ns lifetime. This kinetics is the same as that observed for AH^+ in water, and the absence of a longer-lived growth with a lifetime close to 8 ns suggested that AH^+@CB[7] did not de-protonate during the excited state lifetime of AH^+. Therefore, the intensity changes at 510 nm are diagnostic for the changes in the AH^+ concentration in water and do not have a contribution from the concentration changes for AH^+@CB[7].

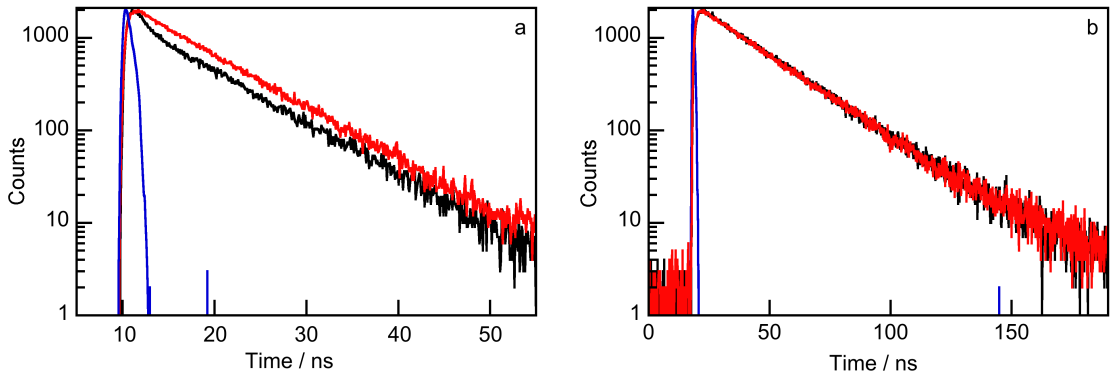

Figure 2.10. (a) Kinetics for the emission of AH^+ at 410 nm at pH 2.0 in the presence of 2.6 μM (black) and 16 μM (red) CB[7]. (b) Kinetics for the emission of A at 510 nm at pH 2.0 in the absence (black) and presence of 2.6 μM (red) CB[7]. The instrument response function is shown in blue.

Table 2.2. The fluorescence lifetimes (τ_i) and pre-exponential factors (A_i) for AH^+ at pH 2.0 in the absence and presence of different concentrations of CB[7].[a]

[CB[7]] / μM	**Emission at 510 nm ("green")**			**Emission at 410 nm ("blue")**		
	τ_1 / ns (A_1)	**τ_2 / ns (A_2)**	**χ^2**	**τ_1 / ns (A_1)**	**τ_2 / ns (A_2)**	**χ^2**
0	1.1 ± 0.1 (-0.49)	24.6 ± 0.1 (0.51)	1.18	-	-	-
2.6	1.1 ± 0.1 (-0.46)	24.5 ± 0.1 (0.54)	1.07	0.9 ± 0.1 (0.59)	7.7 ± 0.1 (0.41)	0.951
16	-	-	-	7.6 ± 0.1	-	1.20

[a], the errors for the pre-exponential factors are ± 0.02.

The longest lifetime observed for the AH^+/A system in the absence and presence of CB[7] is 25 ns, and the dynamics of the excited state is much faster compared to the millisecond time scale for the formation of the AH^+@CB[7] complex (see below). Therefore, the changes in emission intensity can be seen as instantaneous when analyzing the kinetics for AH^+@CB[7] complex formation, and the excited state dynamics of AH^+ is decoupled from the dynamics for CB[7] complex formation.

2.3.5 Dynamics of complexation studied by stopped-flow

The kinetics of complexation between AH^+ and CB[7] was studied by stopped flow. Two solutions, one containing CB[7] and a second containing AH^+/A, were mixed in a 1:1 volume ratio. The concentrations stated are those for the final mixed solution. The

kinetic experiments were performed at pH 2.0 where the guest is completely protonated (AH^+), pH 5.5 where 97% of the guest present in water is A and two intermediate pH values of 3.8 and 5.0 where 61% and 9% of the guest is protonated. The signal to noise ratios for the traces decreased with an increase in pH and as a result experiments could not be performed at higher pH values than 5.5. At all pH values, mixing of the guest (AH^+/A) with CB[7] led to a decrease of the emission intensity at 510 nm (Figure 2.11) and an increase of the emission intensity at 410 nm (Figure 2.12).

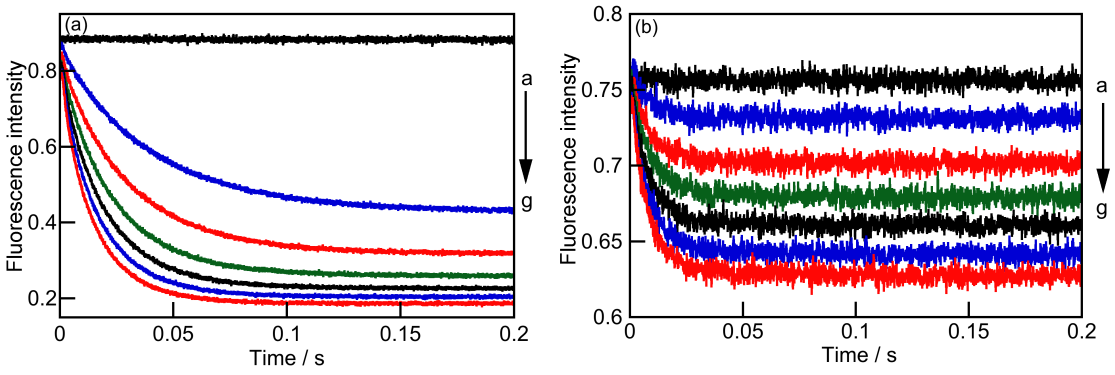

Figure 2.11. Stopped-flow traces at pH 2.0 (left) and 5.5 (right) measured for the "green" intensity change when mixing AH^+/A (1 μM) with different CB[7] concentrations: Left: 0 (a) , 3 (b), 5 (c), 7 (d), 9 (e), 11 (f) and 13 μM (g). Right: 0 (a), 5 (b), 8 (c), 11 (d), 14 (e), 17 (f), and 20 μM (g).

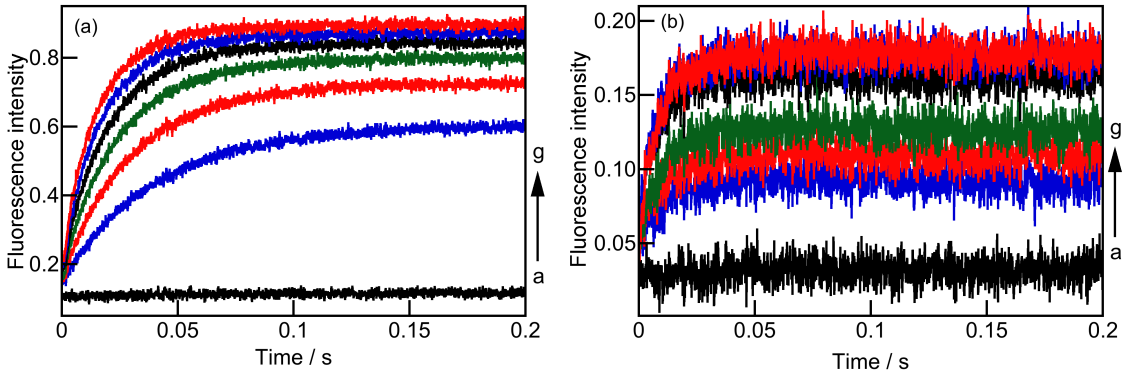

Figure 2.12. Stopped-flow traces at pH 2.0 (left) and 5.5 (right) measured for the "blue" intensity change when mixing AH^+/A (1 μM) with different CB[7] concentrations: Left: 0 (a) , 3 (b), 5 (c), 7 (d), 9 (e), 11 (f) and 13 μM (g). Right: 0 (a), 5 (b), 8 (c), 11 (d), 14 (e), 17 (f), and 20 μM (g).

It is important to note that at pH 2.0, AH^+ in the CB[7] complex does not deprotonate and the emission intensity at 510 nm corresponds to the concentration of AH^+ in water, where excited A is formed from the adiabatic deprotonation of the excited state of AH^+. The intensity increase at 410 nm corresponds to the formation of AH^+@CB[7]. At pH 5.5, the intensity at 510 nm corresponds the sum of the intensities for A in water and A@CB[7] and the emission intensity at 410 nm corresponds to the concentration of AH^+@CB[7] because, at this pH, AH^+ in water deprotonates readily. At the intermediate pH values of 3.8 and 5.0, the intensity at 510 nm corresponds to the concentrations of A in water, A@CB[7], and AH^+ in water that forms excited A adiabatically. At all pH values, the same observed rate constants were recovered from the kinetics measured at 410 and 510 nm, indicating that the kinetics are coupled, as would be expected for the relaxation kinetics of a system where the various species are in equilibrium.

2.3.5.1 Control experiments for stopped-flow

For stopped-flow experiments it is important to establish whether the kinetics is measured for a sufficiently long time for the system to reach equilibrium. This can be tested by comparing the final intensities for the stopped-flow traces and steady state emission spectra at different concentrations of CB[7]. The amplitude of the emission intensity change in the stopped-flow experiment at 0.2 s for the highest CB[7] concentration used in the kinetic experiments was normalized to the amplitude at the same CB[7] concentration in the fluorescence steady-state experiments. The normalized amplitudes from the stopped-flow experiments were the same as the amplitudes from the binding isotherm experiments at all pH values (Figure 2.13 and 2.14) indicating that equilibration was achieved within the 0.2 s time scale of the kinetic experiments. The overlap between the intensities is worse at the higher pH values because the signal-to-noise ratio is lower for the kinetic experiment.

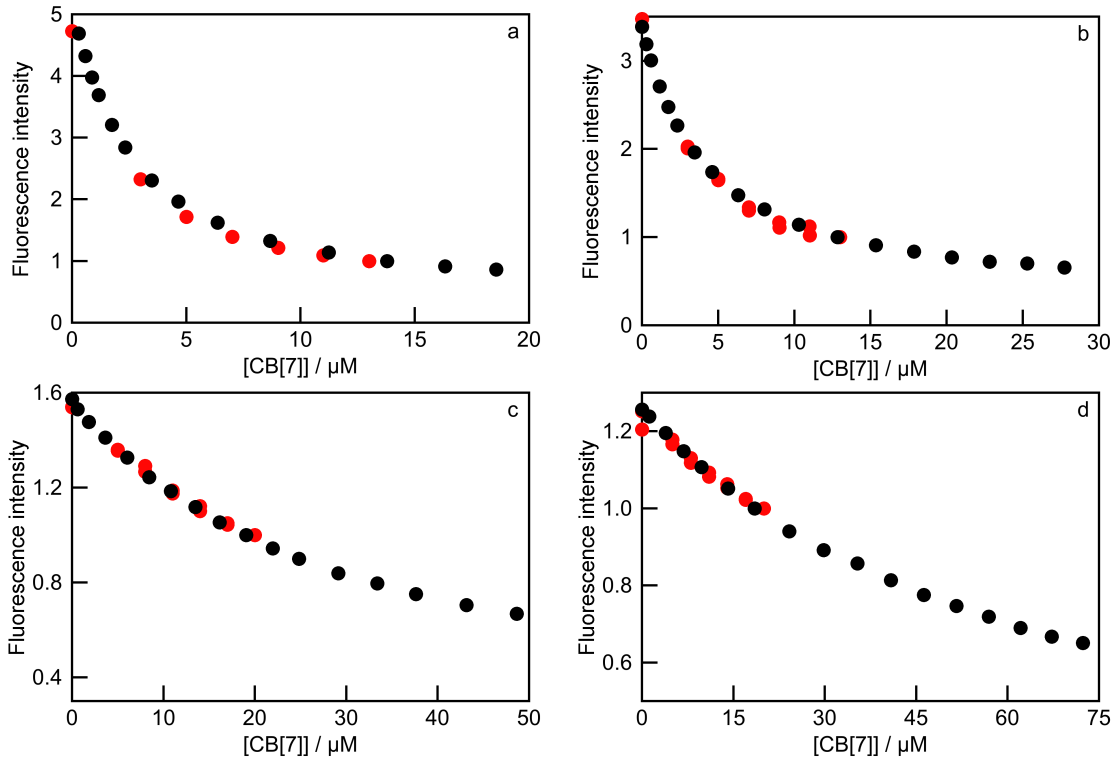

Figure 2.13. Comparison of the changes in the equilibrium "green" emission intensity for 1 μM A/AH$^+$ with CB[7] concentration obtained from the steady-state measurements (black) and stopped-flow kinetic traces (red) at pH values of 2.0 (a), 3.8 (b), 5.0 (c), and 5.5 (d).

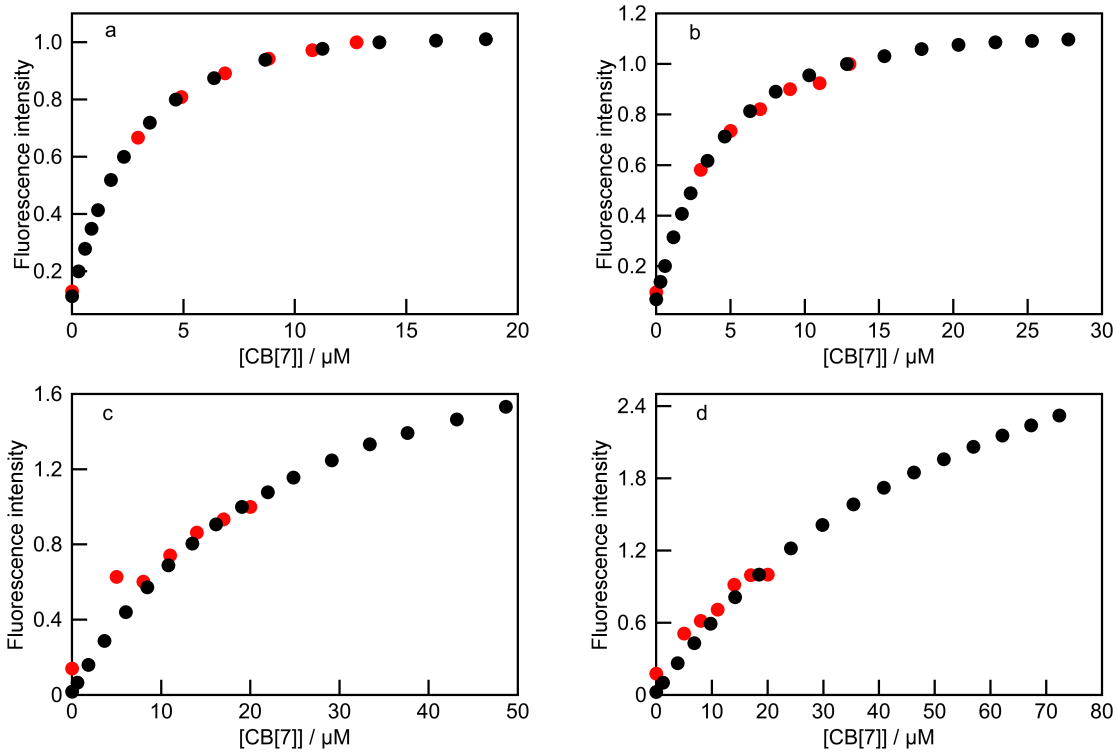

Figure 2.14. Comparison of the changes in the equilibrium "blue" emission intensity for 1 μM A/AH$^+$ with CB[7] concentration obtained from the steady-state measurements (black) and stopped-flow kinetic traces (red) at pH values of 2.0 (a), 3.8 (b), 5.0 (c), and 5.5 (d).

Experiments at pH 2.0 and 3.8 were performed in unbuffered solutions, where the pH was adjusted with the addition of HCl in the presence of 20 mM NaCl, while measurements at pH 5.0 and 5.5 required the use of sodium acetate as a buffer ([Na$^+$] = 20 mM) to adjust the pH. A control experiment was performed at pH 4.3, where samples were prepared in the presence of HCl/NaCl or acetate buffer, and the kinetics for complex formation was measured. The dependence of the observed rate constants with CB[7] was similar, with a slightly lower slope observed for the experiments performed in acetate buffer (Figure 2.15). This difference is very small and could be attributed to the variation observed between independent experiments or it could also indicate the weak

binding of acetic acid to CB[7]. However, this control experiment showed that the large differences in the dependencies of the observed rate constants with the CB[7] concentration (Figure 2.16) are not due to a counter-ion effect.

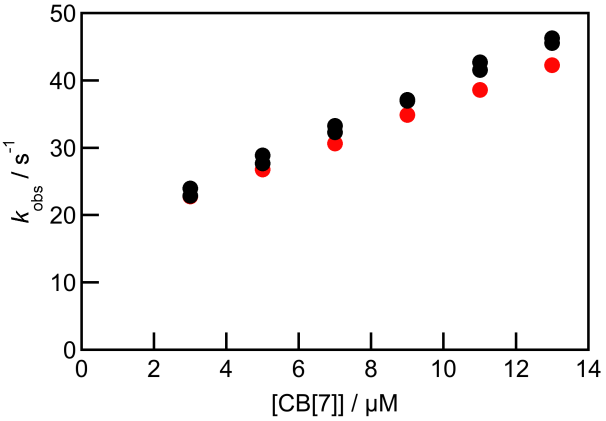

Figure 2.15. Dependence of the observed rate constant on CB[7] concentration for the complexation of AH^+/A (1 μM) for experiments performed in the presence of NaCl/HCl (black) or sodium acetate buffer (red) at pH 4.3.

2.3.5.2 Analysis of the kinetic data

The kinetics observed at different pH values were different as shown in Figure 2.16. The kinetics at pH 2.0 and 3.8 were fit to the sum of two exponentials, while the kinetics at pH 5.0 and 5.5 were mono-exponential. The relaxation kinetics for the lowest observed rate constant at pH 2.0 and 3.8 is slower than the relaxation kinetics at pH 5.5, and a steeper dependence of the observed rate constant with the CB[7] concentration was observed at the lower pH values. The errors for the measured rate constants are higher at pH 5.5 because the signal-to-noise ratio was lower, corresponding to smaller amount of CB[7] complex formed.

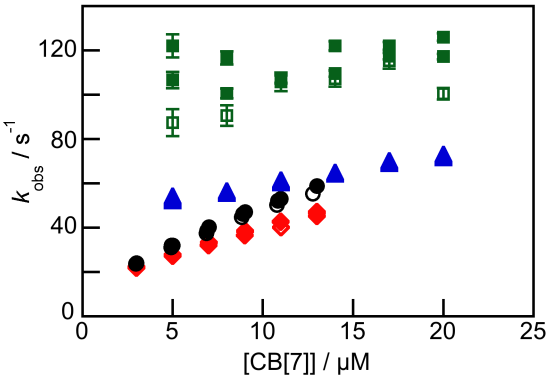

Figure 2.16. Dependence of the observed rate constant with the CB[7] concentration at different pH values (pH 2.0: ○, ●, black; pH 3.8: ♢, ◆, red; pH 5.0: Δ, ▲, blue; and pH 5.5: □, ■, green). The solid and open symbols are the values recovered for the kinetics measured for the "green" and "blue" emission, respectively. For pH values where the open symbols are not shown, they are the same as the closed symbols. The error bars are smaller than the symbols for all pH values, with the exception of pH 5.5. The observed rate constants for pH 2.0 and 3.8 correspond to the lowest values recovered from a fit of the kinetics to the sum of two exponentials. The kinetics for pH 5.0 and 5.5 were fit to a mono-exponential function.

The kinetics at pH 2.0 were fit to the sum of two exponentials, from which two observed rate constants, k_{obs1} and k_{obs2}, were obtained. The slower of these two kinetics (k_{obs2}) were similar for the kinetics measured in the "blue" and "green" region. The values for k_{obs1} were scattered probably due to the small amplitude of this component at the CB[7] concentrations used for the experiment. To improve the precision of the fits, the kinetics was fit to a mono-exponential function by starting the fit at incrementally longer delays after the start of the reaction until a constant value for k_{obs2} was obtained and the residuals were random (Figure 2.1). These k_{obs2} values were then fixed for the fit of the entire kinetic trace to recover the values for k_{obs1}.

In principle, the two relaxation times could correspond to two different processes. If k_{obs2} corresponded to the reaction of AH^+ with CB[7] leading to direct inclusion of AH^+, then the ratio of the slope of a linear dependence between k_{obs2} and the CB[7]

concentration ($3.4 \pm 0.2 \times 10^6$ M^{-1} s^{-1}, average from two kinetic studies with the emission collected in the green region and one in the blue region) and the intercept (14.6 ± 0.8 s^{-1}) should correspond to β_{11}^{AH}. However, this ratio ($(2.3 \pm 0.2) \times 10^5$ M^{-1}) is much lower than the β_{11}^{AH} value of $(4.9 \pm 0.1) \times 10^5$ M^{-1} determined from the binding isotherm studies. This analysis showed that the kinetics for the two relaxation processes are correlated.

CB[n]s are known to form exclusion complexes with ammonium groups of organic amines followed by the inclusion of the hydrophobic moiety into the cavity.[129,163] The slower kinetics observed at pH 2.0 is consistent with a mechanism where an exclusion complex, denoted AH^+•CB[7], is formed in which the positively charged guest interacts with the carbonyl groups at the portal of CB[7] without the inclusion of the anthracene moiety into the CB[7] cavity in addition to a pathway where the anthracene moiety is included directly. Inclusion of the anthracene moiety to form AH^+@CB[7] occurs either from the exclusion complex (pathway "z", Scheme 2.6) or directly ("pathway "x").

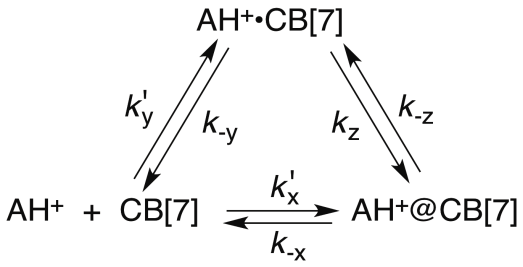

Scheme 2.6. Mechanism used to analyze the kinetic data at pH 2.0

The kinetics was analyzed using the mechanism shown in Scheme 2.6. The formation of AH^+•CB[7] was assumed to be in fast equilibrium (β_y). With this assumption, the two relaxation processes are related to the three equilibria as shown in equations 2.19 and

2.20 and the association rate constant, k'_{+}(AH) and the dissociation rate constant, k_{-}(AH) are defined[39] as in equations 2.21 and 2.22

$$k_{obs1} = k'_{y}[\mathrm{CB[7]}] + k_{-y} \quad \text{(Eq 2.19)}$$

$$k_{obs2} = \frac{k'_{+}(\mathrm{AH})[\mathrm{CB[7]}]}{1 + \beta_{y}[\mathrm{CB[7]}]} + k_{-}(\mathrm{AH}) \quad \text{(Eq 2.20)}$$

$$k'_{+}(AH) = k_{z}\beta_{y} + k'_{x} \quad \text{(Eq 2.21)}$$

$$k_{-}(AH) = k_{-x} + k_{-z} \quad \text{(Eq 2.22)}$$

Fits of the dependence of k_{obs2} with the CB[7] concentration to equation 2.20 (Figure 2.17 and Table 2.3) led to an average β_{y} value of (2.6 ± 0.6) × 10^{4} M^{-1}, k'_{+}(AH) value of (4.9 ± 0.4) × 10^{6} M^{-1} s^{-1}, and k_{-}(AH) value of 10 ± 1 s^{-1}. The ratio between k'_{+}(AH) and k_{-}(AH) is (4.9 ± 0.6) × 10^{5} M^{-1}, which is equal to the β_{11}^{AH} value ((4.9 ± 0.1) × 10^{5} M^{-1}) determined from the binding isotherm. The equality of these values suggests that the mechanism proposed is consistent with the kinetic and the binding isotherm data.

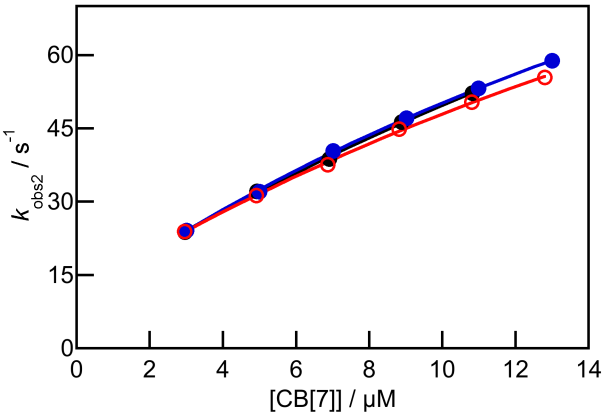

Figure 2.17. Fits to equation 2.20 for the dependence of k_{obs2} with CB[7] concentration obtained from two sets of experiments performed in the "green" region (black and blue) and one set of experiment performed in the "blue" region (red) at pH 2.0.

Table 2.3. Results from the fits shown in Figure 2.17 for the k_{obs2} dependence with the CB[7] concentration at pH 2.0.

Emission	k'_{+}**(AH) / 10^{6} M^{-1} s^{-1}**	k_{-}**(AH) / s^{-1}**	β_y **/ 10^{4} M^{-1}**
Green (expt 1)	5.4 ± 0.3	9.2 ± 0.9	3.2 ± 0.5
Green (expt 2)	4.7 ± 0.6	11 ± 2	2 ± 1
Blue	4.7 ± 0.5	11 ± 1	2.7 ± 0.8

The k_{obs1} values increased with the CB[7] concentration; however, the data had large errors and showed significant scatter as shown in Figure 2.18. Due to these reasons the fitting of the data was not possible. The value of k_{-y} is estimated to be between 100 and 130 s^{-1}, which is ten times higher than the rate constant for the exit of AH^{+} from the

inclusion complex (k_{-}(AH) = 10 s^{-1}), supporting the assumption that the formation of the exclusion complex occurs as a fast equilibrium. The value for k_y estimated from the β_y and k_{-y} values is between 2.7×10^6 and 3.5×10^6 M^{-1} s^{-1}, which would lead to an increment for the k_{obs1} value of ca. 30 s^{-1} for an increase in 10 μM of the CB[7] concentration. This increment is within the scatter observed for the experimental data.

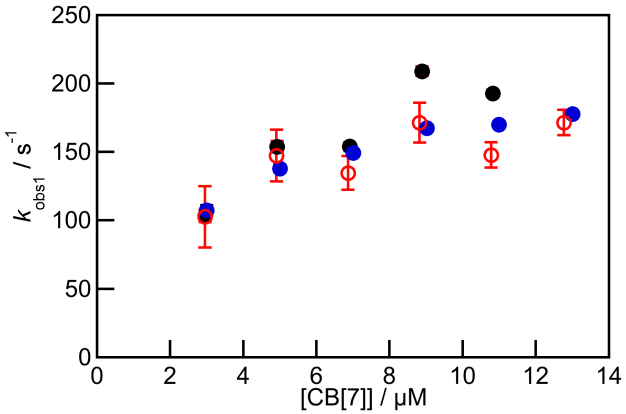

Figure 2.18. Dependence of k_{obs1} with CB[7] concentration at pH 2.0 recovered from the fits of the stopped-flow traces to the sum of two exponentials by fixing k_{obs2} to the value obtained from the systematic fits. The data points correspond to the experiments performed in the "green" (black, blue) and "blue" region (red).

At pH 5.5, deprotonated A is the predominant species in water (97%). The ground state pK_a of AH^+@CB[7] being higher than the pH of the solution, the hydronium ion concentration is sufficiently high to protonate the A@CB[7] complex and form AH^+@CB[7]. The mechanism includes the fast equilibration between A and CB[7] followed by slow protonation and deprotonation steps (Scheme 2.7). Deprotonation of AH^+@CB[7] and exit of AH^+ from AH^+@CB[7] are competitive, and the latter reaction needs to be accounted for in the fit of the data.

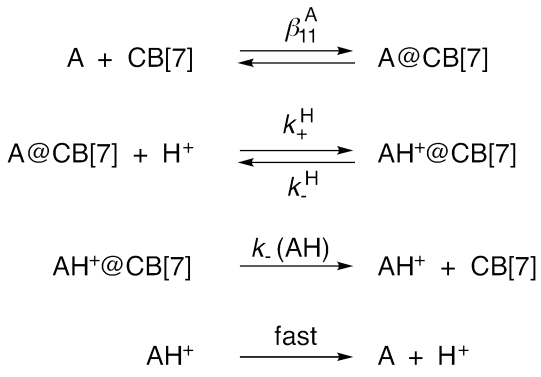

Scheme 2.7. Mechanism used to analyze the kinetic data at pH 5.5.

The data at pH 5.5 were analyzed using a global analysis method (Scheme 2.8), where the kinetics at all CB[7] concentrations for two independent experiments collected for the "green" emission were analyzed simultaneously. The data from the kinetics in the "blue" region were not used because of the poor signal-to-noise ratio. The value for the equilibrium constant for A@CB[7] was fixed as 390 M^{-1}, and this equilibrium was assumed to be fast. Assuming that the association rate constant of A with CB[7] will be at least as high as the overall association rate constant for AH^+ of 4.9×10^6 M^{-1} s^{-1}, then the dissociation rate constant for A from A@CB[7] will be at least 1.3×10^4 s^{-1}, which is ten times faster than the time resolution of the stopped-flow experiment. This calculation is consistent with the assumption of a fast equilibrium for A@CB[7]. The dissociation of AH^+@CB[7] needs to be included in the model because the value for the rate constant of this process (10 s^{-1}) corresponds to 10% of the observed rate constant. This value was also fixed in the model. The protonation and deprotonation reaction for A/AH^+ in water is faster than the time resolution of the experiment, and the concentration of hydronium ion is constant as the solution was buffered. For this reason, the deprotonation reaction for AH^+ in water is not included in the model used for fitting the kinetics.

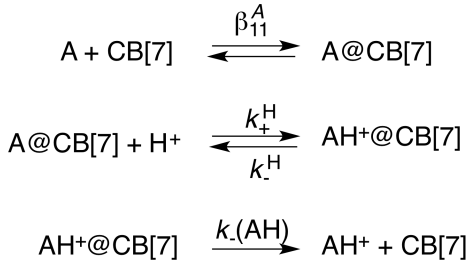

Scheme 2.8. Model used for the global analysis of the kinetic data measured at pH 5.5 for the mixing of A/AH$^+$ with CB[7].

Global analysis of the kinetics at pH 5.5 led to the recovery of a protonation rate constant (k_+^H) of (1.5 ± 0.4) × 10^9 M^{-1} s^{-1} for A@CB[7] and a deprotonation rate constant of (k_-^H) of 89 ± 7 s^{-1} for AH$^+$@CB[7]. The pK_a^{CB} value calculated from these rate constants is 7.3 ± 0.2, which is in agreement with the reported value of 7.1 ± 0.2 determined from a pH titration experiment.[165] The residuals for the global analysis for the two individual stopped-flow experiments performed at pH 5.5 are shown in Figure 2.19.

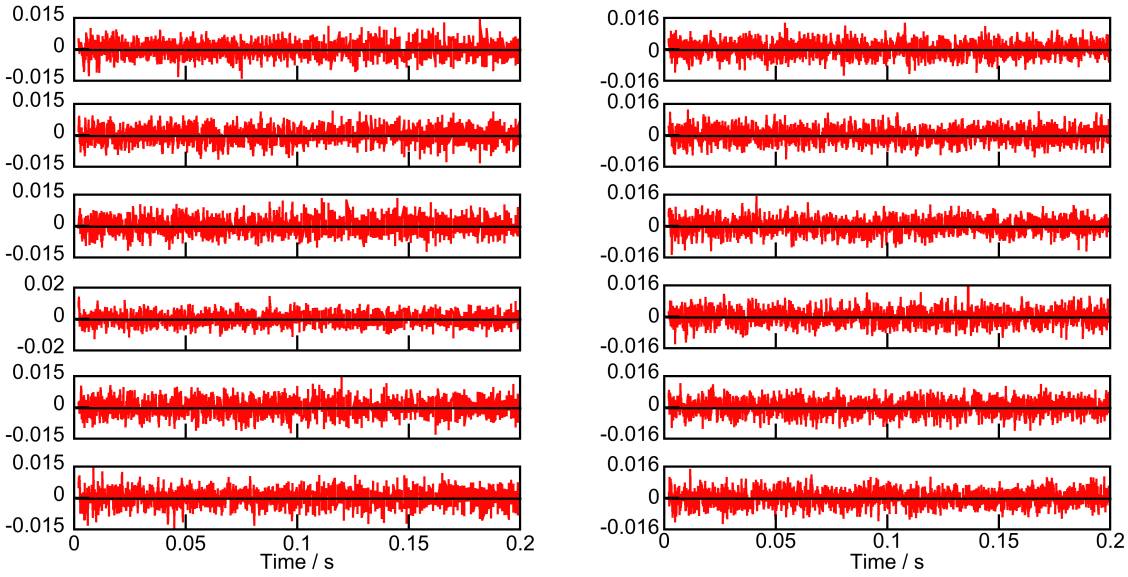

Figure 2.19. Residuals for the fits of the stopped-flow traces for the mixing of A/AH^+ with CB[7] at pH 5.5 using the global analysis model described in Scheme 2.8. The concentrations of CB[7] from the top to the bottom are: 20, 17, 14, 11, 8, and 5 μM.

A quantitative analysis of the kinetics at pH 3.8 and 5 is not feasible because the model requires the inclusion of both the low and high pH mechanisms observed for the binding of AH^+ and A. The model would include too many parameters to fit the data. However, the changes can be explained qualitatively based on the relative contributions from the formation of the exclusion complex AH^+•CB[7] and the complex with neutral A, A@CB[7]. The overall equilibrium constant for the formation of the former is 69 times higher than that for the latter. At pH 3.8, where 61% of the guest in water is in the protonated form and the remaining 39% is deprotonated, the kinetics is dominated by the binding of AH^+ with CB[7] with the observed decay did not fit to a mono-exponential function. However, the amplitude of the fast component is smaller at pH 3.8 than at pH 2. (Table 2.4) This difference increased from 11% for a CB[7] concentration of 5 μM to 32% for a CB[7] concentration of 13 μM. This increase is expected because the

formation of A@CB[7] will be more prominent at the higher CB[7] concentration. The formation of A@CB[7] is followed by immediate protonation of the complex (~2.4×10^5 s^{-1}) because of the high hydronium ion concentration at this pH. This reaction path leads to a decrease of the contribution from AH^+@CB[7] formation through the exclusion complex. This effect is observed as a decrease in the slope for the dependence of k_{obs2} with the CB[7] concentration without a large change in the intercept.

Table 2.4. Pre-exponential factors for k_{obs1} at pH 2.0 and 3.8 from the fits of the kinetic traces to the sum of two exponentials by fixing k_{obs2}, and the difference between the two values.

[CB[7]] / μM	**Pre-exponential factors**		**% difference**
	pH 2.0	**pH 3.8**	
3	0.057	0.059	- 3.4%
5	0.093	0.083	11%
7	0.118	0.095	20%
9	0.154	0.117	24%
11	0.185	0.139	25%
13	0.240	0.163	32%

The kinetics at pH 5 was adequately fit to a mono-exponential function. In water, 9% of the guest is in the form of AH^+ while 91% corresponds to A. The kinetics is dominated by the binding of A, but a slow down was observed for the kinetics when compared with the kinetics at pH 5.5. This slow down was caused by the formation of the AH^+•CB[7] exclusion complex that removes A and free CB[7] from solution. The lower free concentrations of A and CB[7] decrease the amount of AH^+@CB[7] formed through the faster reaction pathway, which is the protonation of the A@CB[7] complex. The binding dynamics of AH^+ and A with CB[7] at any pH can be defined by Scheme 2.9

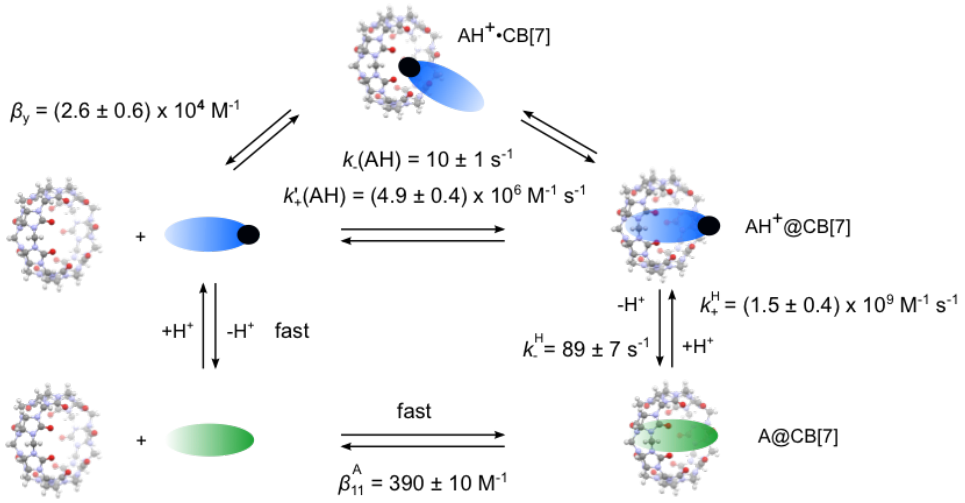

Scheme 2.9. Binding dynamics of AH^+ and A with CB[7], and rate constants for the protonation of A@CB[7] and deprotonation of AH^+@CB[7]. The kinetics for the binding of AH^+ occurs through two pathways, and the association and dissociation rate constants are those for the combined pathways.

2.3.6 Equilibrium and rate constants from "apparent" values

The equilibrium constant K_{AH} was calculated to be $(2.3 \pm 0.3) \times 10^6$ M^{-1} (Eq 2.23) using the previously determined values of 130 ± 10 M^{-1} and 21 ± 2 M^{-1} for the binding of

the first and second Na^+ cation to CB[7],[136] and the average β_{11} value of $(4.9 \pm 0.1) \times 10^5$ M^{-1}. The same multiplication factor was used to calculate the value of the association rate constant ($k_+(AH)$) as $(2.3 \pm 0.2) \times 10^7$ $M^{-1}s^{-1}$ from the overall association rate constant $k'_+(AH)$. It is important to note that the latter value includes the pathway for the formation of the exclusion complex.

$$K_{AH} = \beta_{11}(1 + K_{01}[Na] + K_{01}K_{02}[Na]^2) \quad \text{(Eq 2.23)}$$

2.4 Discussion

The complexation dynamics of AH^+ with CB[7] can be compared to previously studied guests. 2-Naphthyl-1-ethylammonium (Scheme 2.10) has the positively charged ammonium group at the end of the molecule separated from the aromatic ring by one carbon. Berberine on the other hand has a positive charge on the nitrogen centrally located in the molecule (Scheme 2.10). In the case of both these molecules only one relaxation kinetics was observed in the stopped-flow experiments without the formation of an exclusion complex.

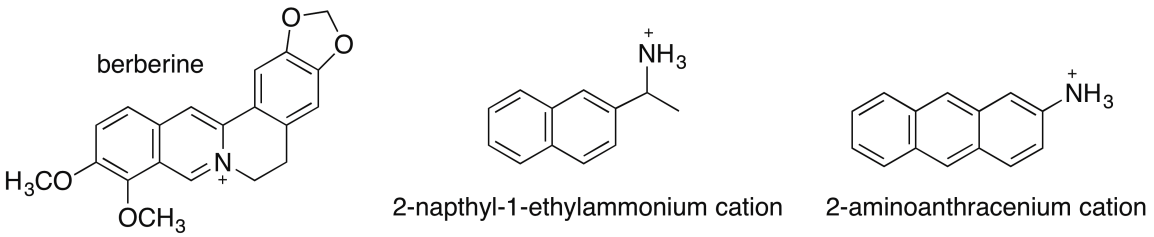

2-napthyl-1-ethylammonium cation

2-aminoanthracenium cation

berberine	2-napthyl-1-ethylammonium cation	2-aminoanthracenium cation
$K = 2.4 \times 10^7$ M^{-1}	$K = 1.1 \times 10^7$ M^{-1}	$K = 2.3 \times 10^6$ M^{-1}
$k_+ = 1.9 \times 10^7$ M^{-1} s^{-1}	$k_+ = 6.3 \times 10^8$ M^{-1} s^{-1}	$k_+ = 2.3 \times 10^7$ M^{-1} s^{-1}
$k_- = 0.81$ s^{-1}	$k_- = 55$ s^{-1}	$k_- = 10$ s^{-1}

Scheme 2.10. Structure, equilibrium constants and association and dissociation rate constants for the binding of berberine,[176] 2-naphthyl-1-ethylammonium cation[136] and AH^+ with CB[7]. The values for K and k_+ for AH^+@CB[7] were calculated from the overall values.

A comparison of the binding properties of the three guests to CB[7] (Scheme 2.10) shows that the position of the positive charge on the guest and the size of the hydrophobic moiety have a significant effect on the binding dynamics. Depending upon the orientation of the molecule while approaching CB[7], either an exclusion or an inclusion complex can be formed. In the case of AH^+, if the anthracene moiety approaches the CB[7] portal an inclusion complex is formed whereas the approach of the amino group at the portals of CB[7] leads to an exclusion complex. The hydrophobic moiety of 2-naphthyl-1-ethylammonium cation is smaller compared to AH^+ and in this case once the exclusion complex is formed the smaller naphthyl group can rotate and enter the cavity. For such instances, the rate constant of inclusion (k_z in Scheme 2.6) is higher than the dissociation of the exclusion complex (k_{-y}), the association rate constant is high, and the exclusion complex is not detected as a defined intermediate. The association rate constant for AH^+ is approximately 25 times lower than that of the 2-naphthyl-1-ethylammonium cation and this is explained by the formation of an exclusion complex. Here, the dissociation of the exclusion complex is competitive with the inclusion by rotation of the anthracene moiety

into the CB[7] cavity. The dissociation rate constant is a factor of ~5 lower for AH^+ than for the 2-naphthyl-1-ethylammonium cation.

The aromatic moiety of berberine is included in the CB[7] cavity,[176] and the central location of the positive charge likely prevents the formation of an exclusion complex. The complexation of berberine to CB[7] was shown to occur through constrictive binding, where the CB[7] portals needs to be distorted for inclusion of the guest to occur. This stereochemical effect led to lower association and dissociation rate constants. The association rate constant for berberine and AH^+ are the same, but different mechanisms led to these values being lower than the association rate constant for the 2-naphthyl-1-ethylammonium cation. Distortion of the host is also responsible for the lower dissociation rate constant observed for berberine when compared to those for AH^+ and the 2-naphthyl-1-ethylammonium cation. These results show that the binding dynamics cannot be predicted from the values of the equilibrium constants because the mechanism for binding differs for the three guests. Berberine has an equilibrium constant similar to that for the 2-naphthyl-1-ethylammonium cation, but the association and dissociation rate constants of berberine are decreased to a similar extent because of the constricted binding mechanism. On the other hand, AH^+ has a lower equilibrium constant because of the slow down of the association process where the exclusion complex is formed, but the dissociation rate constant is affected to a lesser extent because of the absence of a constrictive binding mechanism. It is important to note that in the case of cyclohexylmethylamine binding to the smaller CB[6], the formation of an exclusion complex and constrictive binding were postulated, leading to very slow kinetics,[129,164] showing that the binding dynamics with CB[n]s can occur over very different time scales.

The role of the protonation of the guest was previously studied for the cyclohexylmethylamine/CB[6] system, where the binding dynamics of the neutral and positively charged guest was uncoupled from the protonation/deprotonation dynamics.[129,164] In the case of AH^+ and A binding to CB[7], the binding dynamics is coupled to the protonation/deprotonation reactions for the CB[7]-bound guest. In both systems, the dynamics is faster for the formation of the CB[n] complex with the neutral guest. However, in the case of AH^+/A binding to CB[7], it was possible to measure the kinetics of the system at different pH values. These studies led to the determination of the different mechanisms, where an exclusion complex is formed when AH^+ binds to CB[7], whereas for A, complexation is fast followed by protonation of the complex (Scheme 2.9).

The protonation rate constant for ammonia in water is 4.3×10^{10} M^{-1} s^{-1},[177] and this value constitutes the highest possible rate constant for the protonation of A in water, which is unknown. The protonation rate constant for A@CB[7] of 1.5×10^9 M^{-1} s^{-1} is ~30 times lower than this upper limit, suggesting that protonation of A@CB[7] is not significantly impeded, which is consistent with the location of the amino group at the portal of CB[7]. The lower value for the protonation rate constant for A@CB[7] is probably related to the fact that the approach of the hydronium ion towards the sides of CB[7] or the portal that does not contain the amino group led to unproductive encounter complexes. In this respect, the protonation rate constant for a guest were the acid/base group was exposed to the water phase while a portion of the guest was bound to CB[7] was the same as for the guest in water,[178] probably because the attack of the hydronium ion was not impeded. The deprotonation rate constant of AH^+@CB[7] is higher (89 s^{-1})

than the rate constant for the exit of AH^+ from AH^+@CB[7] (10 s^{-1}). However, the deprotonation reaction is not observable at low pH values because the protonation process is too fast. For example, at pH 2.0, the protonation process for A@CB[7] has a pseudo-first order rate constant of 1.5×10^7 s^{-1}.

2.5 Conclusions

In conclusion, the studies on the binding dynamics of AH^+ and A with CB[7] provided further evidence that different mechanisms occur for the binding of guests with CB[n]s. The binding dynamics of a neutral guest was shown to be faster than that for the corresponding positively charged guest. However, the binding constant is higher for the charged guest than for the neutral guest, mainly because of the charge-dipole interaction between the guest and the carbonyl groups at the portal of CB[n]. The size of the guest and the position of the positive charge on the guest affect the type of mechanism for the binding dynamics and affect the magnitude of the association and dissociation rate constants. Positive charges located at one end of the guest are more likely to lead to the formation of exclusion complexes when compared with molecules with centrally located positive charges. In addition, the requirement for distortion of CB[n] to accommodate the guest can lead to a significant slow down of the dynamics, but has a much smaller effect on the equilibrium constant as the required distortions of the host will occur for both the association and dissociation processes.

The coupling of the binding dynamics of A@CB[7] and AH^+@CB[7] to the deprotonation and protonation reactions of these complexes made it possible to measure the protonation and deprotonation rate constants. The determination of these rate

constants showed that the pK_a shift observed for the CB[7] bound guest was due mainly to a decrease of the deprotonation rate constant because of the stabilization of the charged species. This result has direct implications on the use of CB[n]s in any application, such as in catalysis, where the lifetime of a charged species is important.

3 Switch In The Guest Binding Mechanism With Cucurbit[7]uril With Sodium Ion As A Non-innocent Competitor

3.1 Introduction

3.1.1 Cation binding to cucurbit[n]urils

The presence of cations are known to affect the binding of the guest molecules to cucurbit[n]urils (CB[n]s).[124,125,129,130] The affinity of CB[n] portals to cations is responsible for this effect. It was shown by several research groups that the CB[n]s can bind to one or two cations at the portals.[121-123] However, the effect of the cations on the binding dynamics of the guest molecule with CB[n]s is not well understood. The guest molecule can bind to CB[n] that is free in water and CB[n]s bound to one sodium ion. The binding of the guest molecule to different CB[n] species present in the solution depends on several factors such as the binding affinity and the structure of the guest molecules included. In general the presence of cations in the system are shown to decrease the binding constant of the guest molecule to CB[n]s.[124,125,127,128] This decrease in binding constant is due to the competitive binding of the cations to CB[n]s which leads to less availability of free CB[7] in the solution for the guest molecule to bind. In the case of binding of very small molecules like THF and benzene to CB[6], the presence of cations in the solution was found to have an opposite effect compared to the general trend

explained above. The binding constants of these small molecules were found to increase in the presence of cations and this is due to the cations acting as a "lid" to the CB[6] portals preventing the escape of the small molecules from the CB[6] cavity.[109,179] CB[n]s are potential candidates for drug delivery systems.[99-102] If CB[n]s are to be used for such applications the understanding of the binding dynamics of the drug molecules in the presence of cations is essential due to the presence of high concentrations of different cations in the body fluids.

3.1.2 Objectives

The binding of 2-naphthyl-1-ethylammonium cation (NpH^+) to CB[7] was studied by Bohne's group previously.[136] Experiments performed at various concentrations of sodium ions revealed that NpH^+ binds only to CB[7] free in solution and not to CB[7] bound to one sodium ion. The objective of the current project is to determine the binding dynamics of a molecule with potentially two different binding sites to CB[7] in the presence of sodium ions. N-phenyl-2-naphthylamine (Ph-A-Np) was chosen as the guest molecule (Scheme 3.1). The naphthyl and phenyl groups in the molecule can bind to CB[7]. However, the binding of the naphthyl group is expected to be stronger than the phenyl group due to the larger size of the naphthyl group which efficiently fills the CB[7] cavity. For example, in the case of binding of 2-anilino-naphthalene-6-sulfonic acid to CB[7] where the phenyl group binds to CB[7], the binding constant was reported[180] to be 600 M^{-1} whereas for 2-naphthylamine where the naphthalene moiety is included in the CB[7] cavity was shown to have a binding constant of 3632 M^{-1}.[181] At higher concentrations of CB[7] a 2:1 host-guest complex could also be formed for Ph-A-Np where both the

naphthyl and the phenyl groups are bound to two different CB[7] molecules. The effect of sodium ions on the binding dynamics of the 1:1 complex and the 2:1 host-guest complex formed between Ph-A-Np and CB[7] was investigated.

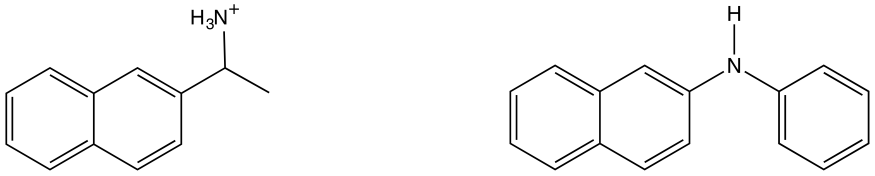

Scheme 3.1. Chemical structures of 2-naphthyl-1-ethylammonium cation (NpH^+, left) and N-phenyl-2-naphthylamine (Ph-A-Np, right).

3.2 Experimental section

3.2.1 Materials

N-phenyl-2-naphthylamine (Aldrich, 97%) was recrystallized once from ethanol. Methanol (Fisher Chemicals, spectral grade, ≥99.9%), sodium chloride (Sigma-Aldrich, BioXtra, ≥99.5%) and standardized volumetric solution of hydrochloric acid (4.0 N, Anachemia) were used as received. Cucurbit[7]uril was synthesized using a modified procedure based on previous literature[169-171] and purified according to the procedure explained in section 2.2.7 of chapter 2. Deionized water (Barnstead NANOpure deionizing systems ≥17.8 MΩ cm) was used to prepare all aqueous solutions.

3.2.2 Sample preparation

A 700 μM stock solution of Ph-A-Np was prepared in methanol. Appropriate amounts of sodium chloride were dissolved in water containing hydrochloric acid to make aqueous solutions of required pH and sodium chloride concentrations. Stock solutions of CB[7] (≈ 1 mM) were prepared by dissolving the solid in aqueous solutions

of required sodium chloride concentration and pH. The CB[7] stock solutions were titrated with cobaltacene solution to determine the actual concentration of the stock solution as explained in section 2.2.9 of chapter 2. For the steady-state fluorescence and lifetime experiments, 3 mL of the aqueous solution containing the required concentration of sodium chloride at pH 1.8 was taken in a cell and appropriate quantity of Ph-A-Np stock solution was injected into the solution in the cell using a gas tight syringe to achieve a final Ph-A-Np concentration of 0.5 μM. Small volumes of CB[7] stock solution were then injected into the cell. For the stopped-flow experiments several solutions of different CB[7] concentrations were prepared by diluting the stock solution in the aqueous solutions of required sodium ion concentration at pH 1.8. Control solutions contained all the chemicals except the fluorophore.

3.2.3 Equipment

Ground state absorption measurements were performed on a Cary 100 spectrophotometer. Steady-state fluorescence measurements were performed on a PTI QM-40 fluorimeter. For the fluorescence emission measurements the samples were excited at 303 nm and the emission was collected between 360-560 nm. The excitation and emission monochromator bandwidths were 2 nm. The sample temperature was maintained at 20 ºC throughout the experiment. The emission spectrum of a control solution containing all the solutions except the fluorophore was subtracted from the sample.

Binding dynamics studies were performed on an Applied Photophysics SX 20 stopped-flow system. The samples were excited at 303 nm using a Hg-Xe vapor lamp.

The excitation monochromator bandwidth was set to 2.3 nm and the emission was collected using a cut-off filter that transmits light above 395 nm. The sample solutions were maintained at a temperature of 20 ºC for 5 min before an experiment was performed. The sample solutions were mixed in a 1:1 volume ratio in the mixing chamber. A minimum of 20 stopped-flow traces were averaged for an experiment to obtain a good signal to noise ratio. The stopped-flow traces for the samples were corrected by subtracting the intensity of a solution containing all the components except Ph-A-Np.

Time-resolved fluorescence lifetime measurements were recorded on an Edinburgh Instruments OB920 single photon counting system. The samples were excited using a 310 nm LED light source. The emission was collected at 438 nm using a monochromator with a 16 nm bandwidth. The number of counts in the maximum intensity channel was 2000. The instrument response function (IRF) was recorded with a light scattering solution of Ludox by recording the emission at the excitation wavelength.

3.2.4 Analysis of fluorescence lifetime data

The fluorescence decay traces were analyzed using FAST software from Edinburgh Instruments. The decay traces were fit by reconvoluting the IRF with the calculated function and comparing it to experimental traces. The fit was considered good if the residuals between the calculated and experimental data were random and the χ^2 values obtained from the fits were close to unity (0.9-1.2).[55] Depending upon the number of species with different lifetimes (τ_i) contributing to the decay, the decay was fit to a mono-exponential function or sum of exponentials as per equation 3.1, where A_i is the

corresponding pre-exponential factor for each lifetime. Due to the presence of very close lifetimes in the decays all the lifetimes were fixed during the fitting procedure for the determination of the A values. In order to obtain reliable lifetimes to be fixed in the fits, the lifetimes from different decays were compared and the lifetime for a specific species was chosen to be fixed for the value recovered from experimental conditions where the A value was highest.

$$I(t) = I_0 \sum_{1}^{i} A_i \; e^{-t/\tau_i} \qquad \text{(Eq 3.1)}$$

3.2.5 Analysis of stopped-flow data

The averaged kinetic traces from the stopped-flow experiments were analyzed by fitting them to the sum of exponential functions (Eq 3.2). The exponential terms in the equation give the observed rate constants (k_{obsi}) for the relaxation processes in the system. The a_i values are the pre-exponential factors whose sum adds up to the amplitude of the kinetic traces and a_0 is the final intensity of the kinetic traces.

$$\Delta I = a_0 + a_1 e^{-k_{obs1}\, t} + a_2 e^{-k_{obs2}\, t} \qquad \text{(Eq 3.2)}$$

The kinetic traces for the experiments performed at 2, 4 and 5 mM sodium ion concentrations were analyzed using Scientist 3 software from Micromath. During the data analysis on Scientist, the sum of the pre-exponential factors was fixed to the amplitude of the stopped-flow trace analyzed. The rate constant closer to the time resolution of the equipment was fixed to 1000 s^{-1} during the fitting process. Stopped-flow fits for the data

for other concentrations of sodium ions were performed on the ProData Viewer software from Applied Photophysics.

3.2.6 Model used in fitting the binding isotherms to a 1:1 complex

The area under the emission spectra was integrated from 360 to 560 nm to construct the binding isotherm. The integrated intensities were then normalized by dividing all the intensities by the intensity for the spectra in the absence of CB[7]. Numerical analysis was employed to fit the binding isotherms using Scientist 3 software from Micromath. The model used for the fitting of the binding isotherms assumed a 1:1 complexation for Ph-A-Np with CB[7] and yielded an overall equilibrium binding constant (β_{11}) for the complexation process. The model was defined as follows: $[CB[7]]_T$ denotes the total concentration of CB[7] and $[G]_T$ denotes the total concentration of guest. Both $[CB[7]]_T$ and $[G]_T$ are defined as independent variables. The equilibrium concentrations of free CB[7] ($[CB[7]]_{eq}$), free guest ($[G]_{eq}$), the 1:1 complex ($[G@CB[7]]_{eq}$), and the fluorescence intensity (I) are defined as dependent variables. R corresponds to the ratio of the fluorescence intensity of the guest in the absence of CB[7] (I_0) to the total guest concentration, while C_{11} is the ratio of the emission efficiencies of the guest in the complex and in water, and β_{11} is the overall equilibrium binding constant for the 1:1 complex. R, C_{11}, and β_{11} were set as parameters.

$$\left[G@CB[7]\right]_{eq} = \beta_{11} \times [G]_{eq} \times \left[CB[7]\right]_{eq} \quad \text{(Eq 3.3)}$$

$$\left[CB[7]\right]_{eq} = \left[CB[7]\right]_{T} - \left[G@CB[7]\right]_{eq} \quad \text{(Eq 3.4)}$$

$$[G]_{eq} = [G]_T - \left[G@CB[7]\right]_{eq} \quad \text{(Eq 3.5)}$$

$$I = R \times \left([G]_{eq} + C_{11} \times \left[G@CB[7]\right]_{eq}\right) \quad \text{(Eq 3.6)}$$

where

$$R = \frac{I_0}{[G]_T} \quad \text{(Eq 3.7)}$$

The concentration constraints for the dependent variables are as follows:

$$0 < \left[CB[7]\right]_{eq} < \left[CB[7]\right]_T \quad \text{(Eq 3.8)}$$

$$0 < [G]_{eq} < [G]_T \quad \text{(Eq 3.9)}$$

$$0 < \left[G@CB[7]\right]_{eq} < [G]_T \quad \text{(Eq 3.10)}$$

3.3 Results

3.3.1 Estimation of pK_a for Ph-AH$^+$-Np in the absence and presence of CB[7]

CB[n]s are known to increase the pK_a of the guest molecule upon binding due to the better stabilization of the protonated molecule by CB[n]s.[108,116,117,165] The experiments were performed at pH 1.8 where most of the guest molecules are unprotonated in solution. This pH was chosen to ensure that the guest molecule is protonated only upon binding with CB[7] (Scheme 3.2). The protonation of the guest upon binding is fast in comparison to the kinetics measured on the stopped-flow system as shown in the case of 2-aminoanthracenium cation (AH$^+$).[156] A protonation rate constant of 1.5×10^9 M^{-1} s^{-1} was

assumed for Ph-A-Np in the presence of CB[7] as in the case of the AH^+-CB[7] system. At pH 1.8, the pseudo-first order protonation rate constant is 2.4×10^7 s^{-1} that corresponds to 0.4 μs which is faster when compared to the 1-2 ms mixing time of the stopped-flow system.

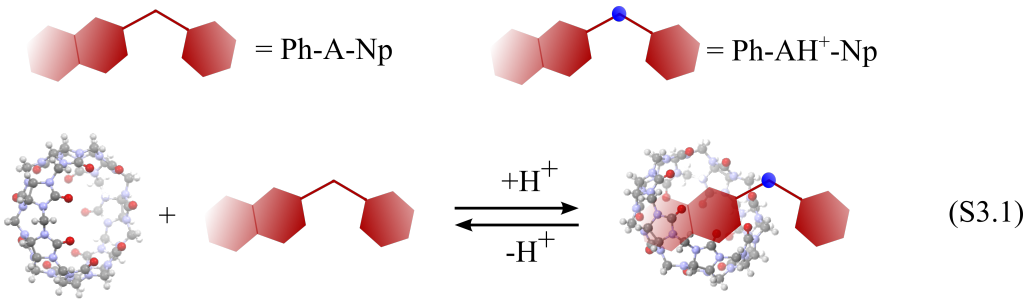

(S3.1)

Scheme 3.2. Schematic representation of the protonation of Ph-A-Np upon binding with CB[7].

The pK_a of the guest molecule in the absence and presence of CB[7] was estimated by absorption measurements. The absorption of Ph-A-Np at 300 nm decreases with the protonation of the molecule. Attaining pH below 0.5 was difficult in aqueous solutions and as a result no absorption measurements were possible below pH 0.5. A pH titration curve for 5 μM Ph-A-Np in the absence of CB[7] (Figure 3.1) showed an inflection point below pH 1. The absorbance stayed constant for pH 1.4 and higher values. This indicates that at a pH value of 1.8 the neutral form of the molecule (Ph-A-Np) is the dominant form present in the solution. In the presence of 25 μM CB[7] the inflection point shifts to between pH 2 and 3 (Figure 3.2) indicating an increase in the pK_a value of Ph-A-Np upon binding with CB[7]. This result means that at pH 1.8 where the experiments were

performed, Ph-A-Np present mostly in its neutral form in aqueous solution becomes protonated when bound to CB[7] (Scheme 3.2).

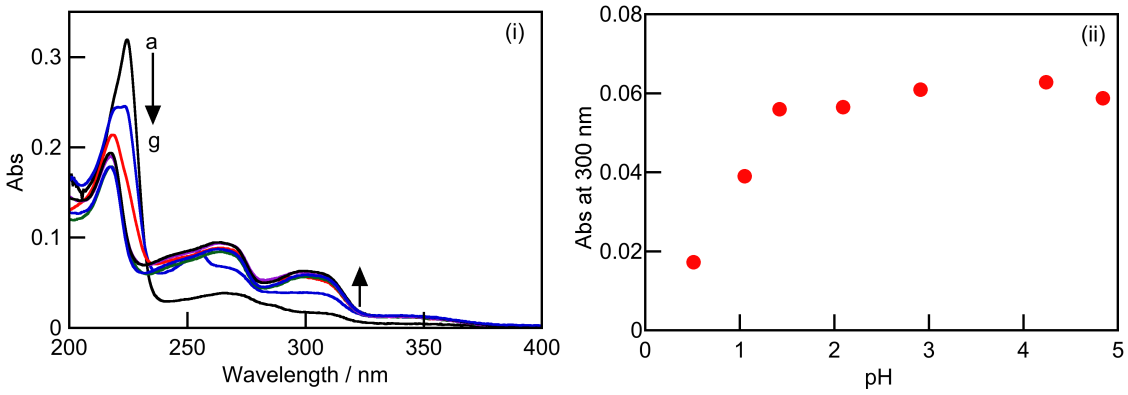

Figure 3.1. Absorption spectra for 5 μM Ph-A-Np in the absence of CB[7] (i) and the corresponding pH titration plot for the absorbance at 300 nm (ii). The pH of the solutions are 0.51 (a), 1.1 (b), 1.4 (c), 2.1 (d), 2.9 (e), 4.2 (f) and 4.8 (g).

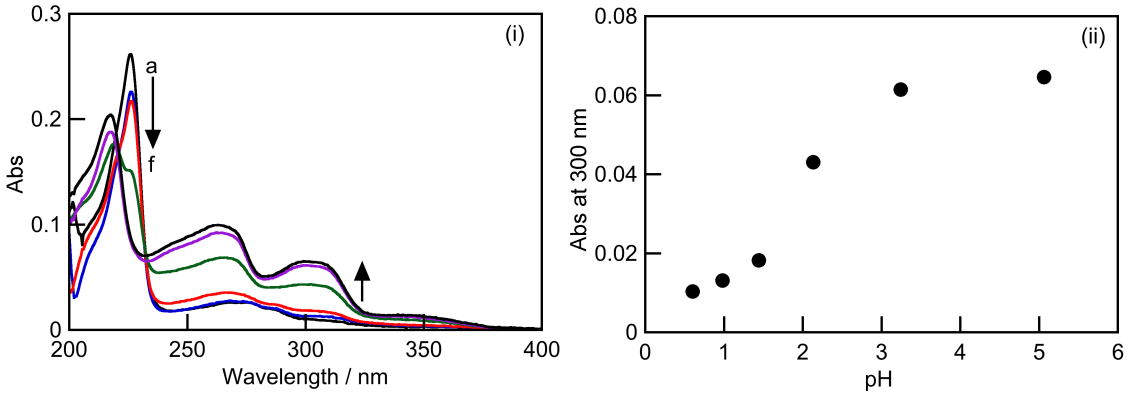

Figure 3.2. Absorption spectra for 5 μM Ph-A-Np in the presence of 25 μM CB[7] (i) and the corresponding pH titration plot for the absorbance at 300 nm (ii). The pH of the solutions are 0.60 (a), 1.0 (b), 1.4 (c), 2.1 (d), 3.2 (e), and 5.1 (f).

3.3.2 Time-resolved fluorescence emission measurements

The fluorescence lifetime experiment provides a measure of the average amount of time a molecule spends in its excited state before returning to its ground state.[53] A fluorophore can have different fluorescence lifetimes depending on the environment in which it is present. For example, AH^+ has a fluorescence lifetime of 1 ns in water which lengthens to 8 ns inside the CB[7] cavity.[156] Analysis of a fluorescence decay trace gives information about the lifetimes of different fluorescent species present in the system and the relative contribution of each of these species (A value) to the fluorescence decay. The A values are a good approximation for the amount of each of the fluorescent species present in the system.

Fluorescence lifetime measurements were used to obtain information about the excited state lifetime of the different species of Ph-A-Np formed in solution in the absence and presence of CB[7]. At pH 5.1, which is well above the pK_a of the molecule, the fluorescence decay for Ph-A-Np in water was mono-exponential and yielded a lifetime of 4.8 ns that was assigned to the excited state decay of the neutral form of the molecule. At pH 0.7, which is close to the estimated pK_a of the molecule, two lifetimes were obtained from the fit of the decay. The longer of the two lifetimes was 1.7 ns and was assigned to the emission from the neutral amine but quenched in the presence of high proton concentration. Aromatic amines are known to undergo fluorescence quenching in the presence of acids.[182,183] The shorter lifetime was less than 0.5 ns which is very close to the time resolution of the equipment and the error value associated with this lifetime was large. Due to the large error associated with this lifetime, accurate measurement of this short lifetime was not possible. This short lifetime was assigned to the emission from the

protonated molecule (Ph-AH$^+$-Np). At pH 1.8, the fluorescence decay was still mono-exponential yielding a lifetime value of 4.6 ns. The absence of a second lifetime at pH 1.8 means that there is no excited state emission from Ph-AH$^+$-Np contributing to the decay. This observation is in agreement with the result that the pK_a of Ph-AH$^+$-Np is less than 1 and at pH 1.8 the predominant species in solution is Ph-A-Np.

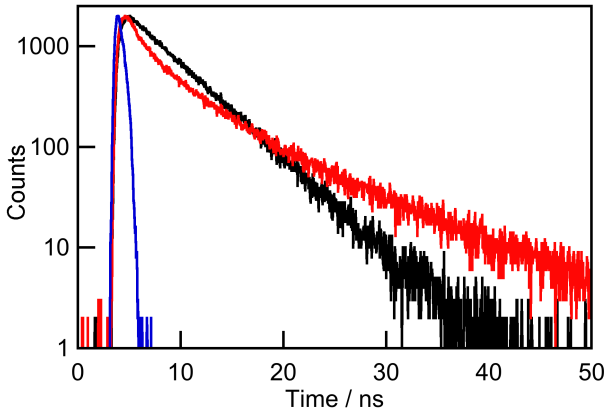

Figure 3.3. Fluorescence lifetime decays for 0.5 μM Ph-A-Np containing 2 mM sodium ion concentration at pH 1.8 in the absence (black) and presence (red) of 25 μM CB[7]. The instrument response function is shown in blue.

In the presence of CB[7], three lifetimes of 1.1, 4.6 and 11 ns were obtained from the lifetime decay (Figure 3.3). The 4.6 ns lifetime is assigned to the unbound Ph-A-Np in solution. CB[7] is shown to lengthen the excited state lifetime of the guest molecule upon complexation.[136,184] The shorter lifetime of 1.1 ns is assigned to the emission from the protonated form of the molecule where the naphthyl group is bound to CB[7] where in the absence of CB[7] this lifetime is close to the time resolution of the equipment (< 0.5 ns). The longer lifetime of approximately 11 ns corresponds to the higher order complex

of Ph-AH$^+$-Np with CB[7] where both the naphthyl and the phenyl rings are bound to two different CB[7] molecules (Scheme 3.3).

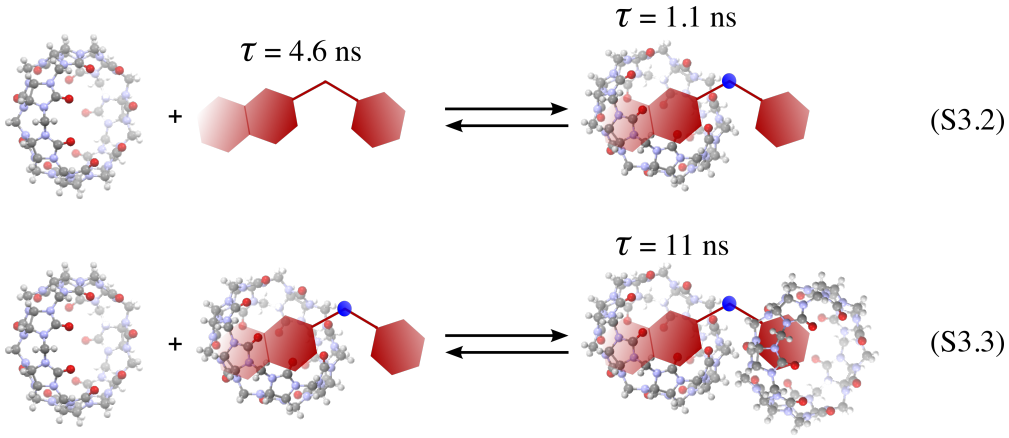

Scheme 3.3. Schematic representation for the sequential formation of 1:1 and 2:1 host-guest complex between CB[7] and Ph-A-Np.

In the presence of CB[7], the relative contributions of the three lifetimes (A values) contributing to the decay was found to depend on the sodium ion concentration in the solution. With increasing sodium ion concentration the contribution from the longer-lived lifetime corresponding to the 2:1 host-guest complex formation was found to increase. However, the absolute A values obtained from the fits were not reliable due to two reasons. Firstly, the compound was found to undergo photodegradation upon irradiation with the LED light source used in the lifetime experiments. Even during the span for the accumulation of one decay (≈ 12 min irradiation with the 310 nm LED), there was slight degradation of the molecule, which leads to inaccuracy in the determination of A values (Figure 3.4 and Table 3.1). Secondly, due to the presence of a very short lifetime and the closeness of this lifetime to the 4.6 ns lifetime for the free molecule in water all the

lifetimes were fixed during the analysis of the lifetime decays. For the decays where the contribution from the short lifetime was low, an accurate determination of the A value was not possible due to the large errors (10-30%) associated with it. Therefore, the time-resolved emission experiments were useful in a qualitative sense to compare the lifetime of the singlet excited-state lifetime of Ph-A-Np in water with the shorter lifetime for Ph-AH^+-Np in the 1:1 complex and the longer one in the 2:1 host-guest complex.

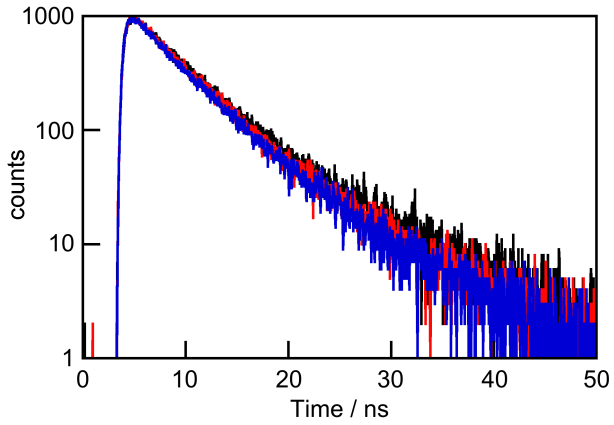

Figure 3.4. Lifetime decays for Ph-A-Np containing 50 mM Na^+ ions at 25 μM CB[7] concentration. The black, red and blue decays were recorded consecutively for the same solution until 1000 counts were reached in the maximum intensity channel.

Table 3.1. The relative contribution to the decay (A value) for different guest species obtained from the fits of the decays shown in Figure 3.4.

Decays shown in Figure 3.4	A_1 (τ_1 = 1.1 ns)	A_2 (τ_2 = 4.6 ns)	A_3 (τ_3 = 11 ns)
Black	0.01 ± 0.01	0.89 ± 0.02	0.10 ± 0.01
Red	0.07 ± 0.01	0.87 ± 0.02	0.06 ± 0.01
Blue	0.13 ± 0.01	0.82 ± 0.01	0.05 ± 0.01

3.3.3 Different CB[7] species present at different Na^+ ion concentrations

Since the singlet excited state lifetime experiments indicated that different mechanisms could be operating at low and high sodium ion concentrations, it is important to consider the relative concentrations of different CB[7] species present in the solution under different sodium ion concentrations. The relative concentrations of free CB[7] and CB[7] bound to one and two sodium ions in solution was calculated by assuming 130 and 21 M^{-1} binding constant values for the binding of one and two sodium ions to CB[7] respectively.[136] The experiments were performed at low and high sodium ion concentrations where the concentration ranged from 2 to 5 mM and 25 to 50 mM respectively. Table 3.2 shows the concentration of free CB[7], CB[7] bound to one sodium ion (CB[7]•Na^+) and CB[7] bound to two sodium ions (Na^+•CB[7]•Na^+) at different sodium ion concentrations used for the experiments. CB[7] bound to two sodium ions are not available for any binding with the guest. Free CB[7] in solution and

CB[7] bound to one sodium are the active host species available to Ph-A-Np for binding. The equilibration between CB[7] and Na^+ is much faster compared to the binding of Ph-A-Np with CB[7]. As a result, at any guest concentration, the relative concentrations of the different CB[7] species can be considered a constant.

Table 3.2. Relative concentrations of different CB[7] species present in solutions at different sodium ion concentrations.

$[Na^+]$ / mM	% $CB[7]_{free}$	% $CB[7]•Na^+$	% $Na^+•CB[7]•Na^+$
2	79	20	1
4	64	33	3
5	58	38	4
25	17	54	29
40	9	49	41
50	7	45	48

3.3.4 Experiments at low sodium ion concentrations

The time resolved fluorescence measurements indicated that the formation of the 2:1 host-guest complex is not very significant at low concentrations of sodium ions. Steady-state fluorescence and stopped-flow experiments were performed at sodium ion concentrations of 2 to 5 mM to understand the binding of Ph-A-Np to CB[7] at low sodium ion concentrations. Steady-state fluorescence measurements were performed at 2 and 4 mM sodium ion concentrations where the changes in fluorescence intensity for Ph-A-Np was monitored with the addition of CB[7]. In both these cases, there is a continuous decrease in the fluorescence intensity accompanied by a blue shift of 17 nm

for the emission maxima with increasing CB[7] concentration (Figure 3.5). This decrease in intensity is consistent with the formation of the comparatively shorter-lived 1:1 complex (Ph-AH$^+$-Np@CB[7]) in the solution. The formation of a 1:1 complex where the phenyl group is bound to CB[7] (CB[7]@Ph-AH$^+$-Np) is also possible but due to the higher binding affinity of naphthyl group to CB[7] compared to the phenyl group, at any given CB[7] concentration, the concentration of CB[7]@Ph-AH$^+$-Np complex can be assumed negligible in the solution.

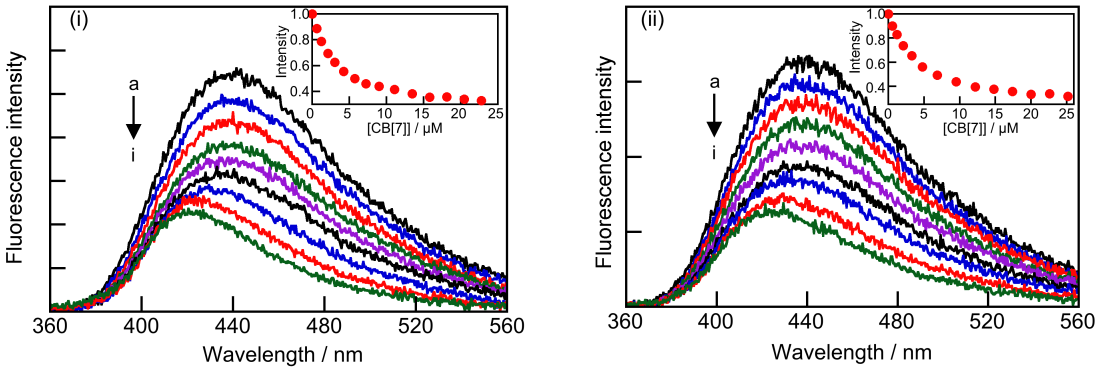

Figure 3.5. Fluorescence emission spectra for 0.5 μM Ph-A-Np in the absence (a, black) and presence (b to i) of up to 25 μM CB[7] for a solution containing 2 (i, left) and 4 mM (ii, right) sodium ions. The insets show the normalized integrated intensities for the emission spectra with CB[7] concentration.

The dependence of the emission intensities for Ph-A-Np on the CB[7] concentration in the presence of 2 and 4 mM sodium ion concentrations did fit well to a 1:1 binding model as shown in Figure 3.6. This result indicated that at lower concentrations of sodium ions there is no significant amount of 2:1 complex (CB[7]@Ph-AH$^+$-Np@CB[7]) formed in the system at least until 25 μM CB[7] concentration where the experiments

were performed. This is consistent with the lifetime data where at low concentrations of sodium ions the amount of 2:1 host-guest complex was quite small (A value < 0.025 ± 0.001). The overall equilibrium binding constants obtained from the fits were (3.6 ± 0.1) × 10^5 and (2.62 ± 0.06) × 10^5 M^{-1} for 2 and 4 mM sodium ion concentrations respectively. The decrease in the overall equilibrium binding constant from 2 to 4 mM sodium ion concentration is due to the competitive binding of sodium ions to CB[7] portals.

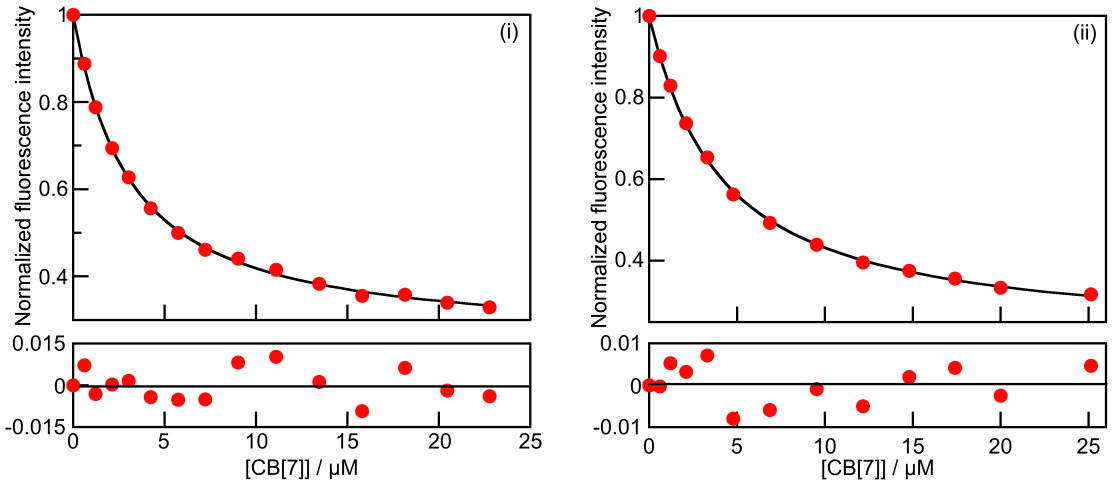

Figure 3.6. Fits for the binding isotherms to a 1:1 binding model and the corresponding residuals for 0.5 μM Ph-A-Np with CB[7] in the presence of 2 (i, left) and 4 mM (ii, right) sodium ions.

Stopped-flow experiments were performed to understand the binding dynamics of the complexation of Ph-A-Np to CB[7] at low sodium ion concentrations. At 2, 4 and 5 mM sodium ion concentrations where the stopped-flow experiments were performed, the stopped-flow traces show a fast relaxation process followed by a slower decay (Figure 3.7). Any equilibrium involving the guest which is faster than the time resolution of the

equipment appears as an offset in the initial intensity in the stopped-flow traces with increasing host concentration. The fast relaxation process in this experiment was very close to the stopped-flow time resolution and as a result along with the offset in the initial intensity this fast relaxation process is part of the decay. This fast kinetics is explained by the fast binding of phenyl ring with the CB[7] cavity. Due to the smaller size of phenyl group compared to the naphthyl group, a weak binding with CB[7] is expected that leads to a faster binding dynamics. Excluding the fast component, the stopped-flow traces follow mono exponential kinetics giving one relaxation lifetime. The slower relaxation kinetics was attributed to the inclusion of the naphthyl moiety into the CB[7] cavity forming the Ph-AH$^+$-Np@CB[7] complex.

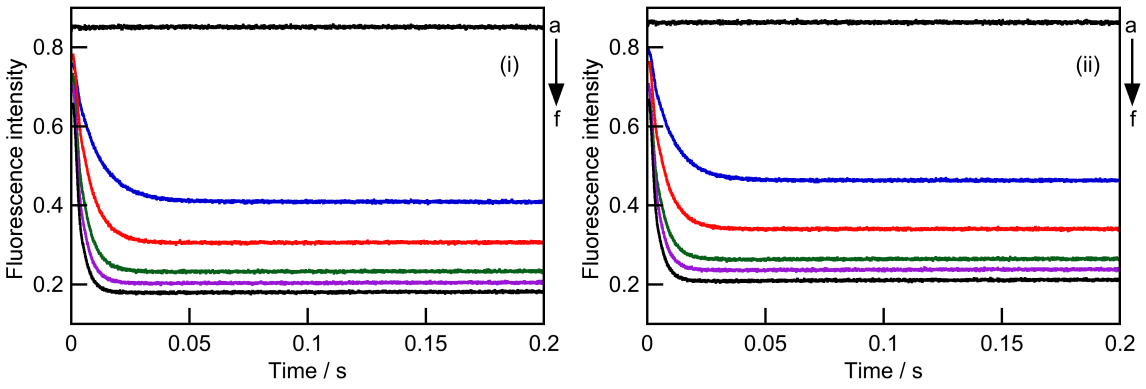

Figure 3.7. Stopped-flow traces for the mixing of 0.5 μM Ph-A-Np with 0 (a, black), 5 (b, blue), 10 (c, red), 15 (d, green), 20 (e, purple) and 25 μM (f, black) CB[7] in the presence of 2 mM (i, left) and 4 mM (ii, right) sodium ion concentration.

At low sodium ion concentrations, consistent with the steady-state fluorescence emission and lifetime data, there is no significant formation of the 2:1 host-gest complex.

The final fluorescence intensity from the stopped-flow traces at lower sodium ion concentration matches the intensity change from the fluorescence emission spectra (Figure 3.8). This shows that at lower sodium ion concentration, the kinetics was measured over a sufficiently long time period for the system to reach equilibrium and that the slow kinetics was completely captured in the stopped-flow traces.

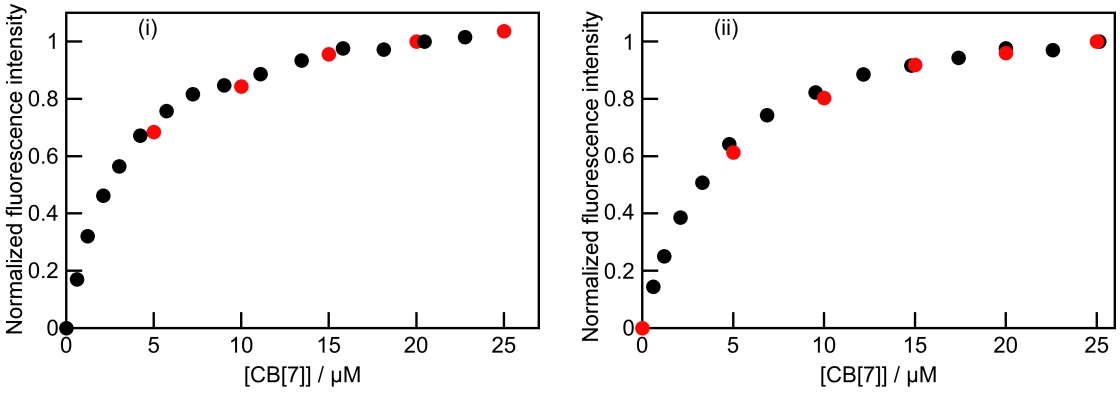

Figure 3.8. Comparison of the final fluorescence intensities from the stopped-flow traces for the mixing of Ph-A-Np with CB[7] (red) with the emission intensities from steady-state measurements (black) for the experiments conducted at 2 (i, left) and 4 mM (ii, right) sodium ion concentration. The amplitudes for both the curves were normalized at the highest CB[7] concentration.

The rate constants determined by stopped-flow measurements in the presence of sodium ions are apparent rate constants and are represented throughout this chapter by the subscript "app". The first and the second numbers on the subscripts associated with any rate constant indicates the number of sodium ions and the guest bound to CB[7] respectively. The observed rate constants for the formation of the 1:1 complex (k_{obs1}) are related to the association (k_{app}^{+}) and dissociation rate constants (k_{app}^{-}) by equation 3.11.

A plot of the observed rate constants obtained from the fits of the stopped-flow traces gives the association and dissociation rate constants for the complexation process from the slope and the intercept respectively. Figure 3.9 shows the dependence of the k_{obs1}, which corresponds to the observed rate constant for the slow relaxation process, on CB[7] concentration for sodium ion concentrations ranging from 0 to 5 mM.

$$k_{obs1} = k_{app}^{+}\left[CB[7]\right] + k_{app}^{-} \qquad \text{(Eq 3.11)}$$

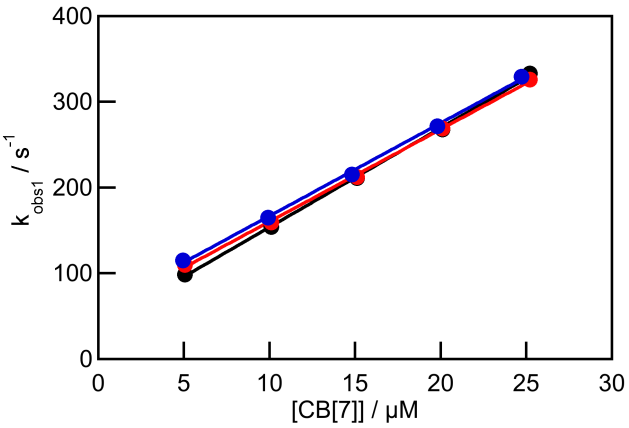

Figure 3.9. Dependence of the observed rate constants on CB[7] concentration for Ph-A-Np in the presence of 2 (black), 4 (red) and 5 mM (blue) sodium ion concentration.

The intercept for the dependence of k_{obs1} with CB[7] (k_{app}^{-}) increases linearly with increasing sodium ion concentration indicating a dissociative mechanism dependent on sodium ion concentration for the Ph-AH^{+}-Np@CB[7] complex (Figure 3.10). This increase in the dissociation rate constant means that in addition to free CB[7], Ph-A-Np binds to CB[7]•Na^{+} displacing the sodium ion from CB[7]•Na^{+}. For a mechanism where the binding of the guest happens with free CB[7] and CB[7]•Na^{+} where sodium ion is

displaced, the apparent dissociation rate constant from the kinetics experiment are related to the dissociation rate constants for the individual dissociation process (k_{11}^{-} and k_{01}^{-}) as follows (see appendix A. 1 for derivation):

$$k_{app}^{-} = k_{11}^{-}[Na^{+}] + k_{01}^{-} \qquad \text{(Eq 3.12)}$$

The values obtained for k_{11}^{-} and k_{01}^{-} for the fit of the dependence of k_{app}^{-} on sodium ion concentration were (6.9 ± 0.2) × 10^{3} M^{-1} s^{-1} and 26 ± 1 s^{-1} respectively.

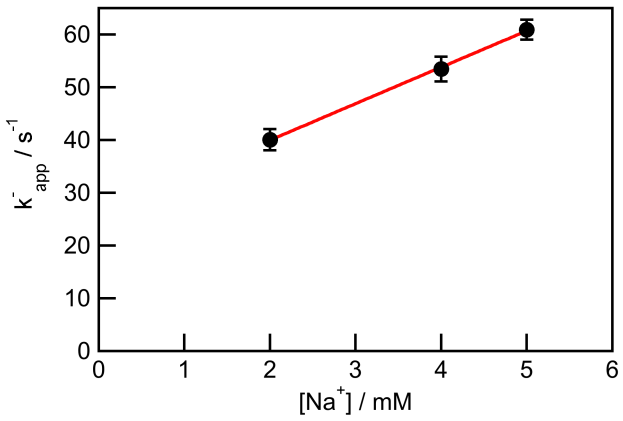

Figure 3.10. Dependence of the dissociation rate constant on the sodium ion concentration for Ph-A-Np binding with CB[7].

There is a very slight decrease in the association rate constant (k_{app}^{+}) from (1.16 ± 0.02) × 10^{7} to (1.08 ± 0.02) × 10^{7} M^{-1} s^{-1} from 2 to 5 mM sodium ion concentration and the decrease is expected due to the decrease of free CB[7] in solution with increasing sodium ion concentration. Unlike the variation in k_{app}^{-} with increasing sodium ion concentration, the changes in k_{app}^{+} are too small to accurately determine individual

values for k_{11}^{+} and k_{01}^{+}. Experiments at higher sodium ion concentrations are not feasible to obtain the individual association rate constants due to different mechanisms for binding at higher sodium ion concentrations (see below). The ratio of apparent association and dissociation rate constants obtained from the kinetic data are related to the overall equilibrium binding constant (β_{11}) as:

$$\beta_{11} = \frac{k_{app}^{+}}{k_{app}^{-}} \qquad \text{(Eq 3.13)}$$

The overall equilibrium binding constant obtained from the kinetics data at 2 and 4 mM sodium ion concentration is (3.0 ± 0.3) × 10^5 M^{-1} and (2.1 ± 0.1) × 10^5 M^{-1} respectively which are very close to the value obtained from the steady-state experiments.

Considering the results from the time-resolved and steady-state fluorescence measurements and the binding dynamics studies the mechanism shown in Scheme 3.4 is proposed for the complexation of Ph-A-Np with CB[7] at low concentrations of sodium ions when the formation of the 2:1 host-guest complex does not occur. At the maximum sodium ion concentration of 5 mM used in the above experiments, the percentage of free CB[7], CB[7]•Na^+ and Na^+•CB[7]•Na^+ are 58, 38 and 4% respectively (Table 3.2). CB[7] bound to two sodium ions is unavailable for any guest binding. The naphthyl group being a better candidate for CB[7] cavity binds with both free CB[7] and CB[7]•Na^+, displacing the sodium ion from CB[7] portal in the latter case. The binding of the phenyl group to free CB[7] is very weak and at any given CB[7] concentration the CB[7]@Ph-AH^+-Np complex is not present in the system in any appreciable quantities at equilibrium. At high CB[7] concentrations where the concentration of Ph-AH^+-

Np@CB[7] is high, the possibility of the formation of a 2:1 host-guest complex increases but this step is not prominent at least until 25 μM CB[7] concentrations where the experiments were performed.

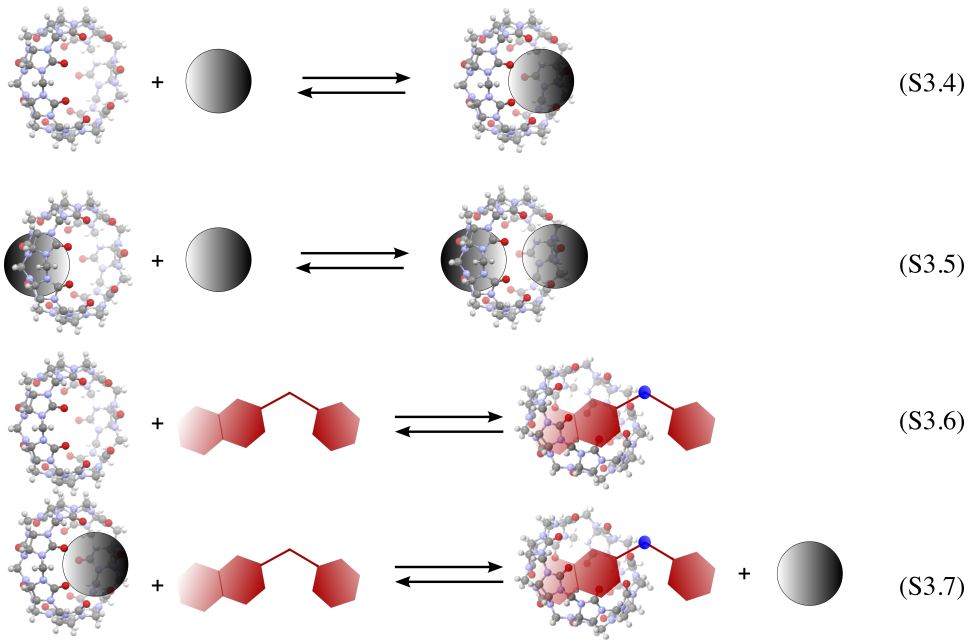

Scheme 3.4. Mechanism of complexation of Ph-A-Np to CB[7] at low sodium ion concentrations.

3.3.5 Experiments at high sodium ion concentrations

Steady-state fluorescence and stopped-flow experiments were performed at high sodium ion concentrations ranging from 25 to 50 mM to understand the mechanism of complexation of Ph-A-Np with CB[7] in the presence of high cation concentration. At 25 and 50 mM sodium ion concentration, there is an initial decrease in the fluorescence intensity with increasing CB[7] concentration followed by an intensity increase with a 12 nm blue shift in the emission spectrum when the CB[7] concentration is raised further

(Figure 3.11). The magnitude for the decrease in intensity with CB[7] concentration at high sodium ion concentration is much smaller when compared to the decrease in intensity observed at low sodium ion concentrations. The CB[7] concentrations at which the fluorescence intensity increases was found to decrease with increasing sodium ion concentration. The increase in fluorescence intensity did not saturate until 40 μM CB[7] concentration indicating a weaker binding process compared to the formation of the 1:1 complex discussed for low sodium ion experiments. An intensity increase in the fluorescence emission spectra was not observed at low sodium ion concentration which suggests that the binding process leading to this increase does not involve free CB[7]. Other than free CB[7], the active host species available for binding to Ph-A-Np is CB[7]•Na^+, which should be responsible for the binding leading to the increase in fluorescence intensity. The increase in intensity is consistent with the formation of the 2:1 host-guest complex where Ph-AH^+-Np has less mobility and has a longer excited state lifetime. The binding isotherms where the intensity decreases and then increases cannot be fit to a binding model which has only one complex, confirming the formation of an additional species in the system other than free Ph-A-Np and Ph-AH^+-Np@CB[7]. The initial decrease in fluorescence intensity is due to the formation of the 1:1 complex, however due to less availability of free CB[7] and CB[7]•Na^+ in solution at high sodium ion concentrations and the propensity to form the 2:1 host-guest complex, there is less amount of Ph-AH^+-Np@CB[7] formed in the system.

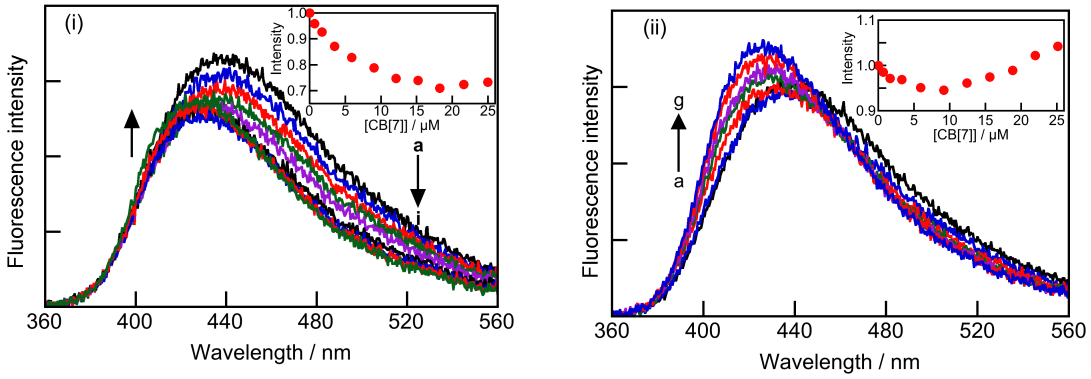

Figure 3.11. Fluorescence emission spectra for 0.5 μM Ph-A-Np in the absence (a, black) and presence (b to i in left panel and b to g in right panel) of up to 25 μM CB[7] for a solution containing 25 (i, left) and 50 mM (ii, right) sodium ions. The insets show the normalized integrated intensities for the emission spectra with CB[7] concentration.

Stopped-flow experiments at high sodium ion concentrations showed no offset in the initial intensity as seen at lower sodium ion concentrations and the kinetics leading to the decrease in fluorescence intensity is followed by a growth kinetics (Figure 3.12). The disappearance of the offset indicates that the binding of phenyl ring to CB[7] is no longer a fast dynamic process with a relaxation time close to the mixing time of the instrument. The growth kinetics became more prominent with increasing sodium ion concentrations indicating that more 2:1 host-guest complex is formed at high sodium ion concentrations (Figure 3.12). The stopped-flow traces could be fit to sum of two exponentials at higher sodium ion concentrations giving two relaxation lifetimes, one for the decay and one for the growth. The decay can be analyzed quantitatively, but the growth could not because the kinetics did not reach saturation (see below).

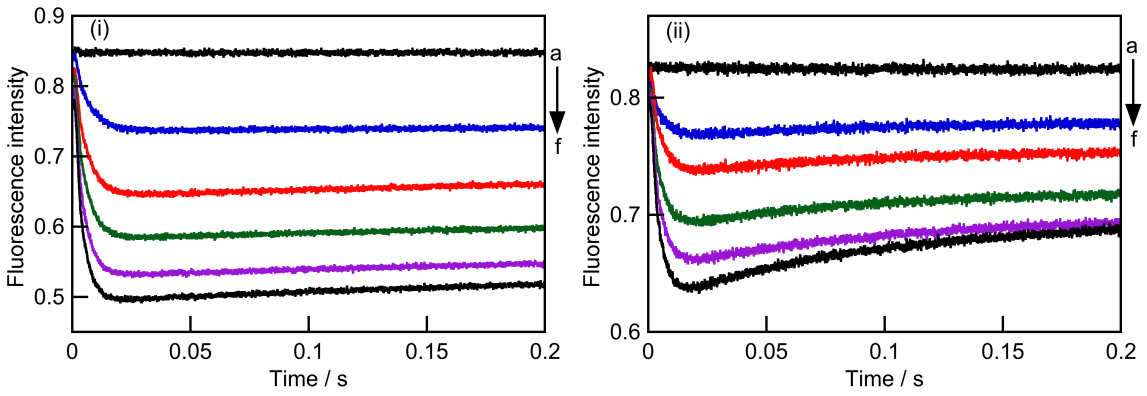

Figure 3.12. Stopped-flow traces for the mixing of 0.5 μM Ph-A-Np with 0 (a, black), 5 (b, blue), 10 (c, red), 15 (d, green), 20 (e, purple) and 25 μM (f, black) CB[7] in the presence of 25 mM (i, left) and 50 mM (ii, right) sodium ion concentration.

The observation that there is negligible formation of the 2:1 host-guest complex at lower sodium ion concentrations where the amount of CB[7]•Na^+ is minimal and the amount of the 2:1 host-guest complex formed increases at high sodium ion concentrations where the amount of CB[7]•Na^+ is very high leads to the conclusion that CB[7]•Na^+ binds to one of the two binding sites present in Ph-A-Np molecule with a higher binding constant compared to free CB[7]. Low sodium ion concentration experiments showed that naphthyl group binding to CB[7]•Na^+ leads to the displacement of sodium ions from CB[7]•Na^+ and vice-versa (step S3.7, Scheme 3.4). This result indicated that the binding of naphthyl group to CB[7]•Na^+ is weaker compared to free CB[7]. Thus the moiety that binds to CB[7]•Na^+ with higher affinity compared to free CB[7] must be the phenyl group. The disappearance of the offset in initial intensity from low to high sodium ion concentration also supports the hypothesis that the binding of the phenyl group to CB[7]•Na^+ is stronger, making the kinetics slower at high sodium ion concentrations. Thus two types of 1:1 complexes are possible, one where the naphthyl group is bound to

free CB[7] (Ph-AH$^+$-Np@CB[7]) and the other where the phenyl group is bound to CB[7]•Na$^+$ (Na$^+$•CB[7]@Ph-AH$^+$-Np). The 2:1 host-guest complex formed from these 1:1 complexes will have the naphthyl and the phenyl group bound to free CB[7] and CB[7]•Na$^+$ respectively (Na$^+$•CB[7]@Ph-AH$^+$-Np@CB[7]).

The observed rate constants corresponding to the decay kinetics (k_{obs1}) is attributed to the formation of both types of 1:1 complexes (Ph-AH$^+$-Np@CB[7] and Na$^+$•CB[7]@Ph-AH$^+$-Np). Only one relaxation kinetics will be observed if the formation of both the 1:1 complexes have similar kinetics. Figure 3.13 shows the dependence of k_{obs1} on CB[7] concentration for high sodium ion concentrations. As is the case at lower sodium ion concentration there is an increase in the dissociation rate constant indicated by the increase in intercept (Figure 3.13) with increasing sodium ion concentration which means a dissociation process dependent on sodium ion concentration. There is also a decrease in the association process with increasing sodium ion concentration indicated by the shallower slope. This decrease is due to the lesser availability of active CB[7] species for binding because of the formation of Na$^+$•CB[7]•Na$^+$.

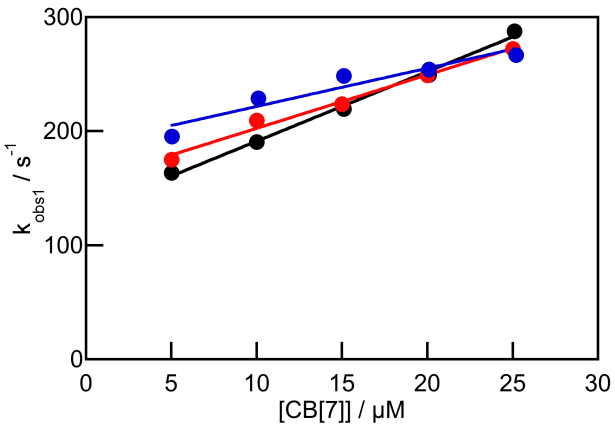

Figure 3.13. Dependence of the observed rate constants on CB[7] concentration for Ph-A-Np in the presence of 25 (black), 40 (red), and 50 mM (blue) sodium ion concentrations.

Unlike the stopped-flow traces for low sodium ion experiments the final intensity of the stopped-flow traces at high sodium ion concentrations does not match the intensity obtained from steady-state measurements. This indicates that the stopped-flow measurements were not done on a long enough time scale to capture the growth kinetics completely. The kinetics leading to the increase in fluorescence intensity can be attributed to the formation of the 2:1 host-guest complex where both the naphthyl and the phenyl groups are bound to CB[7]. Since the growth kinetics does not level off, accurate observed rate constants could not be obtained from the stopped-flow traces for k_{obs2}.

Stopped-flow experiments were performed at very high CB[7] concentrations (160-340 μM) in the presence of 25 and 50 mM sodium ion concentration to determine if a better understanding of the growth kinetics could be obtained (Figure 3.14). At these high concentrations of CB[7] the kinetics for the formation of the 1:1 complex becomes very fast and is a pre-equilibrium step in the kinetic measurements and only the kinetics for the growth is observed. The growth kinetics at 25 mM sodium ion concentration almost

levels off at around 3 s whereas the kinetics at 50 mM sodium ion concentration levels off by 1 s. All the kinetic traces recorded at high CB[7] concentrations fit best to a sum of three exponentials which indicated that there are more relaxation processes contributing to these kinetics other than the simple formation of the 2:1 host-guest complex. It is impossible to distinguish the kinetics associated with the formation of the 2:1 host-guest complex from the three relaxation times obtained from the fits.

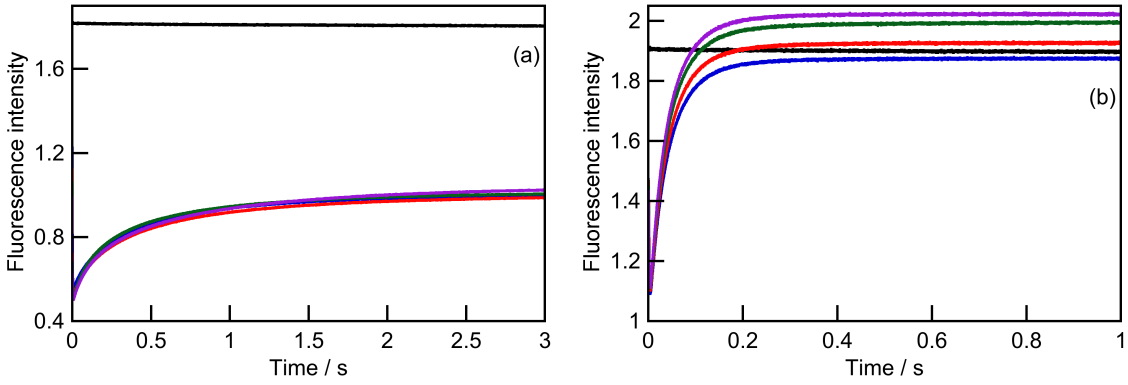

Figure 3.14. (a, left) Stopped-flow traces for the mixing of 1.5 μM Ph-A-Np with 0 (black), 160 (blue), 190 (red), 220 (green) and 250 μM (purple) CB[7] in the presence of 25 mM sodium ion concentration. (b, right) Stopped-flow traces for the mixing of 1.5 μM Ph-A-Np with 0 (black), 250 (blue), 280 (red), 310 (green) and 340 μM (purple) CB[7] in the presence of 50 mM sodium ion concentration.

Based on the experimental results, the mechanism shown in Scheme 3.5 is proposed for the complexation of Ph-A-Np with CB[7] at high sodium ion concentrations. Due to the higher concentration of CB[7]•Na^+ compared to free CB[7] in solution two different 1:1 complexes are formed by the binding of the phenyl group to CB[7]•Na^+ and naphthyl group to either available free CB[7] or CB[7]•Na^+, where the sodium ion is displaced in

the latter case as shown in steps S3.10 to S3.12 in Scheme 3.5. At high sodium ion concentrations only a small amount of free CB[7] is available in solution compared to CB[7]•Na^+. The binding of the naphthyl group to CB[7]•Na^+ is weaker compared to its binding to free CB[7] because sodium ions kick out the naphthyl moiety with a rate constant of $(6.9 \pm 0.2) \times 10^3$ M^{-1} s^{-1} (step S3.7, Scheme 3.4). Even though the binding of phenyl group is stronger to CB[7]•Na^+ than to free CB[7], this binding is still weaker compared to the binding of naphthyl group to CB[7] probably due to its relatively smaller size. As a result, the overall amount of the 1:1 complex formed at high sodium ion concentration is less compared to the amount formed at low sodium ion concentrations. However there are three different pathways for the formation of the 2:1 host-guest complex (S3.13 to S3.15, Scheme 3.5) at high sodium ion concentrations compared to 1 step at low sodium ion concentrations which leads to the formation of more 2:1 host-guest complex at high sodium ion concentrations.

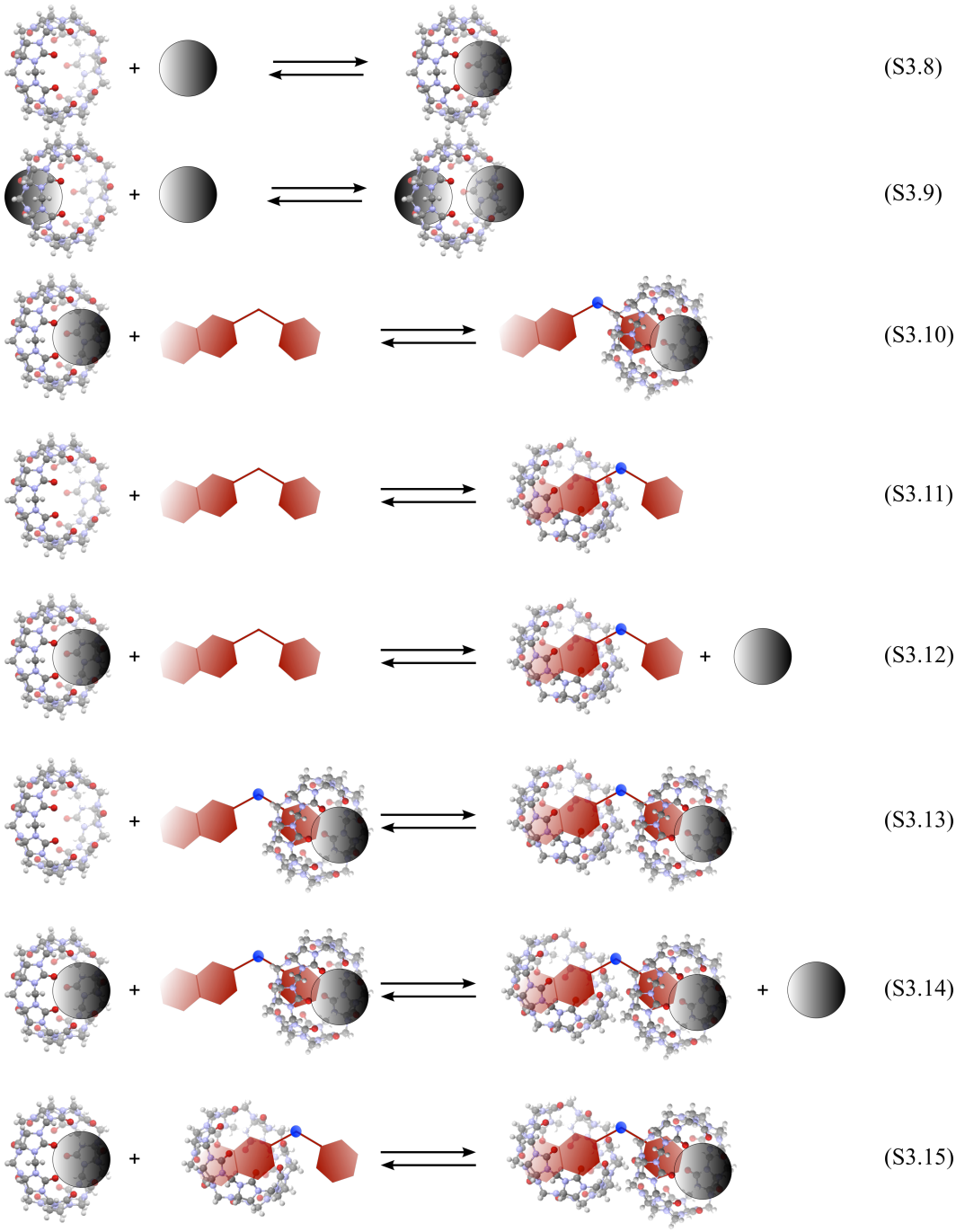

Scheme 3.5. Mechanism of complexation of Ph-A-Np to CB[7] at high sodium ion concentrations.

3.4 Discussion

CB[7] forms stable 1:1 complexes with a variety of guest molecules. These guests include aromatic amines like NpH^+ and AH^+ and the naturally occurring alkaloid, berberine with a positive charge located centrally on the aromatic ring.[136,156,176] The studies on NpH^+ and AH^+ were done in the presence of sodium ions and in these cases sodium ions did not take part in the binding processes of the guest with CB[7], except being a "sponge" taking away free CB[7] in solution available for guest binding. However, in the case of Ph-A-Np, the results show that sodium ions are not just innocent spectators, but can actually participate in the binding of the guest to CB[7]. The reactivity leading to loss of color for the natural plant pigment, 3',4',7-trimethoxyflavilium ion (B-TMF) was reported recently to be inhibited by the formation of a 2:1 host-guest complex with CB[7].[185] B-TMF has a centrally located positive charge and two different binding sites for CB[7]. The studies on berberine and B-TMF were done in the absence of sodium ions. The mechanism of binding with CB[7] for the guest molecules mentioned differ greatly among them. Berberine and NpH^+ has equilibrium constants that are of the same order of magnitude whereas AH^+ and B-TMF have similar equilibrium binding constants but are an order of magnitude lower compared to berberine and NpH^+. The dissociation rate constants for the complexes formed by NpH^+, AH^+, B-TMF and Ph-AH^+-Np are of the same order of magnitude with the value for AH^+ slightly lower compared to the other three complexes. Berberine on the other hand has a dissociation rate constant an order of magnitude lower compared to all the other guests and this low dissociation rate constant was proposed to be due to the constrictive binding of berberine with CB[7]. Two different aspects need to be addressed to rationalize the different binding behavior of

these guest molecules with CB[7]. Firstly, the role of sodium ions in the binding mechanism for the guest with CB[7] and secondly, the role of different binding sites on the guest available to CB[7].

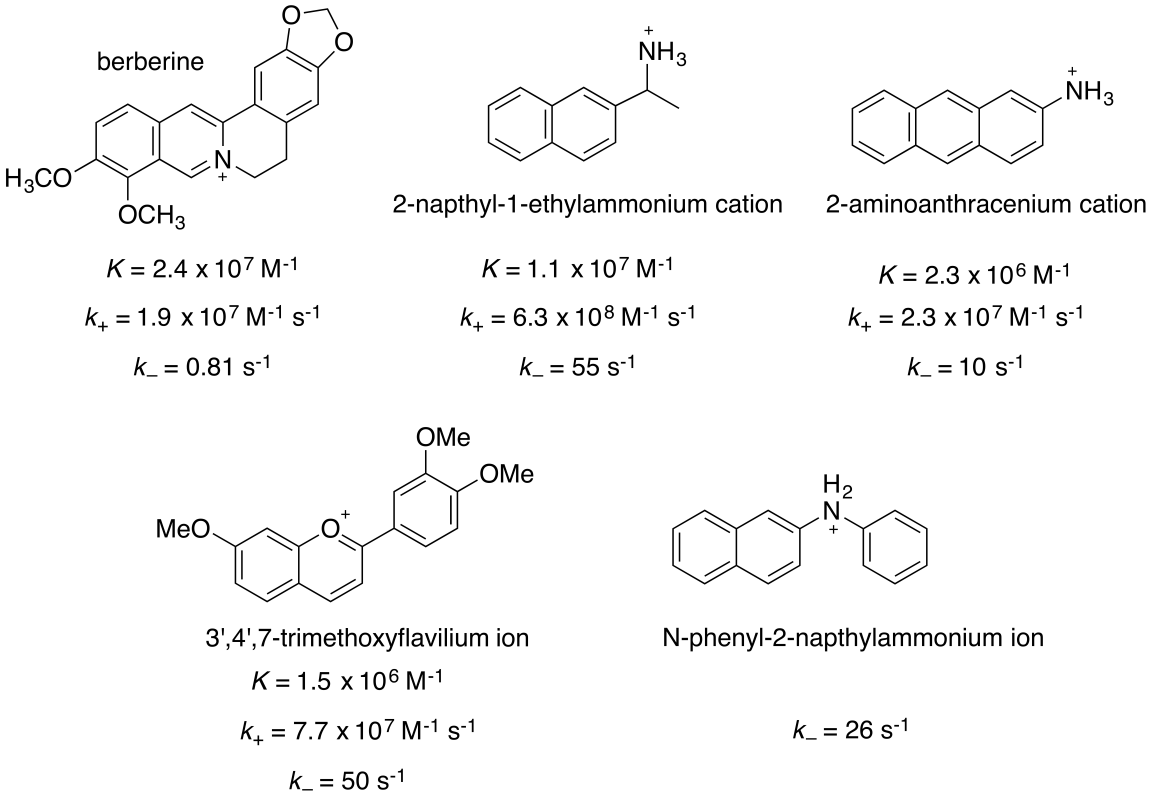

Scheme 3.6. Structure, equilibrium constants and association and dissociation rate constants for the binding the 1:1 binding of berberine, NpH^+, AH^+ and B-TMF. The dissociation rate constant for Ph-AH^+-Np is also shown. The values for K and k_+ for NpH^+@CB[7] and AH^+@CB[7] were calculated from the overall values.

The mechanism for complexation for Ph-A-Np with CB[7] was different at low and high concentrations of sodium ions. A convenient pH regime to conduct the experiments was determined first. Due to the low pK_a value for Ph-A-Np (< 1), a pH value where free

guest was unprotonated and the bound guest undergoes fast protonation was chosen. The experiments performed at pH 1.8, which is in between the pKa for the free, and the bound guests meets both the above-mentioned criteria, thus avoiding any complications in the analysis that could arise due to the adiabatic deprotonation of free protonated guest molecules in the excited state as reported in the case of AH^+.[156]

The kinetic experiments performed at low sodium ion concentrations give direct evidence for the involvement of sodium ions in the binding mechanism for Ph-A-Np with CB[7] (Figure 3.10). A k_{01}^{-} value of 26 s^{-1}, which is of the same order of magnitude as for NpH^+ and AH^+ and in between the values obtained for these two guests suggests that unlike the case of berberine where the dissociation rate constant is an order of magnitude lower there is no constrictive binding mechanism operating in the case of Ph-A-Np. The dissociation rate constant for NpH^+ was independent of the sodium ion concentration but a k_{11}^{-} value of 6.9×10^3 M^{-1} s^{-1} in the case of Ph-A-Np indicates that the residence time of this guest in the CB[7] cavity can be modulated by changing the concentration of sodium ions in solution.

The agreement between the intensities derived from steady-state and stopped-flow fluorescence measurements (Figure 3.8) confirms that no kinetic step leading to the 1:1 complex formation was missed in the kinetic experiments. The stopped-flow experiments also give evidence of a fast binding process that was assigned to the weak binding of the phenyl group to CB[7]. The absence of any evidence for the 2:1 host-guest complex formation at low sodium ion concentration confirms that the binding between the phenyl group and CB[7] is weak, making Ph-AH^+-Np@CB[7] the only 1:1 complex present in the solution at equilibrium.

At high sodium ion concentrations the concentration of free CB[7] in solution is very low and the fast kinetic process observed at low sodium ion concentrations disappeared. This disappearance of the offset further confirms the hypothesis that the fast kinetic process observed at low CB[7] concentration must involve free CB[7] binding to the phenyl group. The observed rate constants do not decrease with increasing sodium ion concentrations, as would be expected if CB[7]•Na^+ was unreactive, suggesting that the binding host species must have switched from free CB[7] to CB[7]•Na^+. Thus the growth kinetics related to the formation of the 2:1 host-guest complex cannot be the binding of free CB[7] to the phenyl group in Ph-AH^+-Np@CB[7] because this kinetics should have been observable at low sodium ion concentrations as well. Combining the information obtained from the different sodium ion concentration experiments, the 2:1 host-guest complex is assumed to be the one where naphthyl group is bound to CB[7] and the phenyl group is bound to CB[7] capped by one sodium ion at its portal.

The analysis of the dissociation rate constants obtained from the observed rate constants at high sodium ion concentrations suggests that the mechanism for the 1:1 complex formation operating at high sodium ion concentrations is different than the low sodium ion concentration experiments. Eq 3.12 predicts a k_{app}^{-} of 199, 302 and 371 s^{-1} for 25, 40 and 50 mM sodium ion concentrations respectively (Figure 3.15). However, the actual values of k_{app}^{-} for these concentrations of sodium ions were 130, 156 and 188 s^{-1} respectively. The fact that the k_{app}^{-} cannot be extrapolated to high sodium ion concentrations implies a different mechanism operating at high sodium ion concentrations.

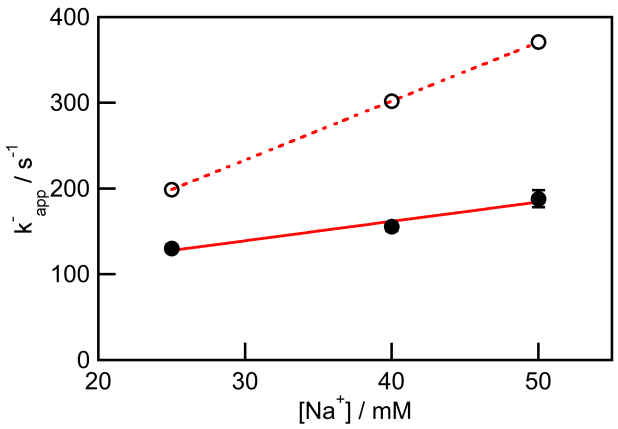

Figure 3.15. Dependence of the dissociation rate constant (black solid circles) on the sodium ion concentration for Ph-A-Np binding with CB[7] at high sodium ion concentrations. Black open circles shows the predicted dependence of binding of Ph-A-Np to CB[7] if the same mechanism is assumed at low and high sodium ion concentrations.

Good values for the kinetics leading to 2:1 host-guest complex could not be obtained from the kinetic experiments. The inconsistency between the emission intensity from the steady state fluorescence experiment and the final intensity from the stopped-flow measurements suggests that the slow kinetics leading to the increase in fluorescence intensity was not completely captured in the kinetic traces. However, there is no doubt that this growth kinetics corresponds to the formation of the 2:1 host-guest complex because of the increase in the fluorescence intensity which can only correspond to a longer-lived and more rigid species in solution than for the binding of Ph-AH^{+}-Np in the 1:1 complex. The experiment performed at high CB[7] concentration in the hope of accurate determination of the growth kinetics showed that the mechanism becomes even more complicated at very high CB[7] concentration. This observation is not surprising because CB[7] is known to form higher order aggregates at high concentrations in the

presence of cations and included guests.[186] CB[7] also forms hydrogels at higher concentrations under acidic conditions arising from the CB[7] aggregates.[187,188] Thus at high CB[7] concentrations, in addition to free CB[7], CB[7]•Na^+ and Na^+•CB[7]•Na^+ higher order aggregates are also present in the system complicating the kinetics leading to the formation of the 2:1 host-guest complex. These aggregates may redistribute during the biding isotherm studies when the solution are equilibrated for a longer time period than in the stopped-flow experiments.

Following the above discussion, it is evident that sodium ions are not innocent spectators in the binding of guests with CB[7]. With the choice of guests with different binding moieties and different experimental conditions sodium ions can switch the mechanism of binding of the guest with CB[7]. In addition, higher order aggregates of CB[7] with sodium ions can complicate the kinetics of the guest with CB[7]. Structural information on the different complexes cannot be obtained at the concentration ranges used for the above experiments. In the absence of any structural data, the following arguments are proposed for the observations for the stronger binding of the phenyl group to CB[7]•Na^+ when compared to free CB[7]. The phenyl group being smaller in size than naphthyl does not efficiently fill the CB[7] cavity as naphthyl does, leading to a stronger binding for naphthyl compared to phenyl group for free CB[7]. Capping of one of the CB[7] portal could inhibit a displacement reaction where the phenyl group in the CB[7] cavity is displaced by the naphthyl group of the guest in solution. The cation capped CB[7] could also strengthen the binding of the phenyl group by preventing the entry of water molecules into the CB[7] cavity. In the case of free CB[7] bound to phenyl group, the portals are exposed in solution and water molecules or other competing guests can

enter the CB[7] cavity and displace the phenyl group, thus weakening the binding of phenyl to free CB[7]. This capping effect is similar to the effect reported in the literature for small molecules[109,179] but instead of slowing down the escape of the included guest as reported for these systems, in the case of Ph-A-Np the binding is strengthened by prevention of other competing species entering the cavity.

Another interesting feature of Ph-A-Np binding to CB[7] is the dependence of the dissociation rate constant for the 1:1 complex formation on the sodium ion concentration. This dependence was not observed in the case of NpH^+ and in both NpH^+ and Ph-A-Np, the binding moiety is the naphthyl group. This striking difference in binding between these two guests could be related to the position and geometry of the positive charge with respect to the naphthyl group. In Ph-A-Np, the amine group is directly attached to the aromatic ring whereas in the case of NpH^+ the amine is one carbon removed from the aromatic ring. Thus the structural differences among guest molecules play a big role in the dynamics of complexation with CB[7].

3.5 Conclusion

Mechanistic studies on the binding behavior of a guest having two different binding sites with CB[7] was investigated in the presence of sodium ions. A switch in the binding mechanism was observed under different concentration regimes of sodium ions. At low sodium ion concentrations, a 1:1 complex formation was observed where the naphthyl group of Ph-A-Np was bound to CB[7]. Sodium ions were found to modulate the residence time of the guest in the 1:1 complex. At high sodium ion concentrations, the binding of the phenyl group to CB[7] was found to be stabilized due to a capping effect

of sodium ions by preventing the entry of competitive guests or water molecules into the CB[7] cavity. This led to an increase in the 2:1 host-guest complex formation where both the naphthyl and the phenyl group was bound to free CB[7] and CB[7] bound to one sodium ion respectively.

4 Binding Dynamics For The Capsule Formation Of Octa Acid With Pyrene Derivatives

4.1 Introduction

4.1.1 Background

The dynamics of complexation for pyrene (Py, Scheme 4.1) to octa acid (OA) was reported previously by our group.[155] Pyrene forms a 2:1 host-guest complex with OA. The proposed mechanism for the formation of the 2:1 complex is shown in Scheme 4.1. The formation of the 1:1 complex is in fast equilibrium compared to the formation of the 2:1 complex. The equilibrium constants and the rate constants in Scheme 4.1 are related as:

$$K_{21} = \frac{k_{21}^{+}}{k_{21}^{-}} \qquad \text{(Eq 4.1)}$$

$$\beta_{21} = K_{11} \times K_{21} \qquad \text{(Eq 4.2)}$$

The overall equilibrium binding constant (β_{21}) for the formation of 2:1 complex was determined by steady-state fluorescence measurements to be (3.19 ± 0.06) × 10^{12} M^{-2}. Combining steady-state fluorescence measurements and kinetic data from stopped-flow fluorescence measurements the individual equilibrium constants (K_{11} and K_{21}) for the 1:1

and 2:1 complex formation were reported to be (4.5 ± 0.6) × 10^5 M^{-1} and (7 ± 1) × 10^6 M^{-1} respectively. Analysis of the kinetic traces also led to the measurement of the association rate constant for the formation of the 2:1 complex (k_{21}^{+}) to be (2.6 ± 0.2) × 10^6 M^{-1} s^{-1}. Using the relationship between the equilibrium constant and rate constants (Eq 4.1) the dissociation of the capsule was found to happen in 2.7 s.

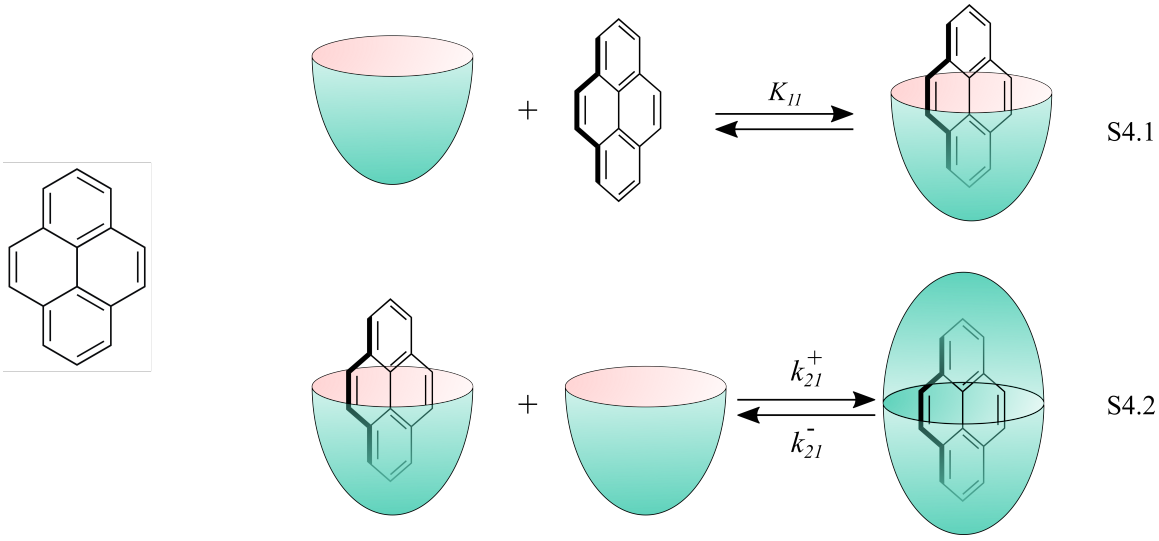

Scheme 4.1. Chemical structure of pyrene (left) and the mechanism (right) of binding of pyrene to OA forming the 2:1 complex. Adapted with permission from the work of Tang et al.[155] Copyright (2012) American Chemical Society.

4.1.2 Objectives

The objective of the present study is to understand how substituents on pyrene affect the complexation dynamics with OA. Minor structural differences in the guest molecule can lead to varied stability and dynamics for the various complex species formed in the system.[147,151,153] 1-Methylpyrene (MePy) and 1-Pyrenemethanol (PyMeOH, Scheme 4.2)

were chosen to study the structure-dynamics relationship for guest binding with octa acid capsules. Unlike Py, MePy and PyMeOH are both unsymmetrical and this could possibly lead to different dynamics of complexation with OA. Two different types of 1:1 complexes are possible with the introduction of a methyl or a hydroxymethyl group on pyrene either by anchoring the substituent to the narrow end of the capsule or by locating them at the wider rim opening (Scheme 4.3).

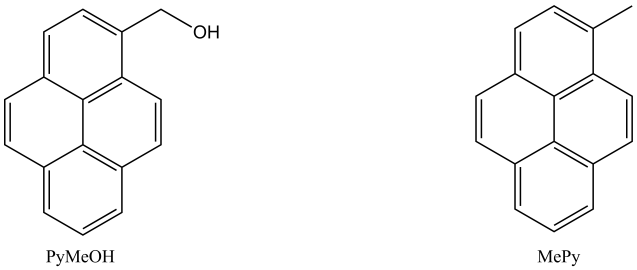

Scheme 4.2. Chemical structures of 1-Pyrenemethanol (PyMeOH) and 1-Methylpyrene (MePy).

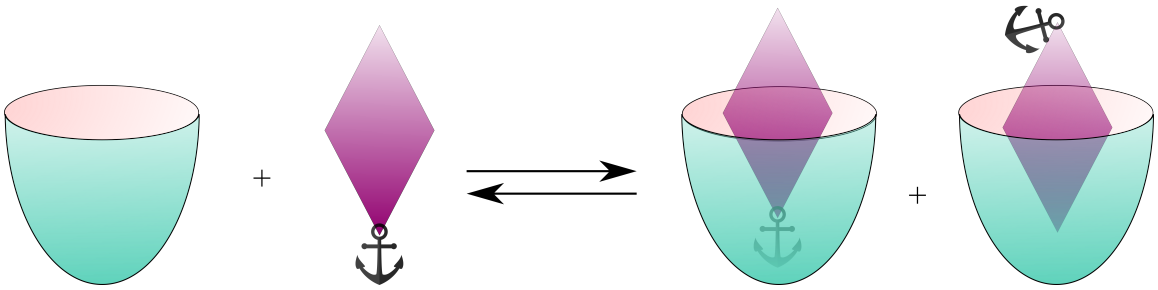

Scheme 4.3. Schematic representation of the two 1:1 complexes that can be formed by an unsymmetrical molecule with OA.

4.2 Experimental section

4.2.1 Materials

1-Methylpyrene (Sigma-Aldrich, ≥ 97%), 1-Pyrenemethanol (Sigma-Aldrich, 98%) sodium tetraborate ($Na_2B_4O_7 \bullet 10H_2O$, BDH, ≥ 98%), nitromethane (Sigma-Aldrich, ≥ 98%), and methanol (Caledon, HPLC grade) were used as received. Octa acid was synthesized by Gibb's group according to the reported procedure.[139,189] Deionized water (Barnstead NANOpure deionizing systems, ≥ 17.8 MΩ cm) was used in the preparation of all aqueous samples.

4.2.2 Sample preparation

A 10 mM solution of borate buffer (pH = 8.9) was prepared from sodium tetraborate. A stock solution of octa acid (300 μM) was prepared by dissolving solid octa acid in borate buffer. Two different stock solutions of 700 μM each were prepared for MePy and PyMeOH in methanol. For the binding isotherm experiments, 3 mL of borate buffer was taken in a 10 × 10 mm quartz cell and appropriate amounts of MePy or PyMeOH stock solutions were injected into the cell to attain a final concentration of 0.2 μM. Small aliquots of octa acid stock solution were added to the cell for the fluorescence emission measurements at different octa acid concentration. For the stopped-flow experiments, a 0.4 μM solution of MePy was prepared in borate buffer. A series of octa acid solutions of required concentrations were also prepared. During the stopped-flow measurements the initial concentrations of MePy and octa acid solutions were halved due to the equal volume mixing of the two solutions during the experiment. For all the experiments, control solutions containing all the components except the fluorophore were prepared.

For time-resolved emission measurements 5 μM solutions each of PyMeOH and MePy was prepared in borate buffer from the respective stock solutions. Required quantities of OA stock solution were added to PyMeOH and MePy solutions to achieve the desired concentrations of OA. Small volumes of liquid nitromethane were then injected into the cell to achieve the desired quencher concentrations.

4.2.3 Equipment

The steady-state fluorescence experiments were performed on a PTI QM-40 fluorimeter. Excitation spectra were collected between 300 and 365 nm at emission wavelengths of 372 nm and 393 nm for PyMeOH and 374 nm for MePy. The emission spectra were collected between 365 and 460 nm at excitation wavelengths of 340 and 347 nm for PyMeOH and 349 nm for MePy. The bandwidths for the excitation and emission monochromators were set to 1 nm. A step size of 0.5 nm and an integration time of 0.5 s were used. A 10 x 10 mm quartz cell with a glass lid was used for the experiment. The glass lid was used instead of a plastic lid to avoid the absorption of the hydrophobic guest onto the plastic lid while the solution inside the cell were mixed during the experiment. The temperature of the sample was kept at 20 ºC throughout the experiment.

Lifetime experiments were performed on an Edinburgh Instruments OB920 single photon counting system. A 335 nm LED was used as the excitation source. The emission from the sample was collected at 393 nm for both PyMeOH and MePy selected with a monochromator with a bandwidth of 16 nm. The number of counts in the maximum intensity channel was set to 10,000. The instrument response function (IRF) was recorded at the excitation wavelength using a Ludox solution.

The dynamics for the binding process were measured in an Applied Photophysics SX20 stopped-flow system. The excitation source for the sample was a Hg-Xe vapor lamp. The samples were excited at 340 and 350 nm for PyMeOH and 349 nm for MePy with an excitation monochromator set to 1 nm bandwidth. The host and guest solutions were mixed in a 1:1 volume ratio in the mixing chamber and the emission from the samples was detected using a 385-423 nm interference filter. The syringes containing the solutions were kept at a temperature of 20 °C for 5 min before each measurement.

4.2.4 Analysis of time-resolved fluorescence decays

FAST software from Edinburgh Instruments was used for the analysis of fluorescence lifetime decays. Due to the long time range collected (2 μs) and the sharpness of the IRF over such long time range, tail fitting was performed on the decays to obtain the lifetimes. The goodness of a fit was judged by the randomness of the residuals and the closeness of χ^2 values from the fits to unity (0.9-1.2).[55] For species i with a lifetime of τ_i the decays were fit to either a monoexponential function or sum of two or three exponentials (Eq 4.3) depending upon the number of species in the solution contributing to the decay and A_i is the pre-exponential factor.

$$\mathrm{I(t)} = \mathrm{I_0} \sum_{1}^{i} A_\mathrm{i}\ e^{-t/\tau_\mathrm{i}} \qquad \text{(Eq 4.3)}$$

Fitting of the quenching plots was performed according to the following equation where k_0 and k_q are the rate constant for the decay in the absence of quencher and the quenching rate constant respectively.

$$\tau^{-1} = k_0 + k_q[Quencher] \quad \text{(Eq 4.4)}$$

4.2.5 Models for analysis of binding isotherms

The integrated intensities under the spectra were normalized by dividing all the intensities by the integrated intensity for the spectrum in the absence of OA. The resulting binding isotherms were then fit with the Scientist 3 software from Micromath using numerical analysis. Three different models were used in the analysis (see below) and in all the models the following independent variables were used:

$[OA]_T$ = total concentration of OA in solution

$[G]_T$ = total concentration of guest in solution

The dependent variables used were:

$[OA]_{eq}$ = equilibrium concentration of free OA in solution

$[G]_{eq}$ = equilibrium concentration of free guest in solution

$[C_{11}]_{eq}$ = equilibrium concentration for the 1:1 complex in solution

$[C_{21}]_{eq}$ = equilibrium concentration for the 2:1 complex in solution

I = Fluorescence intensity

The parameters in the fitting procedures were:

R = Ratio of guest fluorescence intensity in the absence of OA and $[G]_T$

F_{11} = Ratio of emission efficiencies for the guest in the 1:1 complex and guest in water

F_{21} = Ratio of emission efficiencies for the guest in the 2:1 complex and guest in water

K_{11} = Equilibrium binding constant for the 1:1 complex formation

K_{21} = Equilibrium binding constant for the 2:1 complex formation

β_{21} = Overall equilibrium binding constant for the 2:1 complex formation

4.2.5.1 Model for a 1:1 binding process

$$[C_{11}]_{eq} = K_{11} \times [G]_{eq} \times [OA]_{eq} \quad \text{(Eq 4.5)}$$

$$[OA]_{eq} = [OA]_T - [C_{11}]_{eq} \quad \text{(Eq 4.6)}$$

$$[G]_{eq} = [G]_T - [C_{11}]_{eq} \quad \text{(Eq 4.7)}$$

$$I = R \times \left([G]_{eq} + F_{11} \times [C_{11}]_{eq}\right) \quad \text{(Eq 4.8)}$$

The concentration constraints for the dependent variables were defined as:

$$0 < [OA]_{eq} < [OA]_T \quad \text{(Eq 4.9)}$$

$$0 < [G]_{eq} < [G]_T \quad \text{(Eq 4.10)}$$

$$0 < [C_{11}]_{eq} < [G]_T \quad \text{(Eq 4.11)}$$

4.2.5.2 Model for an overall 2:1 binding process

$$[C_{21}]_{eq} = \beta_{21} \times [G]_{eq} \times [OA]_{eq}^2 \quad \text{(Eq 4.12)}$$

$$[OA]_{eq} = [OA]_T - 2\times[C_{21}]_{eq} \quad \text{(Eq 4.13)}$$

$$[G]_{eq} = [G]_T - [C_{21}]_{eq} \quad \text{(Eq 4.14)}$$

$$I = R \times \left([G]_{eq} + F_{21} \times [C_{21}]_{eq}\right) \quad \text{(Eq 4.15)}$$

The concentration constraints for the dependent variables were defined as:

$$0 < [OA]_{eq} < [OA]_T \quad \text{(Eq 4.16)}$$

$$0 < [G]_{eq} < [G]_T \quad \text{(Eq 4.17)}$$

$$0 < [C_{21}]_{eq} < [G]_T \quad \text{(Eq 4.18)}$$

4.2.5.3 Global fit model for a sequential binding mechanism

In the global fits, the fluorescence intensity changes with OA concentration for the increasing and decreasing peaks for the guests were fit simultaneously to the following model. The superscripts "r" and "d" represents the parameters and variables corresponding to the rising and decreasing peak respectively.

$$[C_{11}]_{eq} = K_{11} \times [G]_{eq} \times [OA]_{eq} \quad \text{(Eq 4.19)}$$

$$[C_{21}]_{eq} = K_{21} \times [C_{11}]_{eq} \times [OA]_{eq} \quad \text{(Eq 4.20)}$$

$$[OA]_{eq} = [OA]_T - [C_{11}]_{eq} - 2\times[C_{21}]_{eq} \quad \text{(Eq 4.21)}$$

$$[G]_{eq} = [G]_T - [C_{11}]_{eq} - [C_{21}]_{eq} \quad \text{(Eq 4.22)}$$

$$I^r = R \times \left([G]_{eq} + F_{11}^r \times [C_{11}]_{eq} + F_{21}^r \times [C_{21}]_{eq}\right) \quad \text{(Eq 4.23)}$$

$$I^d = R \times \left([G]_{eq} + F_{11}^d \times [C_{11}]_{eq} + F_{21}^d \times [C_{21}]_{eq}\right) \quad \text{(Eq 4.24)}$$

The concentration constraints for the dependent variables were defined as:

$$0 < [OA]_{eq} < [OA]_T \quad \text{(Eq 4.25)}$$

$$0 < [G]_{eq} < [G]_T \quad \text{(Eq 4.26)}$$

$$0 < [C_{11}]_{eq} < [G]_T \quad \text{(Eq 4.27)}$$

$$0 < [C_{21}]_{eq} < [G]_T \quad \text{(Eq 4.28)}$$

4.2.6 Analysis of kinetic traces from stopped-flow

The stopped-flow traces were analyzed by fitting the individual traces to a sum of exponential functions (Eq 4.29) or by using a global analysis method where all the traces recorded for the guest at different concentrations of OA were simultaneously fit to a defined model. The fit to a sum of exponentials is defined by an offset (a_0) and the sum of exponentials terms, each of which has a corresponding observed rate constant (k_{obsi}) and an amplitude of a_i. Global analysis was performed with the Prokineticist II software from Applied Photophysics. In both the fitting procedures, the goodness of the fit was judged by the randomness of the residuals.

$$\Delta I = a_0 + a_1 e^{-k_{obs1}\,t} + a_2 e^{-k_{obs2}\,t} \qquad \text{(Eq 4.29)}$$

4.3 Results

Where indicated the experiments were performed by a co-op student in the lab, Adam Gaudes, under my supervision.

4.3.1 Steady-state fluorescence measurements

The excitation and emission spectra for PyMeOH and MePy in borate buffer are red shifted by ca. 5 nm compared to those of Py (Figure 4.1). The shape of the emission spectrum for PyMeOH is very similar to that of Py with most of the vibrational fine structure present in the spectrum. In the case of MePy, the emission spectrum is not as structured as that for Py.

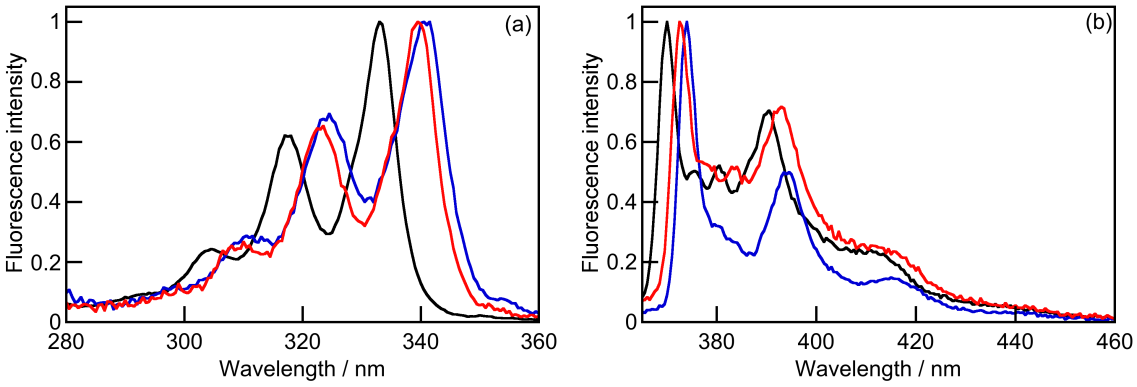

Figure 4.1. Fluorescence excitation (a) and emission (b) spectra for 0.2 µM Py (black), MePy (blue) and PyMeOH (red) in borate buffer. Each spectrum is normalized at the highest intensity peak.

The effect of the substituents on the pyrene molecule on the binding properties with OA was investigated by steady-state fluorescence measurements. Figure 4.2 shows the fluorescence excitation spectra for 0.2 μM PyMeOH at varying concentrations of OA. The changes in the excitation spectra for PyMeOH at different concentrations of OA follow the same trend as that of Py with OA.[155] With increasing OA concentration, the spectra show a decrease in the intensity for the peak at 340 nm and a new band appears centered around 347 nm. The decrease in intensity at 340 nm corresponds to the decrease in the concentration of free PyMeOH in solution and the increase in intensity at 347 nm can be attributed to the increase in the concentration of the host-guest complex formed. The relative intensity of the two bands at 340 and 347 nm in the excitation spectra is largely dependent on the emission wavelength at which the excitation spectrum is collected (Figure 4.2). The excitation spectrum collected at 393 nm shows about equal intensity for 0.2 μM PyMeOH free in solution and the complex with OA with clear isoemissive points in the spectrum. However, the intensity for the band corresponding to the complex formation is very low when the excitation spectrum is collected at 372 nm emission wavelength and the isoemissive points disappears. The disappearance of the isoemissive points in the spectrum at a different emission wavelength is indicative of more than two species in the solution. The presence of 1:1 complex between PyMeOH and OA in addition to free PyMeOH in solution and the 2:1 complex could explain the difference in the excitation spectra at two different wavelengths. Binding isotherms were constructed by integration of areas under two different peaks for the excitation spectra collected at the emission wavelength of 393 nm. The shapes of the two binding isotherms are different especially at lower concentrations of OA where the possibility of formation

of 1:1 complex is high (Figure 4.3). This difference in shape for the binding isotherms also indicates the presence of a third species in the solution.

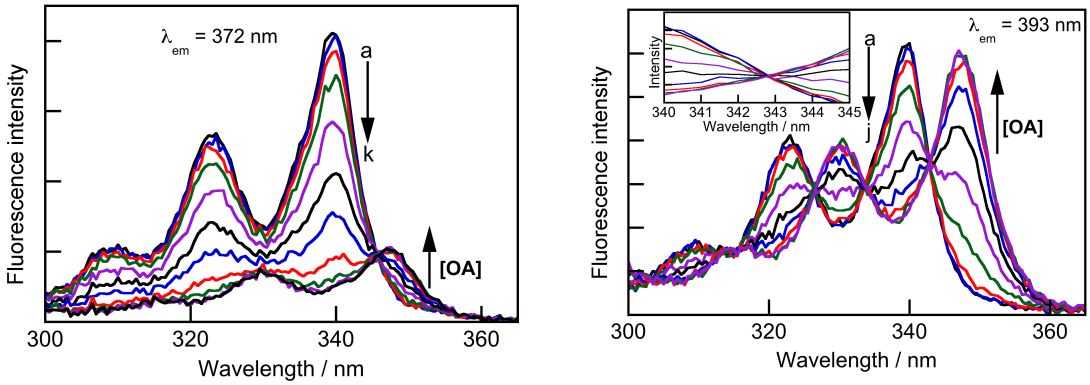

Figure 4.2. Fluorescence excitation spectra at emission wavelengths of 372 nm (left) and 393 nm (right) for 0.2 µM PyMeOH in the absence (a, black) and presence of up to 7.1 µM OA (b to k). The inset in figure b shows the sharp isoemissive point around 343 nm.

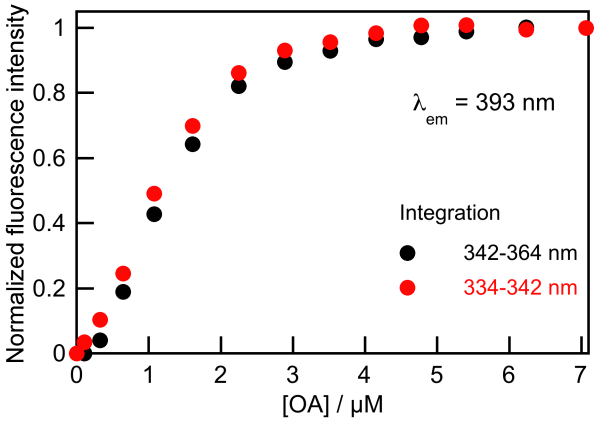

Figure 4.3. Binding isotherms obtained by integrating the area under the excitation spectra (λ_{em} = 393 nm) between 342-364 nm (black) and 334-342 nm (red). The binding isotherm obtained from the decreasing peak was inverted and the amplitude for both the binding isotherms were normalized at the highest OA concentration.

The presence of two different emission bands corresponding to different species in the solution allowed the excitation of the sample at two different wavelengths to collect emission spectra with different shapes and opposite trends for the intensity changes. Exciting the sample at 340 nm led to a continuous decrease in intensity, while the intensity increased for excitation at 347 nm (Figure 4.4). In both cases complete complex formation was observed when the fluorescence intensity remained constant with further increases in the OA concentration.

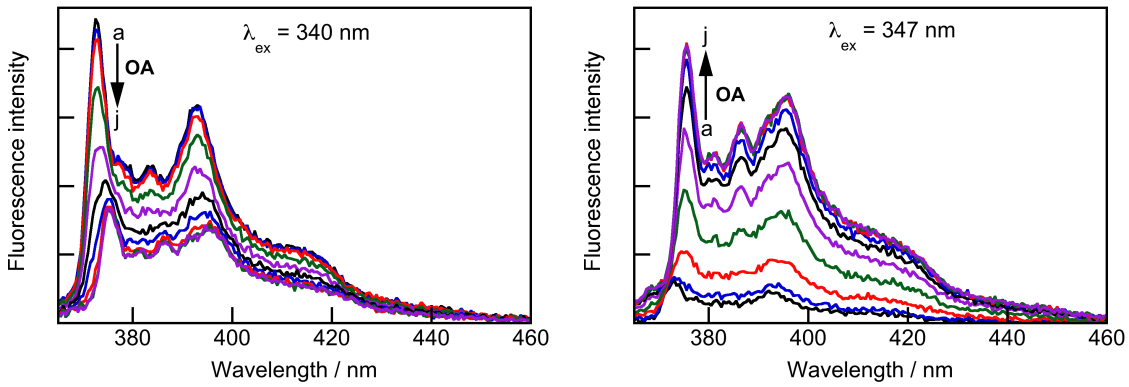

Figure 4.4. Fluorescence emission spectra for 0.2 µM PyMeOH at excitation wavelengths of 340 nm (left) and 347 nm (right) in the absence (black) and presence of up to 7.1 µM OA (b-j).

The binding isotherms obtained from the decreasing peak for both the excitation (λ_{em} = 393 nm) and the emission spectrum (λ_{ex} = 340 nm) were fit to an overall 2:1 binding model (Figure 4.5). An average value of (1.18 ± 0.04) × 10^{12} M^{-2} was obtained from the fits for the overall equilibrium binding constant (β_{21}^{PyMeOH}), which is slightly lower but of the same order of magnitude as for Py with OA (3.19 ×10^{12} M^{-2}).

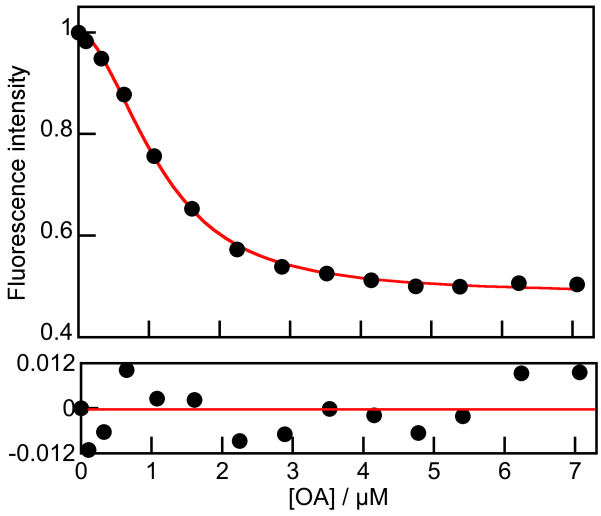

Figure 4.5. Fits for the dependence of fluorescence emission intensity on OA concentration for the excitation spectra (λ_{em} = 393 nm) and the corresponding residuals for an overall β_{21} binding model.

Similar observations for the fluorescence properties as explained in the case of PyMeOH were observed for MePy (Figure 4.6). The relative intensities of the bands corresponding to the guest in solution and in the 2:1 complex in the excitation spectrum depended on the emission wavelength and different emission spectra could be obtained by exciting the sample at either one of the two peak wavelengths of the excitation spectrum. The comparison of binding isotherms obtained by the integration of the area under the increasing and the decreasing peak of the excitation spectrum collected for the emission at 374 nm is shown in Figure 4.7.

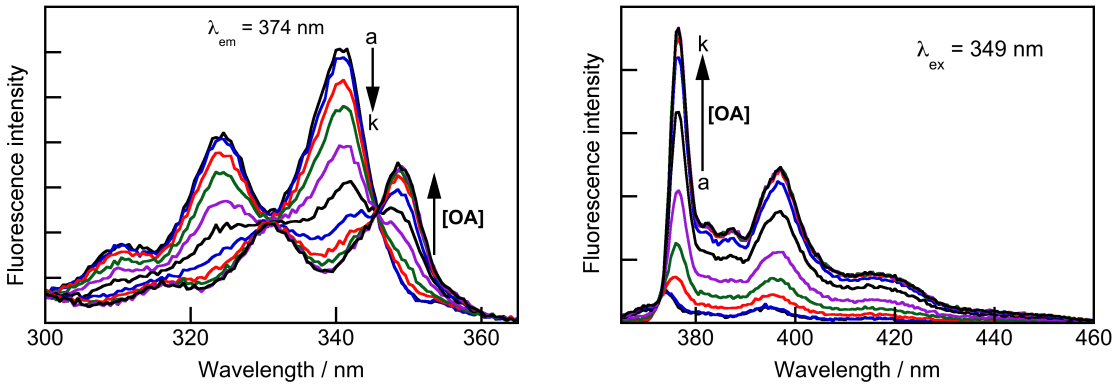

Figure 4.6. Fluorescence excitation (left, λ_{em} = 374 nm) and emission spectra (right, λ_{ex} = 349 nm) for 0.2 µM MePy in the absence (a, black) and presence of up to 4.2 µM OA (b-k).

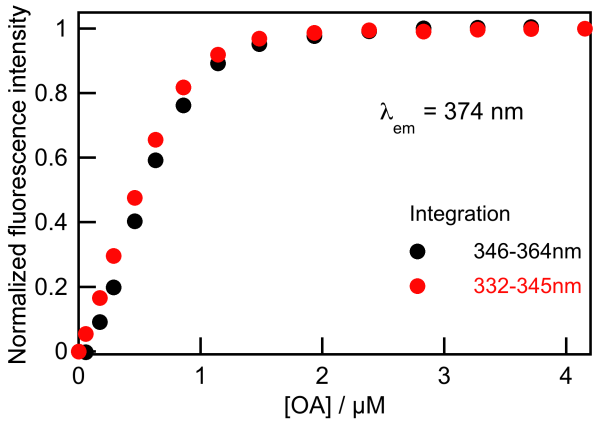

Figure 4.7. Binding isotherms obtained by integrating the area under the excitation spectra (λ_{em} = 374 nm) between 346-364 nm (black) and 332-345 nm (red). The binding isotherm obtained from the decreasing peak was inverted and the amplitude for both the binding isotherms were normalized at the highest OA concentration.

The binding isotherms obtained for MePy binding to OA is steeper and achieves the saturation point at lower OA concentrations compared to the binding behavior for PyMeOH. This trend is indicative of a stronger binding between MePy and OA compared

to PyMeOH. A global fit was performed where the changes in the excitation spectra (λ_{em} = 374 nm) with the addition of OA where the integrated area between 346 to 364 nm for the intensity increase and 332 to 345 nm for the intensity decrease were fit simultaneously. The binding isotherm did not fit very well to the overall binding model used in the case of Py and PyMeOH. The non-random residuals obtained in this case indicate that the fit is not adequate (Figure 4.8a). A better fit was obtained for the binding isotherms when the sequential formation of a 1:1 complex followed by the 2:1 complex is considered (Figure 4.8b), where the magnitude of the residuals is lower than for the overall model (Figure 4.8a). The residuals for the fits are better when compared to the overall binding model, however, a slight systematic deviation in the residuals could indicate the presence of another species in solution in addition to the free guest, the 1:1 complex and the 2:1 complex (see discussion below). The binding constant values for the formation of the 1:1 complex (K_{11}^{MePy}) and the 2:1 complex (K_{21}^{MePy}) recovered from the fits were (1.60 ± 0.47) × 10^6 M^{-1} and (1.41 ± 0.14) × 10^7 M^{-1} yielding a β_{21}^{MePy} value of (2.26 ± 0.70) ×10^{13} M^{-2} which is an order of magnitude greater than the overall binding constant for PyMeOH with OA.

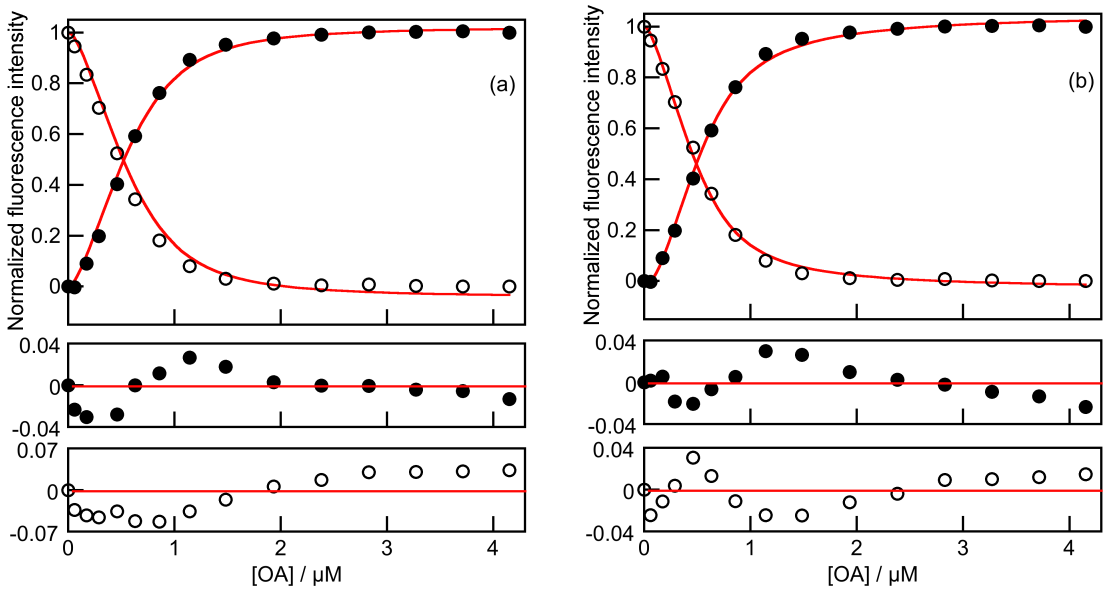

Figure 4.8. Fits and the corresponding residuals for the global fits of the binding isotherms obtained from the increasing (black solid circles) and decreasing peaks (black open circles) of the excitation spectra (λ_{em} = 374 nm) to an overall 2:1 binding model (a, left) and a sequential binding model (b, right). The amplitudes for all the binding isotherms were normalized for comparison.

4.3.2 Stopped-flow measurements

The binding kinetics for the complexation of MePy and PyMeOH were investigated by stopped-flow measurements. Figure 4.9 shows the stopped-flow traces obtained for the complexation for 0.2 μM PyMeOH with different concentrations of OA. The experiments were performed by exciting the sample at 340 or 350 nm where respectively a decrease or an increase in fluorescence intensities were observed with complex formation. Similar to what was observed for pyrene complexation with octa acid, a gradual increase in the offset for the initial intensity was observed in the case of PyMeOH. This offset in intensity is indicative of a kinetic relaxation process faster than

the time resolution of the equipment (Figure 4.10). This fast component is attributed to the kinetics related to the formation of the 1:1 complex.

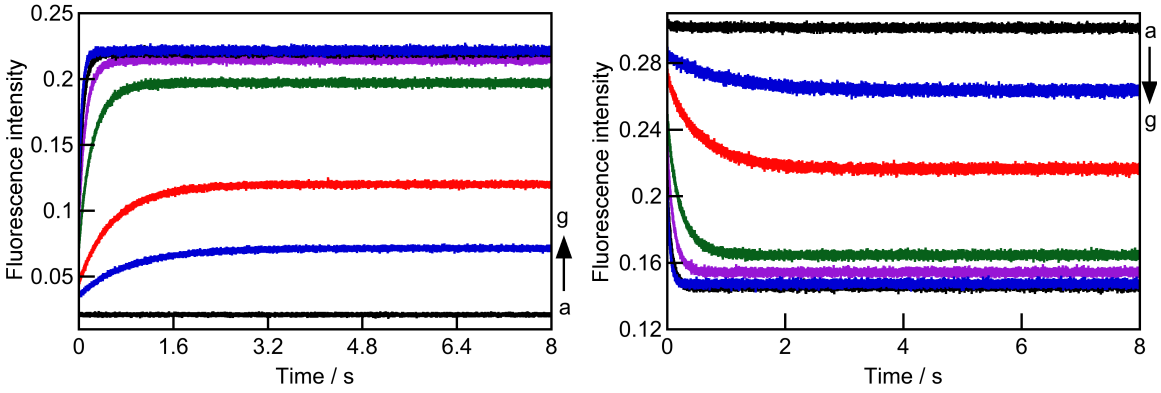

Figure 4.9. Stopped-flow traces for the excitation at 350 (left) and 340 nm (right) for the mixing of 0.2 μM PyMeOH with 0 (a, black), 0.70 (b, blue), 1.0 (c, red), 2.0 (d, green), 3.0 (e, purple), 4.0 (f, black) and 5.0 μM (g, blue) OA. All the concentrations mentioned are after mixing.

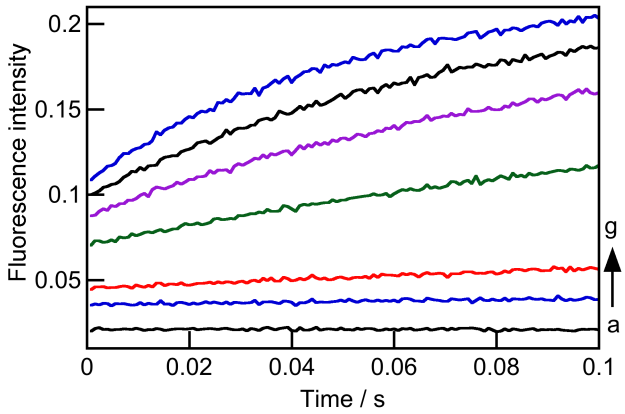

Figure 4.10. The offset in initial intensity for the stopped-flow traces (λ_{ex} = 350 nm) observed for the mixing of 0.2 μM PyMeOH with 0 (a, black), 0.7 (b, blue), 1.0 (c, red), 2.0 (d, green), 3.0 (e, purple), 4.0 (f, black) and 5.0 μM (g, blue) OA.

Assuming the formation of the 1:1 complex to be a pre-equilibrium step in the stopped-flow experiment, the initial intensity of the stopped-flow traces at various concentrations of OA can be used to construct a binding isotherm to estimate the equilibrium binding constant (K_{11}^{PyMeOH}) for the 1:1 complex. The fitting of this binding isotherm (Figure 4.11) gave a K_{11}^{PyMeOH} value of (1.3 ± 0.3) × 10^5 M^{-1}. This value is slightly lower but of the same order of magnitude as that of Py complexation with OA (4.5 × 10^5 M^{-1}). From the K_{11}^{PyMeOH} obtained from the kinetic data and the β_{21}^{PyMeOH} obtained from the steady-state measurements, a K_{21}^{PyMeOH} value of (9 ± 2) × 10^6 M^{-1} was calculated from Eq 4.2. This value is the same as was obtained for pyrene (7 × 10^6 M^{-1}).

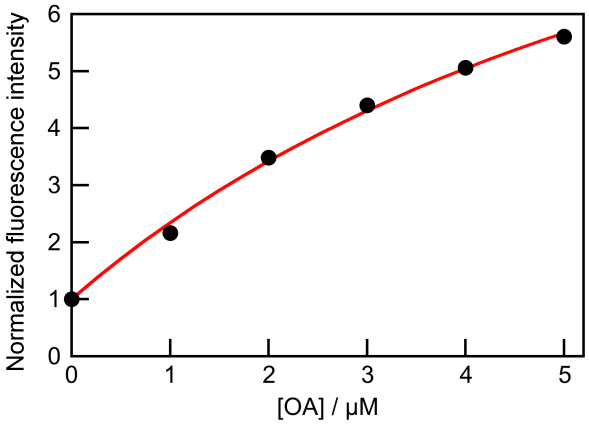

Figure 4.11. Fit to a 1:1 binding model for the binding isotherm obtained from the offset of initial intensity (λ_{ex} = 350 nm) normalized at 0 μM OA concentration obtained from the stopped-flow traces for the mixing of PyMeOH with OA.

A global analysis was performed on all the stopped-flow traces shown in Figure 4.9 to the model described in Scheme 4.4 where the formation of the 1:1 complex was assumed to be in fast equilibrium. The equilibrium binding constant value for the

formation of 1:1 complex obtained from the initial intensity offset in the stopped-flow traces was fixed during the fitting process. The fixed value of the K_{11}^{PyMeOH} was varied between the error limits obtained from the binding isotherm fit. The residuals obtained were mostly random around zero (Figure 4.12) and the values obtained for the association rate constant (k_{21}^{+}) and dissociation (k_{21}^{-}) rate constants recovered from the fits for the 2:1 complex formation are summarized in Table 4.1. An average value of (4.8 ± 0.7) × 10^6 M^{-1} s^{-1} and (0.77 ± 0.02) s^{-1} was obtained for k_{21}^{+} and k_{21}^{-} respectively. This dissociation rate constant corresponds to a capsule opening time of 1.3 s, which is twice as fast as the capsule dissociation time for pyrene. The ratio of the association and dissociation rate constants recovered from global analysis gave a value of (6.2 ± 0.9) × 10^6 M^{-1} which is the same as the K_{21}^{PyMeOH} value obtained from the β_{21}^{PyMeOH} from the steady-state fluorescence measurement and K_{11}^{PyMeOH} obtained from the initial intensity offset data from stopped-flow.

$$PyMeOH + OA \underset{}{\overset{K_{11}^{PyMeOH}}{\rightleftharpoons}} PyMeOH@OA \qquad \text{(Eq 4.30)}$$

$$PyMeOH@OA + OA \underset{k_{21}^{-}}{\overset{k_{21}^{+}}{\rightleftharpoons}} OA@PyMeOH@OA \qquad \text{(Eq 4.31)}$$

Scheme 4.4. Model used in the global fitting procedure for the stopped-flow traces obtained for the mixing of PyMeOH with OA.

Global analysis was also performed by fitting the stopped-flow traces to the model used in the case of Py where the dissociation rate constant term in Eq 4.31 of Scheme 4.4

is not considered in the fit. This mechanism also gave a good fit with random residuals giving an average association rate constant of (9 ± 2) × 10^6 M^{-1} s^{-1} which led to the calculated dissociation rate constant of (1.0 ± 0.2) s^{-1} which matches the recovered k_{21}^{-} value from the global fit to the mechanism shown in Scheme 4.4.

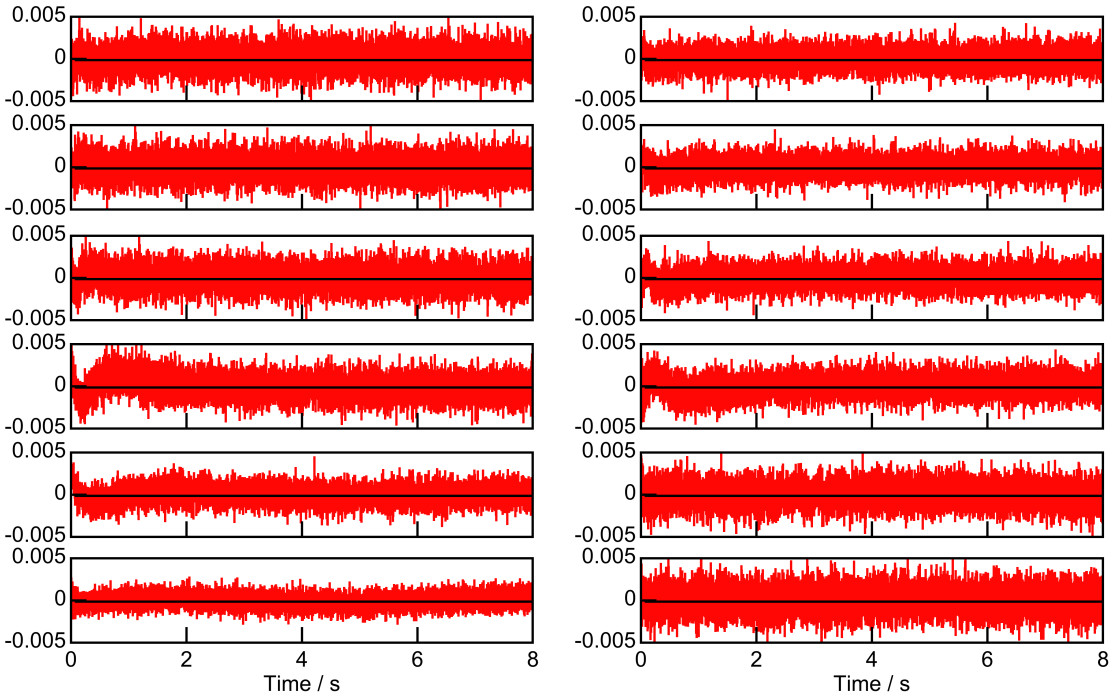

Figure 4.12. Residuals for the global analysis for the stopped-flow traces for the increasing (left) and decreasing peaks (right) to the model in Scheme 4.4. In each panel, the concentration of OA increases from 0.7 to 5 μM from bottom to top.

Table 4.1. Table summarizing the fit results for the global analysis performed on the stopped-flow traces for the mixing of PyMeOH with OA to the model in Scheme 4.4. The parameter K_{11}^{PyMeOH} was fixed during the fits.

K_{11}^{PyMeOH} / 10^5 M^{-1}	k_{21}^{+} / 10^6 M^{-1} s^{-1}	k_{21}^{-} / s^{-1}
1.28	4.69 ± 0.03	0.77 ± 0.01
1.55	4.18 ± 0.03	0.76 ±0.01
1.00	5.51 ± 0.03	0.79 ± 0.01

The stopped-flow traces obtained for MePy at different concentrations of OA are shown in Figure 4.13. The kinetic traces collected at the decreasing peak in the excitation spectra had poor signal-to-noise ratio and were not analyzed. The increase in the offset as seen in the case of PyMeOH was also observed in the case of MePy. However, this increase in offset was smaller compared to PyMeOH and had a linear dependence on the OA concentration. As a result, accurate determination of the equilibrium constant for 1:1 complex formation was not possible from the kinetic data.

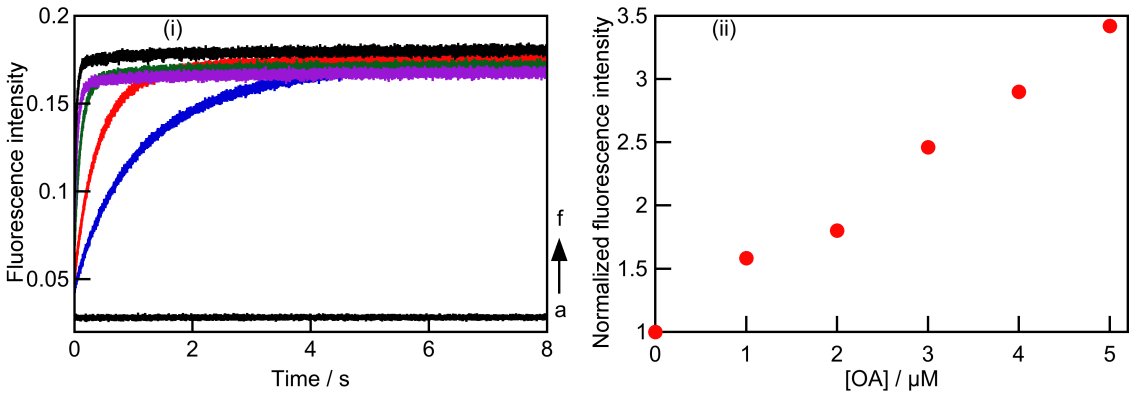

Figure 4.13. (i, left) Stopped-flow traces for the excitation at 349 nm for the mixing of 0.2 μM MePy with 0 (a, black), 1.0 (b, blue), 2.0 (c, red), 3.0 (d, green), 4.0 (e, purple) and 5.0 μM (f, black) OA. All the concentrations mentioned are after mixing. (ii, right) Offset in initial intensity normalized at 0 μM OA concentration obtained from the stopped-flow traces for the mixing of MePy with OA.

Global analysis of the stopped-flow traces to the model shown in Scheme 4.4 where PyMeOH was replaced by MePy gave a systematic deviation in the beginning of the residuals for all the traces indicating that the model used is not the correct one (Figure A. 1, appendix). This result indicates that there are more equilibria associated with the capsule formation of OA with MePy other than a simple and sequential formation of the 1:1 and the 2:1 complex as will be addressed in the discussion section. Of the several fitting models tried, the best fit was obtained for the mechanism shown in Scheme 4.5. In this mechanism, the formation of different types of 1:1 complex was assumed and the binding constant for one of those complexes were considered to be higher than the other (see discussion below). The capsule formation was assumed to happen from both the 1:1 complexes. The binding constant value for the formation of the less stable 1:1 complex of MePy with OA was assumed to be the same as that for the 1:1 complex formation for PyMeOH with OA and was fixed in the fitting procedure. Only the forward rate constants

were considered for the formation of the 1:1 and 2:1 complexes. The residuals obtained for the fits were random compared to the other models used in the analysis (Figure 4.14, see Appendix A. 3 for other models tried). Fits where the dissociation rate constants were included led to six floating parameters in the fit and the values recovered for the dissociation rate constants were larger than the time resolution of the equipment.

$$MePy + OA \underset{}{\overset{{}^{1}K_{11}^{MePy}}{\rightleftharpoons}} {}^{1}MePy@OA \qquad \text{(Eq 4.32)}$$

$$MePy + OA \xrightarrow{{}^{2}k_{11}^{+}} {}^{2}MePy@OA \qquad \text{(Eq 4.33)}$$

$${}^{1}MePy@OA + OA \xrightarrow{{}^{1}k_{21}^{+}} OA@MePy@OA \qquad \text{(Eq 4.34)}$$

$${}^{2}MePy@OA + OA \xrightarrow{{}^{2}k_{21}^{+}} OA@MePy@OA \qquad \text{(Eq 4.35)}$$

Scheme 4.5. Model used in the global fitting procedure for the stopped-flow traces obtained for the mixing of MePy with OA.

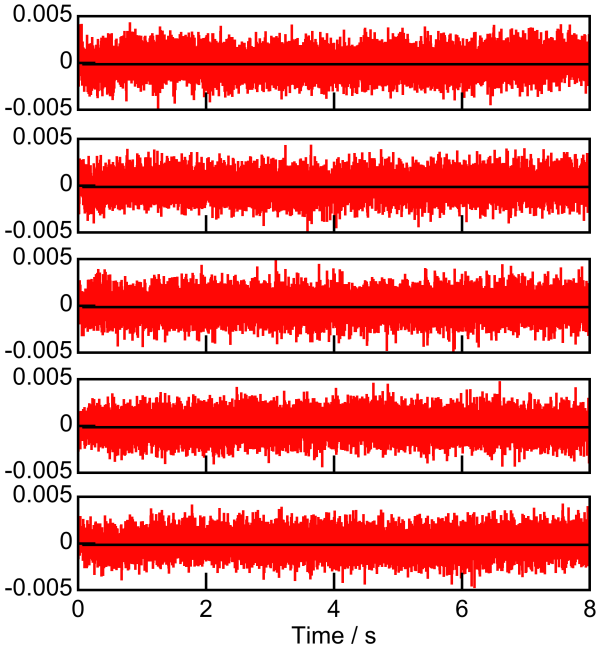

Figure 4.14. Residuals for the global fits performed on the stopped-flow traces for the mixing of MePy with OA to the model shown in Scheme 4.5. The concentration of OA increases from 1 to 5 μM from bottom to top panel. The value for ${}^{1}K_{11}^{MePy}$ fixed in the fits was 1.3×10^5 M^{-1}.

The global fits for the stopped-flow traces shown in Figure 4.13 gave an association rate constant (${}^{2}k_{11}^{+}$) of $(2.1 \pm 0.2) \times 10^5$ M^{-1} s^{-1} for the formation of the more stable 1:1 complex. The dissociation rate constant for this stable 1:1 complex (${}^{2}k_{11}^{-}$) calculated from the equilibrium binding constant (K_{11}^{MePy}) and ${}^{2}k_{11}^{+}$ was (0.13 ±0.04) s^{-1}. This dissociation rate constant for the 1:1 complex is lower than the dissociation rate constant for the 2:1 capsule with Py as the guest. Two different association rate constants of (6.8 ± 0.1) $\times 10^6$ and $(1.53 \pm 0.02) \times 10^5$ M^{-1} s^{-1} were recovered for the formation of the 2:1 complex from the less and more stable 1:1 complexes respectively (${}^{1}k_{21}^{+}$ and ${}^{2}k_{21}^{+}$). Since the different 1:1 complexes result in the same 2:1 complex and the equilibrium binding constants for the formation of the two different 1:1 complex is not available, separate

dissociation constants cannot be calculated for the 2:1 complex formation (see discussion below).

4.3.3 Time-resolved fluorescence measurements

Preliminary experiments on time-resolved fluorescence measurements described below were performed by Adam Gaudes.

Time resolved fluorescence quenching experiments were performed to see if the presence of a 1:1 complex could be detected at equilibrium. The guest free in water, in the 1:1 complex and the 2:1 complex in principle can have different excited state lifetimes. This difference is due to the different degrees of protection experienced by the guest molecule in different environments. The addition of a fluorescence quencher to a solution containing different species of the guest can differentially quench the lifetimes of the guest species. The differential quenching of the guest depends on the accessibility of the quencher to the guest molecule. Free guest in water is accessible to the quencher whereas the partially or fully protected guest in the 1:1 and the 2:1 complex is not as easily quenched. In order to improve the collection times on the single photon counter, the lifetime experiments were performed at 5 μM guest concentration in the case of PyMeOH and MePy. A simulation of the concentrations of different guest species in solution at varying host concentrations was done using the binding constant values obtained from the steady-state and stopped-flow studies. The ideal host concentration where maximum concentration of the 1:1 complex is observed was used for the experiments to see if the presence of a 1:1 complex could be detected by lifetime experiments.

The fluorescence decay of PyMeOH in the absence of OA is mono exponential with a lifetime of 126 ns. At high concentrations of OA (35 μM) where mostly 2:1 complex is present the decay was again mono exponential with a longer lifetime of ca. 237 ns which was assigned to the 2:1 complex. A quenching experiment was performed by adding nitromethane to a solution containing 5 μM PyMeOH and 6 μM OA. Good fits were obtained when the decays were fit to a sum of two exponentials for all quencher concentrations (Figure 4.15 and Table 4.2). The lifetime of PyMeOH free in water was found to be quenched efficiently whereas the longer lifetime of 237 ns was quenched very inefficiently by increasing concentrations of the quencher (Figure 4.16). The quenching rate constants obtained for free guest and the 2:1 complex was found to be (5.9 ± 0.1) × 10^9 M^{-1} s^{-1} and (1.2 ± 0.1) × 10^7 M^{-1} s^{-1} respectively. A third lifetime corresponding to the 1:1 complex was not evident in the lifetime decays for PyMeOH. Forcing the fluorescence decays to fit to a sum of three exponentials revealed a lifetime intermediate to that of the free guest and the 2:1 complex. However, the A values recovered from these fits had errors greater than the values themselves showing no reliability for the presence of this third lifetime. Therefore, the fluorescence lifetime experiments do not reveal the presence of the 1:1 complex in the case of PyMeOH.

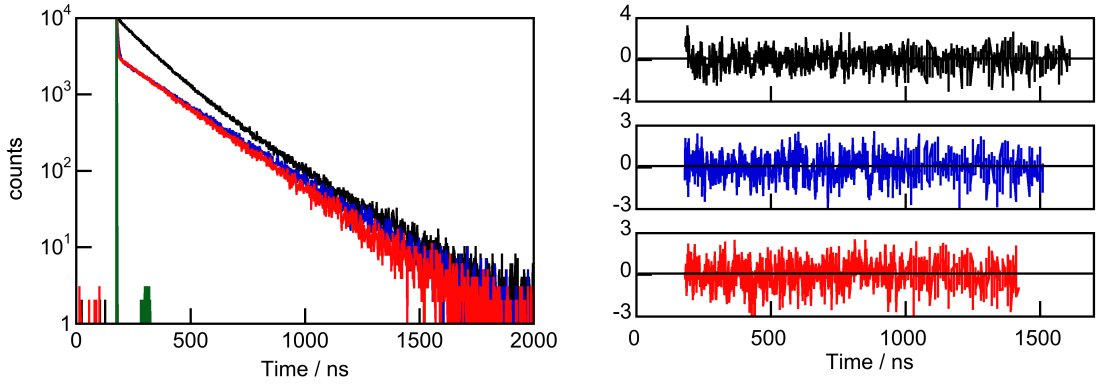

Figure 4.15. Fluorescence lifetime decays (left) and the residuals for the fits of the decays to sum of two exponentials (right) for 5 µM PyMeOH and 6 µM OA in borate buffer in the presence of 0 (black), 0.03 (blue) and 0.06 M (red) nitromethane. The IRF is shown in green with the decays.

Table 4.2. Fluorescence lifetimes and A values for the fits of the decays to sum of two exponentials for 5 µM PyMeOH in the presence of 6 µM OA at varying nitromethane concentrations.

[Nitromethane] / M	τ_1 / ns	τ_2 / ns	A_1	A_2	χ^2
0	126	240	0.72	0.28	1.009
0.03	5.41	221	0.77	0.23	0.975
0.06	2.77	206	0.82	0.18	1.166

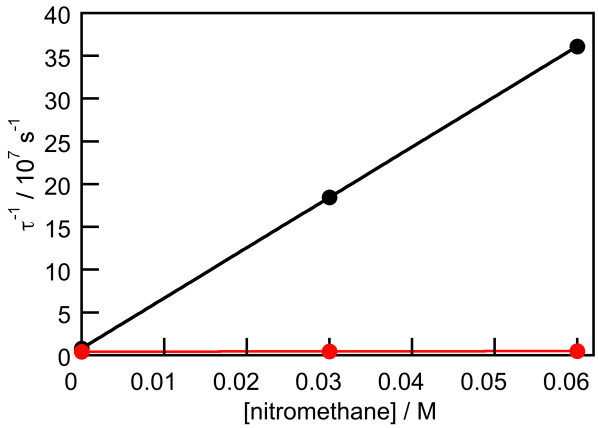

Figure 4.16. Quenching plot for a solution containing 5 µM PyMeOH and 6 µM OA in borate buffer. The black and red solid circles represent the lifetime for free PyMeOH and the 2:1 complex with OA respectively.

The same experiment was performed in the case of MePy and OA. Analysis of the fluorescence decay of MePy in borate buffer in the absence of OA revealed a single lifetime of 90 ns. In the presence of high OA concentrations a single exponential decay was observed with a lifetime of 215 ns corresponding to the lifetime of MePy inside the OA capsule. Quenching experiments performed using a solution containing 5 μM MePy and 5 μM OA gave quenching rate constants of $(6.3 \pm 0.1) \times 10^9$ M^{-1} s^{-1} and $(9 \pm 2) \times 10^6$ M^{-1} s^{-1} for the free guest and the 2:1 complexes respectively. However, the lifetime decays in the presence of the quencher gave high χ^2 values and/or systematic deviation in residuals when fit to sum of two exponentials. (Figure 4.17 and Table 4.3) Fitting the traces to sum of three exponentials led to improved χ^2 values and residuals indicating the presence of a third species in solution. This species had a lifetime in between that of the free guest and the 2:1 complex and the quenching rate constant for this species varied between 0.3×10^8 to 1.1×10^8 M^{-1} s^{-1} for repeated experiments (Figure 4.18). This

variability is likely due to the low contribution from this species to the lifetime decay (A value ≤ 5%, table XX). This lifetime is assigned to the 1:1 complex present in the system. In the absence of the quencher this third lifetime not detected possibly due to its closeness to the lifetime of the guest free in solution or the 2:1 complex. As a result, the lifetime for the 1:1 complex in the absence of the quencher was estimated from extrapolation of the lifetime for this species in the presence of the quencher.

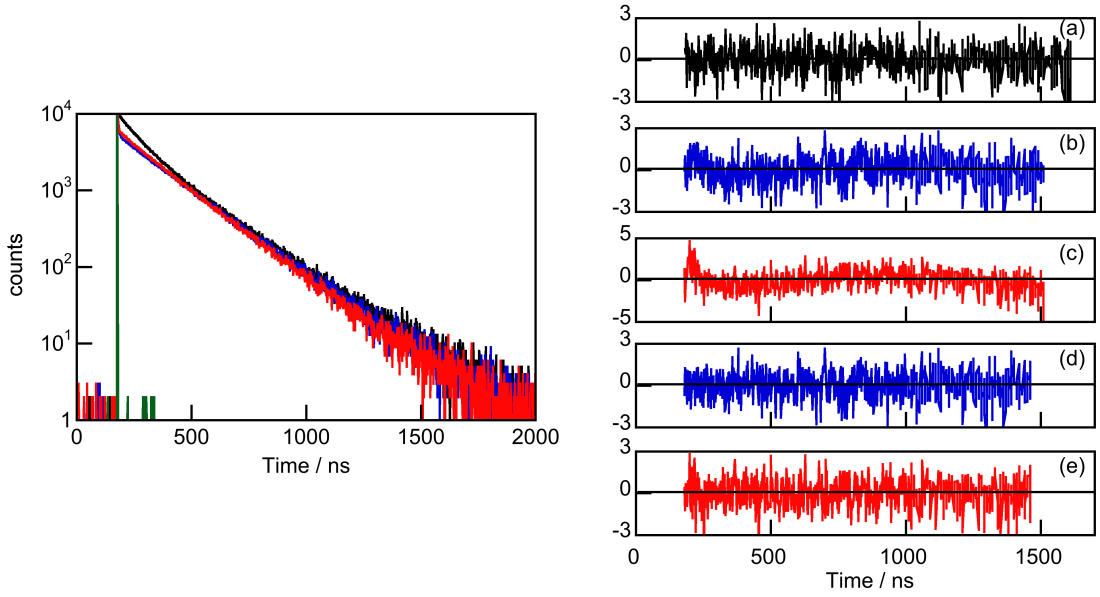

Figure 4.17. Fluorescence lifetime decays (left) and the residuals for the fits of the decays (right) to sum of two exponentials (a, b and c) and three exponentials (d and e) for 5 µM MePy and 5 µM OA in borate buffer in the presence of 0 (black), 0.03 (blue) and 0.06 M (red) nitromethane.

Table 4.3. Fluorescence lifetimes and A values for the fits of the decays to sum of two and three exponentials for 5 μM PyMeOH in the presence of 5 μM OA at varying nitromethane concentrations.

[Nitromethane] / M	τ_1 /ns	τ_2 /ns	τ_3 /ns	A_1	A_2	A_3	χ^2
0	89.6	-	215	0.57	-	0.43	1.073
0.03	5.49	-	196	0.56	-	0.44	1.386
0.06	3.00	-	182	0.58	-	0.42	1.269
0.03	5.08	112	204	0.56	0.05	0.39	1.156
0.06	2.63	81.5	188	0.59	0.04	0.37	1.051

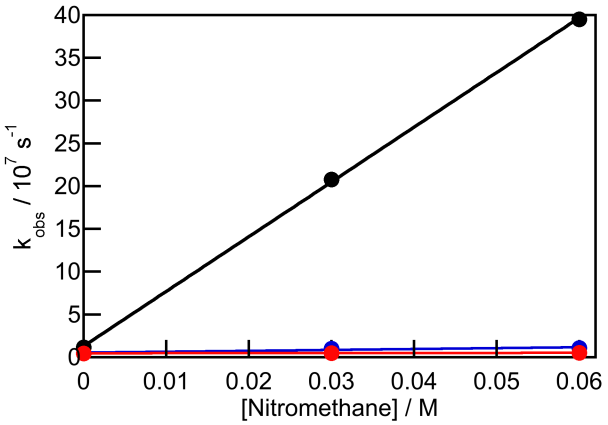

Figure 4.18. Quenching plot for a solution containing 5 μM MePy and 5 μM OA in borate buffer. The black, blue and red solid circles represent the lifetime for MePy free in water, 1:1 complex and 2:1 complex with OA respectively.

4.4 Discussion

The introduction of substituents on Py brings about interesting changes to the thermodynamics and kinetics of its complexation with OA. The introduction of the

methyl group to pyrene results in a more hydrophobic molecule, which prefers to be encapsulated in the hydrophobic OA cavity. The relatively hydrophilic hydroxymethyl substituent, which is capable of hydrogen bonding with water, is not as good a candidate to occupy the OA cavity. This is evident from the binding isotherms (Figure 4.19) and the equilibrium binding constant values for the three molecules. The binding isotherm for PyMeOH is shallower compared to Py, which indicates a weaker binding, yielding an overall equilibrium binding constant (β_{21}) value of (1.18 ± 0.04) × 10^{12} M^{-2} compared to (3.19 ± 0.06) × 10^{12} M^{-2} for Py. In the case of MePy, the binding isotherm is steeper when compared to Py with a β_{21} value of (2.26 ± 0.70) × 10^{13} M^{-2} which is an order of magnitude greater when compared to either Py or PyMeOH. The overall and individual equilibrium binding constants obtained for all the three guests with OA is summarized in Table 4.4.

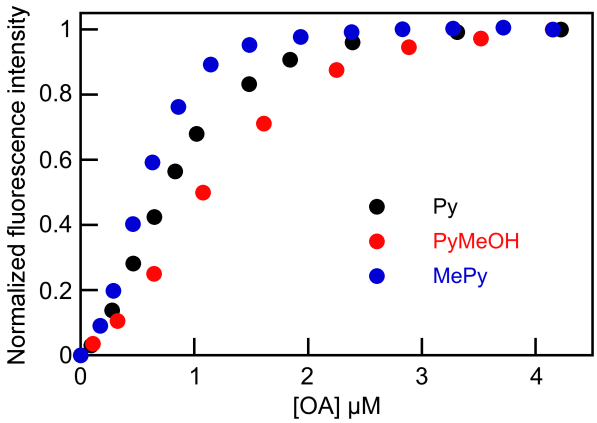

Figure 4.19. Comparison of binding isotherms for Py (black), PyMeOH (red) and MePy (blue). All the binding isotherms were normalized at 4.2 μM OA. The binding isotherm for Py was taken from previous work.[155]

Table 4.4. Overall and individual binding constants for Py, PyMeOH and MePy.

Guest	β_{21} / 10^{12} M^{-2}	K_{11} / 10^{5} M^{-1}	K_{21} / 10^{6} M^{-1}
Py[a]	3.19 ± 0.06	4.5 ± 0.6	7 ± 1
PyMeOH	1.18 ± 0.04	1.3 ± 0.3	9 ± 2
MePy	22.6 ± 0.7	16 ± 5	14 ± 1

[a] the values for Py were taken from previous work.[155]

In all three cases, there is a positive cooperativity indicated by the sigmoidal shape of the binding isotherm which means that the binding constant for the 2:1 complex is higher compared to that for 1:1 complexation. The fact that the binding isotherms for Py and PyMeOH fit to an overall equilibrium binding model indicates that the concentration of the 1:1 complex is low in relative terms compared to the concentration of free guests and the 2:1 complexes. Stopped-flow experiments also showed that the formation of 1:1 complexes for Py and PyMeOH correspond to fast equilibria compared to the formation of the 2:1 complex. However, the binding isotherm for MePy could only be fit if the sequential formation of the 1:1 and the 2:1 complex was taken into account. Unlike the case for Py and PyMeOH, the 1:1 complex for MePy with OA has a higher stability and this complex is present in appreciable amounts, especially at lower OA concentrations. This observation can be explained by considering the structures of the different 1:1 complexes formed by these molecules. Py being a symmetrical molecule can form only one type of 1:1 complex with OA. On the other hand, PyMeOH and MePy form two different 1:1 complexes with OA (Scheme 4.3). The first type of 1:1 complex formed by

the encapsulation of the hydrophilic hydroxymethyl group in the OA cavity is not very favorable (Scheme 4.6). But the equivalent of this complex formed by MePy with OA is more stabilized due to the hydrophobicity of the methyl group and the favorable CH_3-π interactions the methyl group can have with the narrower rim of the OA molecule (Scheme 4.7). Ramamurthy's research group has shown that the hydrophobic alkyl side chains substituted on phenyl group can be anchored at the narrow rim of OA cavity leading to better stabilization for that particular orientation of guest molecules in the OA cavity.[145,150] The enhanced stability of the 1:1 complex formed by MePy with OA by an order of magnitude compared to Py and PyMeOH is explained by the anchoring of the methyl group at the narrow rim of the OA cavity. The second type of 1:1 complex is formed when the methyl or hydroxymethyl group of the encapsulated guest point towards the wider rim of the OA molecule, exposed to the solvent molecules. In the case of PyMeOH this orientation would lead to a more stable 1:1 complex whereas in the case MePy this orientation leads to lower stability of the 1:1 complex when compared to the first type of 1:1 complex discussed above (Scheme 4.6 and Scheme 4.7). In both cases, the most stable of the two 1:1 complexes can be considered to be predominantly present in solution, and the major species contributing to the formation of the 2:1 complex is the more stable 1:1 complex.

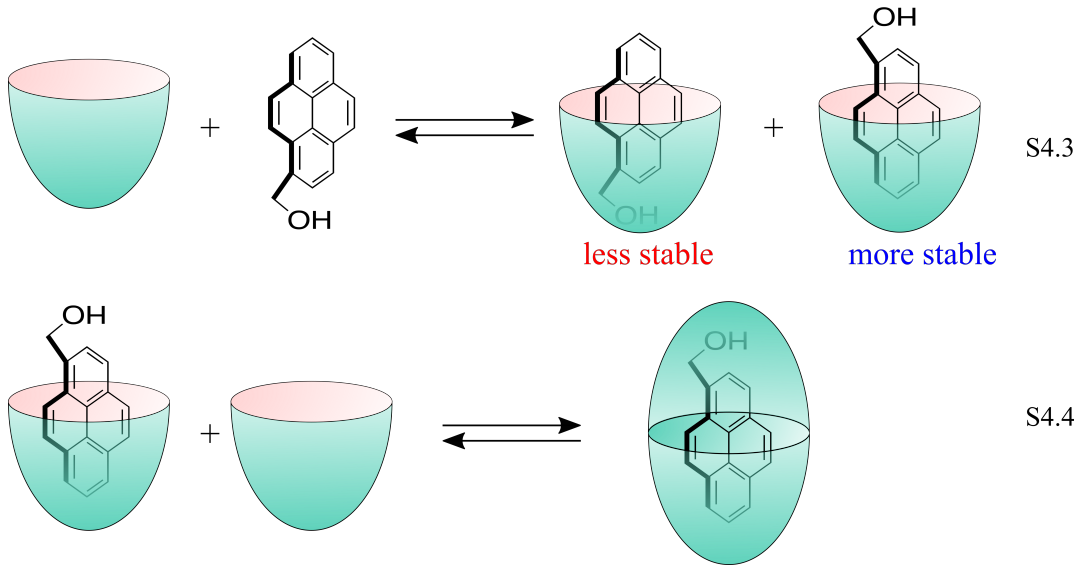

S4.3

S4.4

Scheme 4.6. The two different types of 1:1 complexes formed by PyMeOH with OA and the formation of the 2:1 complex from the more stable 1:1 complex.

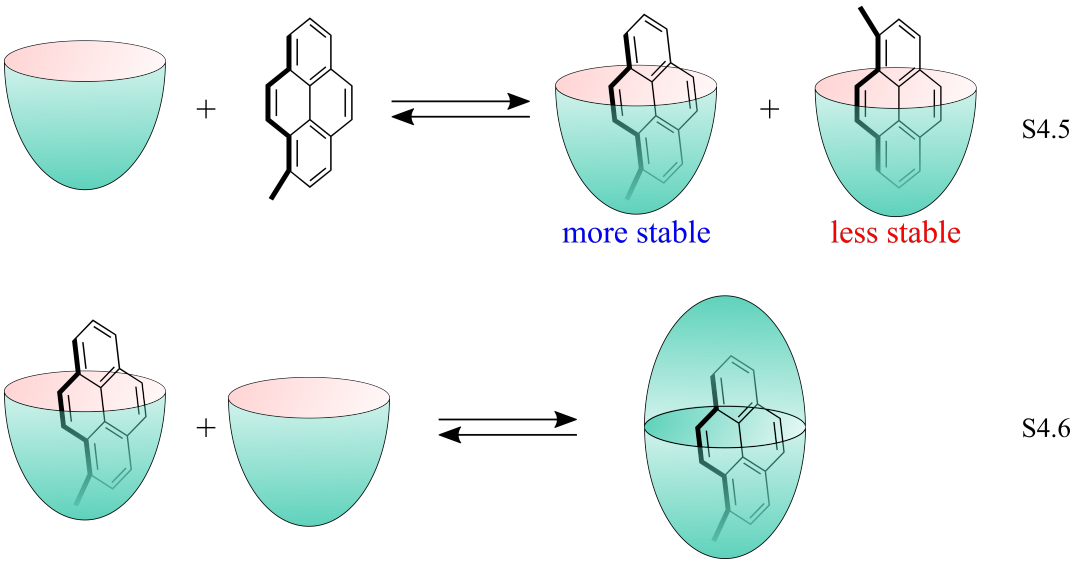

S4.5

S4.6

Scheme 4.7. The two different types of 1:1 complexes formed by MePy with OA and the formation of the 2:1 complex from the more stable 1:1 complex.

Simulations performed using the individual equilibrium binding constants listed in Table 4.4 reveal that the relative concentrations of the 1:1 complex species is highest in the case of MePy compared to either Py or PyMeOH (Figure 4.20). The anchoring of methyl group in the OA cavity increases the binding constant for the formation of the 1:1 complex for MePy leading to higher concentration ratio for the 1:1 complex and the free guest in solution especially at lower OA concentrations. This appreciable amount of 1:1 complex is responsible for the inadequate fits obtained for an overall equilibrium binding model (β_{21}) for MePy. Even though better fits were obtained when the 1:1 complex formation was taken into account, the small systematic deviation seen in the residuals for the fitting of the binding isotherms can be explained by the formation of the two different 1:1 complex formed. The formation of the less stable 1:1 complex for MePy can be assumed to have a maximum equilibrium binding constant of 1.3×10^5 M^{-1} which is the binding constant for the stable 1:1 complex for PyMeOH with OA. Incorporating the binding step for the less stable 1:1 complex formation in the fitting of binding isotherm for MePy resulted in the insensitivity of the fit to the change in parameters during the fitting process. Owing to the lower binding constant for Py and PyMeOH compared to MePy, the amount of 1:1 complex formed is much smaller and the respective binding isotherms could be adequately fit to a 2:1 overall equilibrium binding model.

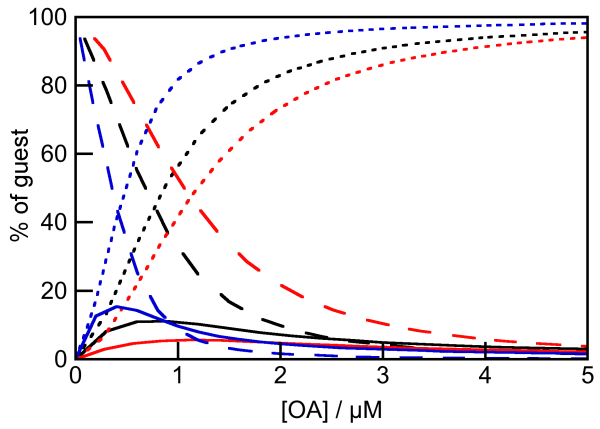

Figure 4.20. The percentage of guest free in solution (long dashed lines), in 1:1 complex (solid lines) and 2:1 complex (short dashed lines) with increasing OA concentration for Py (black), PyMeOH (red) and MePy (blue).

The presence of a lifetime for the 1:1 complex in the fluorescence lifetime studies for MePy confirms the results obtained from the steady-state measurements. In the case of MePy at lower concentrations of OA, considerable amount of the 1:1 complex is present in the system in order to be detected in the lifetime measurements. A quenching rate constant for the lifetime for the 1:1 complex intermediate to that of free MePy and the 2:1 complex suggests that the guest in the 1:1 complex is partially exposed to the solvent where the quencher can access the guest easier than the 2:1 complex. But due to the weak binding between PyMeOH and OA the amount of 1:1 complex present in the system is very low to be detected by lifetime measurements under the experimental conditions.

The presence of the transient 1:1 complexes is more evident in the kinetic data for both PyMeOH and MePy. The offset in the initial intensity for the stopped-flow traces of PyMeOH and MePy is the result of a fast relaxation process, which arises from the fast equilibrium for the 1:1 complex formation. The offset in intensity in the case of PyMeOH

is large enough for the determination of K_{11} from the data. However, no information on the dynamics for this fast equilibrium can be obtained from kinetic data. The stopped-flow traces for PyMeOH follow mono exponential kinetics that corresponds to the formation of the 2:1 complex (Figure 4.21).

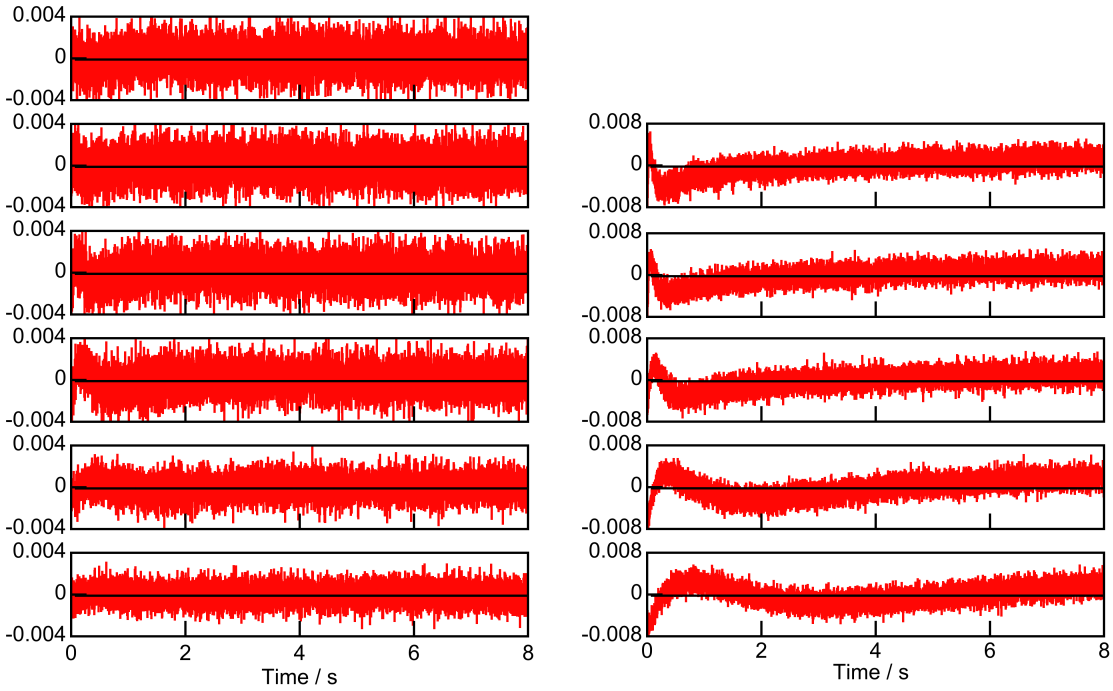

Figure 4.21. Residuals for the fits of the increasing intensity stopped-flow traces for PyMeOH (left) and MePy (right) to a mono exponential function. From bottom to top panels OA concentration increases from 0.7 to 5 μM for PyMeOH and 1 to 5 μM for MePy.

In the case of MePy, the offset in intensity was smaller in magnitude compared to PyMeOH and fitting the stopped-flow traces to mono exponential kinetics gave residuals with large systematic deviations (Figure 4.21). The traces could be fit well to the sum of

two exponentials, which indicates that there are two relaxation processes observable in the system. Following the discussion of the stability of the different 1:1 complexes formed by MePy, the equilibrium leading to the offset in the initial intensity arises from the formation of the less stable 1:1 complex whereas one of the relaxation processes observed in the stopped-flow traces can be attributed to the more stable 1:1 complex for MePy with a higher binding constant. The second relaxation process is explained by the 2:1 complex formation. However, the relaxation process cannot be equated with the observed rate constants recovered from the kinetics because the sequential reactions are coupled. The data has to be fit to the mechanism proposed. A good fit for the stopped-flow traces to the mechanism shown in Scheme 4.5 where the formation of the less stable complex was considered to be in fast equilibrium and the formation of the more stable 1:1 complex and the 2:1 complex was assumed to be slower further supports the presence of three complexes and the sequential mechanism proposed. Introduction of dissociation rate constants for the formation of the 1:1 complexes and the 2:1 complex led to the recovery of random numbers for the dissociation rate constant values probably due to their very small values. The calculation of the dissociation rate constant for the 1:1 complex formation from the kinetic and steady-state results revealed that the introduction of a methyl group on pyrene brings about a very slow dissociation rate constant for the more stable 1:1 complex. The decrease in the dissociation rate constant is from at least 1,000 s^{-1}, the time-resolution of the stopped-flow for pyrene to 0.13 s^{-1} for MePy showing that the "anchoring effect" of a single methyl group is very significant.

Due to the complexity in the dynamics introduced by the methyl group in MePy accurate determination of the dissociation rate constant for the 2:1 complexation was not

possible for this guest. An order of magnitude increase for the association rate constant for the formation of the 2:1 complex from the less stable complex compared to the more stable 1:1 complex shows the increase in stability of the complex formed when methyl group anchored at the narrow rim of the OA molecule. The mechanism of dissociation for the 2:1 complex in the case of MePy can be rationalized as follows. The steady-state and stopped-flow fluorescence measurements have proved beyond doubt that the anchoring of methyl group in OA cavity increases the stability of the complex formed. The major pathway leading to the dissociation of the 2:1 complex can thus be considered to happen from the opposite side of the anchoring of methyl group (major pathway, Scheme 4.8). A similar capsule opening time as that of pyrene can be assumed in the case of MePy since the OA molecule coming off the 2:1 complex experiences similar environment in the case of MePy and Py.

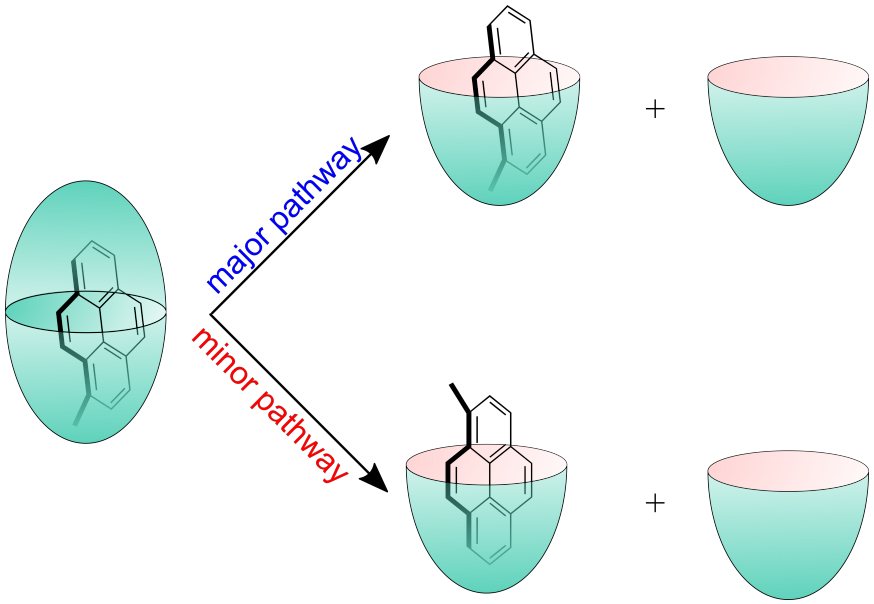

Scheme 4.8. Proposed mechanism for the dissociation of the 2:1 capsule complex for MePy with OA.

Table 4.5. Association and dissociation rate constant parameters obtained experimentally for the formation of 2:1 complex for the guests with OA.

Guest	k_{21}^{+} / 10^6 M^{-1} s^{-1}	k_{21}^{-} / s^{-1}
Py[a]	2.6 ± 0.2	0.37 ± 0.06
PyMeOH	4.8 ± 0.7	0.77 ± 0.02
MePy	6.8 ± 0.1 ($^1k_{21}^{+}$) 0.15 ± 0.01 ($^2k_{21}^{+}$)	-

[a] the values for Py were taken from previous work.[155]

The association and dissociation rate constant parameters for the formation of the 2:1 complex for all the three guests with OA are summarized in Table 4.5. The trend in the dissociation rate constants for Py, PyMeOH and MePy parallels the hydrophobicity of the guest. Where Py had a capsule opening time of 2.7 s, the dissociation of the capsule with PyMeOH as the guest happens almost twice as fast. The faster dissociation for PyMeOH is likely due to the position of the hydroxyl group at the wide opening where the two half-capsules join. Access of water to the region where the two half-capsules join is likely to be possible during the partial opening, or breathing motion, which was shown to occurs in microseconds.[149] The hydration of the hydroxyl group can then provide a driving force for the capsule to open faster followed by the fast exit of the pyrene moiety

from the 1:1 complex.[155] On the other hand the capsule opening time for MePy could be compared to that of Py assuming that the capsule opens from the side that does not have the methyl substituent, which must be similar in the case of Py and MePy. One of the association rate constants for the formation 2:1 complex for MePy and the association rate constant for the formation of PyMeOH are of the same order of magnitude compared to that of pyrene. However, the second association rate constant for MePy where the 2:1 complex is formed from the more stable 1:1 complex, the association rate constant is an order of magnitude lower compared to other association rate constant.

In the case of the complex formed by MePy, the dissociation of the capsule corresponds to the release of the guest from the capsule into water. In the case of Py, the guest is released in 2.7 s when one of the capping OA molecules dissociates. The opening of the capsule in the case of MePy from the side that does not contain the methyl group (major pathway, Scheme 4.8) can be assumed to happen on the same time scale as that for Py. Since the capsule opening on the side of the guest that does not contain the methyl group is faster than the capsule opening on the side of the methyl group (minor pathway, Scheme 4.8), the rate-determining step in the dissociation of the complex is the exit rate of MePy from the 1:1 complex. The dissociation rate constant corresponding to the exit of MePy from the 1:1 complex corresponds to ca. 8 s which is almost three times slower than the capsule dissociation for Py. Thus comparing the three guests, the dissociation of the capsulle for PyMeOH and MePy are faster and slower respectively compared to Py.

4.5 Conclusion

Equilibrium and kinetic studies were performed on two unsymmetrical pyrene derivatives to understand the complex formation of these molecules with OA. OA usually forms only 2:1 capsule complexes with large neutral molecules. The major technique used widely in the characterization of these complexes is NMR and requires high reagent concentrations, which prevents the observation of any transient species in solution. The more sensitive fluorescence techniques revealed the presence of 1:1 complexes for these large neutral guest molecules with OA. The results show that the substituents on pyrene can largely affect the binding dynamics of the guest with OA. Where Py molecule has a residence time of 2.7 s in the OA capsule, the addition of a hydrophilic hydroxymethyl group to pyrene decreases the residence time to 1.3 s inside the capsule. The addition of a hydrophobic methyl group increases the stability of the 1:1 complex from which the 2:1 complex is formed by decreasing the dissociation dynamics for the 1:1 complex.

Summary

The overarching theme of this thesis is the exploration of mechanistic diversity exhibited by supramolecular host-guest systems. The dynamics leading to two different aspects of CB[7]-guest chemistry that could have potential applications were probed in two of the projects. Structural variations of guests leading to different binding dynamics for OA, which are a relatively new class of supramolecular hosts finding wide applications in supramolecular photochemical reactions, were explored in the third project.

The projects described in this thesis give a better understanding on the complexity of supramolecular systems, which can only be understood well by probing the dynamics of the system. The dynamic studies on the complexation of AH^+ with CB[7] reveals a triangular mechanism involving the free guest and the guest in an exclusion and inclusion complex with the host. These studies also revealed the mechanism leading to pK_a shift for the guest molecule upon binding with CB[7]. The presence of sodium ions brought about a switch in the mechanism of binding with CB[7] for the guest, Ph-A-Np with two different binding sites. Sodium ions, usually known to weaken and slow down the binding of guests with CB[7] was found to stabilize the complex formation for the 2:1 complex in this particular case. Modulation of the capsule opening time releasing the guest for OA-guest system was found to happen by changing the substituents on the guest.

Supramolecular systems are used increasingly in functional materials where complex functions are achieved by the different “compartments” of the supramolecular systems working together. Dynamic studies leading to the understanding of functions achieved by

these supramolecular systems is of utmost importance for the design of such functional materials. The studies presented in this thesis lay the groundwork for understanding the mechanism behind the complex formation of some supramolecular systems that can have applications in acid-base catalysis, drug delivery and photochemistry in nano containers.

References

(1) Steed, J. W.; Turner, D. R.; Wallace, K. J. *Core concepts in supramolecular chemistry and nanochemistry*; Wiley, 2007.

(2) Lehn, J. M. *Chemical Society Reviews* **2007**, *36*, 151.

(3) Lehn, J. M. *Supramolecular chemistry: concepts and perspectives*; VCH: Weinheim ; Cambridge, 1995.

(4) Atwood, J. L. *Comprehensive supramolecular chemistry*; Pergamon: Oxford, 1996.

(5) Lehn, J. M. *Proceedings of the National Academy of Sciences* **2002**, *99*, 4763.

(6) Pedersen, C. J. *Journal of the American Chemical Society* **1967**, *89*, 7017.

(7) Pedersen, C. J. *Journal of the American Chemical Society* **1967**, *89*, 2495.

(8) Pedersen, C. J. *Journal of the American Chemical Society* **1970**, *92*, 386.

(9) Pedersen, C. J.; Frensdorff, H. K. *Angewandte Chemie International Edition* **1972**, *11*, 16.

(10) Lehn, J. M. *Angewandte Chemie International Edition* **1988**, *27*, 89.

(11) Dietrich, B.; Lehn, J. M.; Sauvage, J. P. *Tetrahedron Letters* **1969**, *10*, 2885.

(12) Dietrich, B.; Lehn, J. M.; Sauvage, J. P. *Tetrahedron* **1973**, *29*, 1647.

(13) Cram, D. J.; Kaneda, T.; Helgeson, R. C.; Lein, G. M. *Journal of the American Chemical Society* **1979**, *101*, 6752.

(14) Trueblood, K. N.; Knobler, C. B.; Maverick, E.; Helgeson, R. C.; Brown, S. B.; Cram, D. J. *Journal of the American Chemical Society* **1981**, *103*, 5594.

(15) Uhlenheuer, D. A.; Petkau, K.; Brunsveld, L. *Chemical Society Reviews* **2010**, *39*, 2817.

(16) Yeates, T. O.; Padilla, J. E. *Current Opinion in Structural Biology* **2002**, *12*, 464.

(17) Liu, Y.; Chen, Y. *Accounts of Chemical Research* **2006**, *39*, 681.

(18) Peczuh, M. W.; Hamilton, A. D. *Chemical Reviews* **2000**, *100*, 2479.

(19) Mammen, M.; Choi, S. K.; Whitesides, G. M. *Angewandte Chemie International Edition* **1998**, *37*, 2754.

(20) Haag, R. *Angewandte Chemie International Edition* **2004**, *43*, 278.

(21) Li, J.; Loh, X. J. *Advanced Drug Delivery Reviews* **2008**, *60*, 1000.

(22) Ueno, M.; Murakami, A.; Makino, K.; Morii, T. *Journal of the American Chemical Society* **1993**, *115*, 12575.

(23) Raynal, M.; Ballester, P.; Vidal-Ferran, A.; van Leeuwen, P. W. N. M. *Chemical Society Reviews* **2014**, *43*, 1734.

(24) Brown, C. J.; Toste, F. D.; Bergman, R. G.; Raymond, K. N. *Chemical Reviews* **2015**, *115*, 3012.

(25) Giansante, C.; Ceroni, P.; Balzani, V.; Vögtle, F. *Angewandte Chemie International Edition* **2008**, *47*, 5422.

(26) Kroon, J.; Oliver, A. M.; Paddon-Row, M. N.; Verhoeven, J. W. *Journal of the American Chemical Society* **1990**, *112*, 4868.

(27) Ward, M. D. *Chemical Society Reviews* **1997**, *26*, 365.

(28) Fabbrizzi, L.; Poggi, A. *Chemical Society Reviews* **1995**, *24*, 197.

(29) You, L.; Zha, D.; Anslyn, E. V. *Chemical Reviews* **2015**, *115*, 7840.

(30) Okamoto, A.; Tanaka, K.; Saito, I. *Journal of the American Chemical Society* **2004**, *126*, 9458.

(31) Liu, G. F.; Ji, W.; Feng, C. L. *Langmuir* **2015**, *31*, 7122.

(32) Maligaspe, E.; D'Souza, F. *Organic Letters* **2010**, *12*, 624.

(33) Hasenknopf, B.; Lehn, J. M.; Boumediene, N.; Dupont-Gervais, A.; Van Dorsselaer, A.; Kneisel, B.; Fenske, D. *Journal of the American Chemical Society* **1997**, *119*, 10956.

(34) Langner, A.; Tait, S. L.; Lin, N.; Rajadurai, C.; Ruben, M.; Kern, K. *Proceedings of the National Academy of Sciences* **2007**, *104*, 17927.

(35) Bohne, C. *Langmuir* **2006**, *22*, 9100.

(36) Bohne, C. *Chemical Society Reviews* **2014**, *43*, 4037.

(37) Pace, T. C. S.; Bohne, C. In *Advances in Physical Organic Chemistry*; Richard, J. P., Ed.; Academic Press: **2007**; Vol. Volume 42, p 167.

(38) Webber, M. J.; Appel, E. A.; Meijer, E. W.; Langer, R. *Nature Materials* **2016**, *15*, 13.

(39) Bernasconi, C. F. *Relaxation Kinetics*; Academic Press, Inc.: New York, 1976.

(40) Eigen, M. In *Nobel lectures in chemistry*; Elsevier: Amsterdam, 1972, p 170.

(41) Caldin, E. F. *Fast Reactions in Solution*; Wiley, 1964.

(42) Berger, R. L.; Balko, B.; Borcherdt, W.; Friauf, W. *Review of Scientific Instruments* **1968**, *39*, 486.

(43) Robinson, B. H. In *Chemical and Biological Applications of Relaxation Spectrometry*.; Wyn-Jones, E., Ed.; Springer Netherlands: 1975, p 41.

(44) Bohne, C. In *Supramolecular Photochemistry: Controlling Photochemical Processes*; John Wiley & Sons, Inc.: **2011**, p 1.

(45) Breusegem, S. Y.; Sadat-Ebrahimi, S. E.; Douglas, K. T.; Clegg, R. M.; Loontiens, F. G. *Journal of Molecular Biology* **2001**, *308*, 649.

(46) Crooks, J. E. *Journal of Physics E: Scientific Instruments* **1983**, *16*, 1142.

(47) Thurn, T.; Bloor, D. M.; Wyn-Jones, E. In *Mixed Surfactant Systems, Second Edition*; CRC Press: 2004.

(48) Verrall, R. E. *Chemical Society Reviews* **1995**, *24*, 135.

(49) Eaton, D. F. *Pure and Applied Chemistry* **1990**, *62*, 1631.

(50) Holden, D. A. In *Handbook of Organic Photochemistry*; Scaiano, J. C., Ed.; CRC Press: 1989; Vol. I, p 261.

(51) O'Connor, D. V.; Phillips, D. *Time-Correlated Single Photon Counting*; Academic Press: Orlando, 1984.

(52) Birch, D. J. S.; Imhof, R. E. In *Topics in Fluorescence Spectroscopy*; Lakowicz, J., Ed.; Plenum Press: **1991**; Vol. 1, p 1.

(53) Lakowicz, J. R. *Principles of Fluorescence Spectroscopy*; Plenum Press: New York, 1983.

(54) Kleinman, M. H.; Bohne, C. In *Molecular and Supramolecular Photochemistry*; Ramamurthy, V., Schanze, K. S., Eds.; Marcel Dekker Inc.: New York, **1997**; Vol. 1, p 391.

(55) Bohne, C.; Redmond, R. W.; Scaiano, J. C. In *Photochemistry in Organized and Constrained Media*; Ramamurthy, V., Ed.; VCH Publishers: New York, 1991, p 79.

(56) Almgren, M.; Grieser, F.; Thomas, J. K. *Journal of the American Chemical Society* **1979**, *101*, 279.

(57) Rinco, O.; Nolet, M.-C.; Ovans, R.; Bohne, C. *Photochemical & Photobiological Sciences* **2003**, *2*, 1140.

(58) Turro, N. J.; Okubo, T.; Chung, C. J. *Journal of the American Chemical Society* **1982**, *104*, 1789.

(59) Scaiano, J. C. In *Reactive Intermediate Chemistry*; Moss, R. A., Platz, M. S., Jonnes Jr., M., Eds.; John Wiley and Sons: 2004, p 847.

(60) Gösch, M.; Rigler, R. *Advanced Drug Delivery Reviews* **2005**, *57*, 169.

(61) Webb, W. W. In *Fluorescence Correlation Spectroscopy*; Rigler, R., Elson, E. S., Eds.; Springer: Berlin, 2001, p 305.

(62) Widengren, J. In *Fluorescence Correlation Spectroscopy*; Rigler, R., Elson, E. S., Eds.; Springer: Berlin, 2001, p 277.

(63) Freeman, R. *A handbook of nuclear magnetic resonance*; Longman Scientific & Technical; Wiley: Harlow, Essex, England, New York, 1987.

(64) Perrin, C. L.; Dwyer, T. J. *Chemical Reviews* **1990**, *90*, 935.

(65) Schuck, P. *Annual Review of Biophysics and Biomolecular Structure* **1997**, *26*, 541.

(66) Green, R. J.; Frazier, R. A.; Shakesheff, K. M.; Davies, M. C.; Roberts, C. J.; Tendler, S. J. B. *Biomaterials* **2000**, *21*, 1823.

(67) Hartley, J. H.; James, T. D.; Ward, C. J. *Journal of the Chemical Society, Perkin Transactions 1* **2000**, 3155.

(68) Perry, J. J. B.; Kilburn, J. D. *Contemporary Organic Synthesis* **1997**, *4*, 61.

(69) Stoddart, J. F. *Annual Reports Section "B" (Organic Chemistry)* **1983**, *80*, 353.

(70) Diederich, F. *Cyclophanes*; Royal Society of Chemistry: Cambridge, 1991.

(71) Forman, J. E.; Barrans, R. E.; Dougherty, D. A. *Journal of the American Chemical Society* **1995**, *117*, 9213.

(72) Crini, G. *Chemical Reviews* **2014**, *114*, 10940.

(73) Del Valle, E. M. M. *Process Biochemistry* **2004**, *39*, 1033.

(74) Böhmer, V. *Angewandte Chemie International Edition* **1995**, *34*, 713.

(75) Zheng, Y. S.; Luo, J. *Journal of Inclusion Phenomena and Macrocyclic Chemistry* **2011**, *71*, 35.

(76) Rudkevich, D. M.; Rebek, J. J. *European Journal of Organic Chemistry* **1999**, *1999*, 1991.

(77) Schneider, H. J.; Schneider, U. *Journal of inclusion phenomena and molecular recognition in chemistry* **1994**, *19*, 67.

(78) Brotin, T.; Dutasta, J. P. *Chemical Reviews* **2009**, *109*, 88.

(79) Holman, K. T. In *Encyclopedia of Supramolecular Chemistry*; Taylor & Francis: 2007; Vol. 1, p 340.

(80) Behrend, R.; Meyer, E.; Rusche, F. *Justus Liebig's Annalen der Chemie* **1905**, *339*, 1.

(81) Freeman, W. A.; Mock, W. L.; Shih, N. Y. *Journal of the American Chemical Society* **1981**, *103*, 7367.

(82) Biedermann, F.; Uzunova, V. D.; Scherman, O. A.; Nau, W. M.; De Simone, A. *Journal of the American Chemical Society* **2012**, *134*, 15318.

(83) Biedermann, F.; Vendruscolo, M.; Scherman, O. A.; De Simone, A.; Nau, W. M. *Journal of the American Chemical Society* **2013**, *135*, 14879.

(84) Rekharsky, M. V.; Mori, T.; Yang, C.; Ko, Y. H.; Selvapalam, N.; Kim, H.; Sobransingh, D.; Kaifer, A. E.; Liu, S.; Isaacs, L.; Chen, W.; Moghaddam, S.; Gilson, M. K.; Kim, K.; Inoue, Y. *Proceedings of the National Academy of Sciences* **2007**, *104*, 20737.

(85) Green, N. M. *Biochemical Journal* **1963**, *89*, 585.

(86) Cao, L.; Šekutor, M.; Zavalij, P. Y.; Mlinarić-Majerski, K.; Glaser, R.; Isaacs, L. *Angewandte Chemie International Edition* **2014**, *53*, 988.

(87) Mock, W. L.; Irra, T. A.; Wepsiec, J. P.; Adhya, M. *The Journal of Organic Chemistry* **1986**, *54*, 5302.

(88) Parvari, G.; Reany, O.; Keinan, E. *Israel Journal of Chemistry* **2011**, *51*, 646.

(89) Pemberton, B. C.; Raghunathan, R.; Volla, S.; Sivaguru, J. *Chemistry - A European Journal* **2012**, *18*, 12178.

(90) Assaf, K. I.; Nau, W. M. *Chemical Society Reviews* **2015**, *44*, 394.

(91) Wang, R.; Yuan, L.; Macartney, D. H. *The Journal of Organic Chemistry* **2006**, *71*, 1237.

(92) Zheng, L.; Sonzini, S.; Ambarwati, M.; Rosta, E.; Scherman, O. A.; Herrmann, A. *Angewandte Chemie International Edition* **2015**, *54*, 13007.

(93) Vallavoju, N.; Sivaguru, J. *Chemical Society Reviews* **2014**, *43*, 4084.

(94) Gadde, S.; Batchelor, E. K.; Weiss, J. P.; Ling, Y.; Kaifer, A. E. *Journal of the American Chemical Society* **2008**, *130*, 17114.

(95) Das, D.; Scherman, O. A. *Israel Journal of Chemistry* **2011**, *51*, 537.

(96) Hennig, A.; Bakirci, H.; Nau, W. M. *Nature Methods* **2007**, *4*, 629.

(97) Dsouza, R. N.; Hennig, A.; Nau, W. M. *Chemistry - A European Journal* **2012**, *18*, 3444.

(98) Ghale, G.; Nau, W. M. *Accounts of Chemical Research* **2014**, *47*, 2150.

(99) Kim, K.; Selvapalam, N.; Ko, Y. H.; Park, K. M.; Kim, D.; Kim, J. *Chemical Society Reviews* **2007**, *36*, 267.

(100) Macartney, D. H. *Israel Journal of Chemistry* **2011**, *51*, 600.

(101) Walker, S.; Oun, R.; McInnes, F. J.; Wheate, N. J. *Israel Journal of Chemistry* **2011**, *51*, 616.

(102) Ghosh, I.; Nau, W. M. *Advanced Drug Delivery Reviews* **2012**, *64*, 764.

(103) Jiang, W.; Wang, Q.; Linder, I.; Klautzsch, F.; Schalley, C. A. *Chemistry – A European Journal* **2011**, *17*, 2344.

(104) Liu, S.; Ruspic, C.; Mukhopadhyay, P.; Chakrabarti, S.; Zavalij, P. Y.; Isaacs, L. *Journal of the American Chemical Society* **2005**, *127*, 15959.

(105) Mukhopadhyay, P.; Zavalij, P. Y.; Isaacs, L. *Journal of the American Chemical Society* **2006**, *128*, 14093.

(106) Rekharsky, M. V.; Yamamura, H.; Ko, Y. H.; Selvapalam, N.; Kim, K.; Inoue, Y. *Chemical Communications* **2008**, 2236.

(107) Barrow, S. J.; Kasera, S.; Rowland, M. J.; del Barrio, J.; Scherman, O. A. *Chemical Reviews* **2015**, *115*, 12320.

(108) Dsouza, R. N.; Pischel, U.; Nau, W. M. *Chemical Reviews* **2011**, *111*, 7941.

(109) Jeon, Y. M.; Kim, J.; Whang, D.; Kim, K. *Journal of the American Chemical Society* **1996**, *118*, 9790.

(110) Kim, J.; Jung, I. S.; Kim, S. Y.; Lee, E.; Kang, J. K.; Sakamoto, S.; Yamaguchi, K.; Kim, K. *Journal of the American Chemical Society* **2000**, *122*, 540.

(111) Day, A. I.; Blanch, R. J.; Arnold, A. P.; Lorenzo, S.; Lewis, G. R.; Dance, I. *Angewandte Chemie International Edition* **2002**, *41*, 275.

(112) Liu, S.; Zavalij, P. Y.; Isaacs, L. *Journal of the American Chemical Society* **2005**, *127*, 16798.

(113) Lee, J. W.; Samal, S.; Selvapalam, N.; Kim, H.-J.; Kim, K. *Accounts of Chemical Research* **2003**, *36*, 621.

(114) Karcher, S.; Kornmueller, A.; Jekel, M. *Acta Hydrochimica et Hydrobiologica* **1999**, *27*, 38.

(115) Buschmann, H. J.; Jansen, K.; Meschke, C.; Schollmeyer, E. *Journal of Solution Chemistry* **1998**, *27*, 135.

(116) Mock, W. L.; Pierpont, J. *Journal of the Chemical Society Chemical Communications* **1990**, 1509.

(117) Barooah, N.; Mohanty, J.; Pal, H.; Bhasikuttan, A. C. *Proceedings of the National Academy of Sciences, India Section A: Physical Sciences* **2014**, *84*, 1.

(118) Saleh, N.; Koner, A. L.; Nau, W. M. *Angewandte Chemie International Edition* **2008**, *47*, 5398.

(119) Barooah, N.; Sundararajan, M.; Mohanty, J.; Bhasikuttan, A. C. *The Journal of Physical Chemistry B* **2014**, *118*, 7136.

(120) Pischel, U.; Uzunova, V. D.; Remon, P.; Nau, W. M. *Chemical Communications* **2010**, *46*, 2635.

(121) Buschmann, H. J.; Cleve, E.; Jansen, K.; Wego, A.; Schollmeyer, E. *Journal of Inclusion Phenomena and Macrocyclic Chemistry* **2001**, *40*, 117.

(122) Buschmann, H. J.; Cleve, E.; Schollmeyer, E. *Inorganica Chimica Acta* **1992**, *193*, 93.

(123) Hoffmann, R.; Knoche, W.; Fenn, C.; Buschmann, H. J. *Journal of the Chemical Society, Faraday Transactions* **1994**, *90*, 1507.

(124) Megyesi, M.; Biczok, L.; Jablonkai, I. *The Journal of Physical Chemistry C* **2008**, *112*, 3410.

(125) Ong, W.; Kaifer, A. E. *The Journal of Organic Chemistry* **2004**, *69*, 1383.

(126) Rekharsky, M. V.; Ko, Y. H.; Selvapalam, N.; Kim, K.; Inoue, Y. *Supramolecular Chemistry* **2007**, *19*, 39.

(127) Shaikh, M.; Mohanty, J.; Bhasikuttan, A. C.; Uzunova, V. D.; Nau, W. M.; Pal, H. *Chemical Communications* **2008**, 3681.

(128) Wyman, I. W.; Macartney, D. H. *Organic & Biomolecular Chemistry* **2008**, *6*, 1796.

(129) Marquez, C.; Nau, W. M. *Angewandte Chemie International Edition* **2001**, *40*, 3155.

(130) Shaikh, M.; Mohanty, J.; Singh, P. K.; Nau, W. M.; Pal, H. *Photochemical & Photobiological Sciences* **2008**, *7*, 408.

(131) Jansen, K.; Buschmann, H. J.; Wego, A.; Dopp, D.; Mayer, C.; Drexler, H. J.; Holdt, H. J.; Schollmeyer, E. *Journal of Inclusion Phenomena and Macrocyclic Chemistry* **2001**, *39*, 357.

(132) Lagona, J.; Mukhopadhyay, P.; Chakrabarti, S.; Isaacs, L. *Angewandte Chemie International Edition* **2005**, *44*, 4844.

(133) Whang, D.; Heo, J.; Park, J. H.; Kim, K. *Angewandte Chemie International Edition* **1998**, *37*, 78.

(134) Márquez, C.; Hudgins, R. R.; Nau, W. M. *Journal of the American Chemical Society* **2004**, *126*, 5806.

(135) Neugebauer, R.; Knoche, W. *Journal of the Chemical Society, Perkin Transactions 2* **1998**, 529.

(136) Tang, H.; Fuentealba, D.; Ko, Y. H.; Selvapalam, N.; Kim, K.; Bohne, C. *Journal of the American Chemical Society* **2011**, *133*, 20623.

(137) Barrett, K. E.; Ganong, W. *Ganong's review of medical physiology*; 24th ed.; McGraw Hill Medical: New York ; London, 2012.

(138) Mezzina, E.; Cruciani, F.; Pedulli, G. F.; Lucarini, M. *Chemistry - A European Journal* **2007**, *13*, 7223.

(139) Gibb, C. L. D.; Gibb, B. C. *Journal of the American Chemical Society* **2004**, *126*, 11408.

(140) Gibb, C. L. D.; Li, X.; Gibb, B. C. *Proceedings of the National Academy of Sciences* **2002**, *99*, 4857.

(141) Gibb, B. C. *Chemistry – A European Journal* **2003**, *9*, 5180.

(142) Li, X.; Upton, T. G.; Gibb, C. L. D.; Gibb, B. C. *Journal of the American Chemical Society* **2003**, *125*, 650.

(143) Gibb, C. L. D.; Gibb, B. C. *Journal of the American Chemical Society* **2006**, *128*, 16498.

(144) Ramamurthy, V.; Jockusch, S.; Porel, M. *Langmuir* **2015**, *31*, 5554.

(145) Jayaraj, N.; Zhao, Y. P.; Parthasarathy, A.; Porel, M.; Liu, R. S. H.; Ramamurthy, V. *Langmuir* **2009**, *25*, 10575.

(146) Podkoscielny, D.; Philip, I.; Gibb, C. L. D.; Gibb, B. C.; Kaifer, A. E. *Chemistry – A European Journal* **2008**, *14*, 4704.

(147) Kaanumalle, L. S.; Gibb, C. L. D.; Gibb, B. C.; Ramamurthy, V. *Journal of the American Chemical Society* **2004**, *126*, 14366.

(148) Kaanumalle, L. S.; Gibb, C. L. D.; Gibb, B. C.; Ramamurthy, V. *Journal of the American Chemical Society* **2005**, *127*, 3674.

(149) Jayaraj, N.; Jockusch, S.; Kaanumalle, L. S.; Turro, N. J.; Ramamurthy, V. *Canadian Journal of Chemistry* **2011**, *89*, 203.

(150) Choudhury, R.; Barman, A.; Prabhakar, R.; Ramamurthy, V. *The Journal of Physical Chemistry B* **2013**, *117*, 398.

(151) Ramamurthy, V. *Accounts of Chemical Research* **2015**, *48*, 2904.

(152) Parthasarathy, A.; Ramamurthy, V. *Journal of Photochemistry and Photobiology A: Chemistry* **2016**, *317*, 132.

(153) Parthasarathy, A.; Kaanumalle, L. S.; Ramamurthy, V. *Organic Letters* **2007**, *9*, 5059.

(154) Parthasarathy, A.; Ramamurthy, V. *Photochemical & Photobiological Sciences* **2011**, *10*, 1455.

(155) Tang, H.; de Oliveira, C. S.; Sonntag, G.; Gibb, C. L. D.; Gibb, B. C.; Bohne, C. *Journal of the American Chemical Society* **2012**, *134*, 5544.

(156) Thomas, S. S.; Bohne, C. *Faraday Discussions* **2015**, *185*, 381.

(157) Klöck, C.; Dsouza, R. N.; Nau, W. M. *Organic Letters* **2009**, *11*, 2595.

(158) Basilio, N.; García-Río, L.; Moreira, J. A.; Pessêgo, M. *The Journal of Organic Chemistry* **2010**, *75*, 848.

(159) Wang, R.; Macartney, D. H. *Organic & Biomolecular Chemistry* **2008**, *6*, 1955.

(160) Koner, A. L.; Ghosh, I.; Saleh, N. i.; Nau, W. M. *Canadian Journal of Chemistry* **2011**, *89*, 139.

(161) Li, S.; Yin, H.; Wyman, I. W.; Zhang, Q.; Macartney, D. H.; Wang, R. *The Journal of Organic Chemistry* **2016**, *81*, 1300.

(162) Barooah, N.; Mohanty, J.; Pal, H.; Bhasikuttan, A. C. *The Journal of Physical Chemistry B* **2012**, *116*, 3683.

(163) Hoffmann, R.; Knoche, W.; Fenn, C.; Buschmann, H. J. *Journal of the Chemical Society, Faraday Transactions* **1994**, *90*, 1507.

(164) Márquez, C.; Hudgins, R. R.; Nau, W. M. *Journal of the American Chemical Society* **2004**, *126*, 5806.

(165) Wang, R.; Yuan, L.; Macartney, D. H. *Chemical Communications* **2005**, 5867.

(166) Schulman, S. G.; Kovi, P. J.; Torosian, G.; McVeigh, H.; Carter, D. *Journal of Pharmaceutical Sciences* **1973**, *62*, 1823.

(167) Rotkiewicz, K.; Grabowski, Z. R. *Transactions of the Faraday Society* **1969**, *65*, 3263.

(168) Vander Donckt, E.; Porter, G. *Transactions of the Faraday Society* **1968**, *64*, 3218.

(169) Day, A.; Arnold, A. P.; Blanch, R. J.; Snushall, B. *The Journal of Organic Chemistry* **2001**, *66*, 8094.

(170) Kim, J.; Jung, I.-S.; Kim, S.-Y.; Lee, E.; Kang, J.-K.; Sakamoto, S.; Yamaguchi, K.; Kim, K. *Journal of the American Chemical Society* **2000**, *122*, 540.

(171) Marquez, C.; Huang, F.; Nau, W. M. *IEEE Transactions on NanoBioscience* **2004**, *3*, 39.

(172) Yi, S.; Kaifer, A. E. *The Journal of Organic Chemistry* **2011**, *76*, 10275.

(173) Da Silva, J. P.; Jayaraj, N.; Jockusch, S.; Turro, N. J.; Ramamurthy, V. *Organic Letters* **2011**, *13*, 2410.

(174) Jiao, D.; Zhao, N.; Scherman, O. A. *Chemical Communications* **2010**, *2007-2009*.

(175) Nijegorodov, N.; Mabbs, R.; Winkoun, D. P. *Spectrochimica Acta Part A: Molecular and Biomolecular Spectroscopy* **2003**, *59*, 595.

(176) Miskolczy, Z.; Biczók, L. *The Journal of Physical Chemistry B* **2014**, *118*, 2499.

(177) Eigen, M. *Angewandte Chemie International Edition* **1964**, *3*, 1.

(178) Basílio, N.; Laia, C. A. T.; Pina, F. *The Journal of Physical Chemistry B* **2015**, *119*, 2749.

(179) Haouaj, M. E.; Ho Ko, Y.; Luhmer, M.; Kim, K.; Bartik, K. *Journal of the Chemical Society, Perkin Transactions 2* **2001**, 2104.

(180) Wagner, B. D.; Stojanovic, N.; Day, A. I.; Blanch, R. J. *The Journal of Physical Chemistry B* **2003**, *107*, 10741.

(181) Wei, F.; Liu, S.-M.; Xu, L.; Cheng, G.-Z.; Wu, C.-T.; Feng, Y.-Q. *Electrophoresis* **2005**, *26*, 2214.

(182) Förster, T. *Chemical Physics Letters* **1972**, *17*, 309.

(183) Tsutsumi, K.; Shizuka, H. *Chemical Physics Letters* **1977**, *52*, 485.

(184) Nau, W. M.; Mohanty, J. *International Journal of Photoenergy* **2005**, *7*, 133.

(185) Held, B.; Tang, H.; Natarajan, P.; da Silva, C. P.; de Oliveira Silva, V.; Bohne, C.; Quina, F. H. *Photochemical & Photobiological Sciences* **2016**.

(186) Da Silva, J. P.; Jayaraj, N.; Jockusch, S.; Turro, N. J.; Ramamurthy, V. *Organic Letters* **2011**, *13*, 2410.

(187) Hwang, I.; Jeon, W. S.; Kim, H.-J.; Kim, D.; Kim, H.; Selvapalam, N.; Fujita, N.; Shinkai, S.; Kim, K. *Angewandte Chemie International Edition* **2007**, *46*, 210.

(188) Pattabiraman, M.; Maddipatla, M. V. S. N.; Ramamurthy, V. *Journal of Photochemistry and Photobiology A: Chemistry* **2016**, *324*, 53.

(189) Liu, S. M.; Whisenhunt-Ioup, S. E.; Gibb, C. L. D.; Gibb, B. C. *Supramolecular Chemistry* **2011**, *23*, 480.

Appendix

A. 1. Derivation for the relationship between the observed rate constant and the concentration of CB[7] for the mechanism shown in Scheme 3.4

$$CB[7] + Na^+ \underset{}{\overset{K_1}{\rightleftharpoons}} CB[7]\bullet Na^+ \quad \text{(A 1)}$$

$$CB[7]\bullet Na^+ + Na^+ \underset{}{\overset{K_2}{\rightleftharpoons}} Na^+\bullet CB[7]\bullet Na^+ \quad \text{(A 2)}$$

$$CB[7] + \text{Ph-A-Np} \underset{k_{01}^-}{\overset{k_{01}^+}{\rightleftharpoons}} \text{Ph-AH}^+\text{-Np@CB[7]} \quad \text{(A 3)}$$

$$CB[7]\bullet Na^+ + \text{Ph-A-Np} \underset{k_{11}^-}{\overset{k_{11}^+}{\rightleftharpoons}} \text{Ph-AH}^+\text{-Np@CB[7]} + Na^+ \quad \text{(A 4)}$$

For convenience of representation in the following derivations Ph-A-Np and Ph-AH$^+$-Np are represented as G and GH$^+$ respectively. The rate equation for the formation of GH$^+$@CB[7] can be written as:

$$\frac{d\left[GH^+@CB[7]\right]}{dt} = k_{01}^+[G]\left[CB[7]\right] - k_{01}^-\left[GH^+@CB[7]\right]$$

$$+k_{11}^+[G][CB[7]\bullet Na^+] - k_{11}^-\left[GH^+@CB[7]\right][Na^+] \quad \text{(A 5)}$$

Equation A6 represents the rate equation for the formation of GH$^+$@CB[7] where a perturbation of equilibrium state happens. For any species concentration [i], the subscript "eq" and "T" represents the equilibrium and total concentrations respectively and $\Delta[i]$ represents the change in concentration of the species between the equilibrium state and time t.

$$\frac{d\left(\left[GH^{+}@CB[7]\right]_{eq}+\Delta\left[GH^{+}@CB[7]\right]\right)}{dt}=$$

$$k_{01}^{+}\left([G]_{eq}+\Delta[G]\right)\left(\left[CB[7]\right]_{eq}+\Delta\left[CB[7]\right]\right)$$

$$-k_{01}^{-}\left(\left[GH^{+}@CB[7]\right]_{eq}+\Delta\left[GH^{+}@CB[7]\right]\right)$$

$$+k_{11}^{+}\left([G]_{eq}+\Delta[G]\right)\left([CB[7]\bullet Na^{+}]_{eq}+\Delta[CB[7]\bullet Na^{+}]\right)$$

$$-k_{11}^{-}\left(\left[GH^{+}@CB[7]\right]_{eq}+\Delta\left[GH^{+}@CB[7]\right]\right)\left([Na^{+}]_{eq}+\Delta[Na^{+}]\right) \quad \text{(A 6)}$$

At equilibrium, equation A5 can be written as

$$\frac{d\left[GH^{+}@CB[7]\right]_{eq}}{dt}=$$

$$k_{01}^{+}[G]_{eq}\left[CB[7]\right]_{eq}-k_{01}^{-}\left[GH^{+}@CB[7]\right]_{eq}+k_{11}^{+}[G]_{eq}[CB[7]\bullet Na^{+}]_{eq}$$

$$-k_{11}^{-}\left[GH^{+}@CB[7]\right]_{eq}[Na^{+}]_{eq}=0 \quad \text{(A 7)}$$

Combining equations A6 and A7 equation A8 is derived

$$\frac{d\Delta\left[GH^{+}@CB[7]\right]}{dt} =$$

$$k_{01}^{+}\left(\left[CB[7]\right]_{eq}\Delta[G] + [G]_{eq}\Delta\left[CB[7]\right] + \Delta[G]\Delta\left[CB[7]\right]\right) - k_{01}^{-}\Delta\left[GH^{+}@CB[7]\right]$$

$$+k_{11}^{+}\left([G]_{eq}\,\Delta[CB[7]{\bullet}Na^{+}] + [CB[7]{\bullet}Na^{+}]_{eq}\Delta[G] + \Delta[G]\Delta[CB[7]{\bullet}Na^{+}]\right)$$

$$-k_{11}^{-}\left([Na^{+}]_{eq}\Delta\left[GH^{+}@CB[7]\right] + \left[GH^{+}@CB[7]\right]_{eq}\Delta[Na^{+}]\right.$$

$$\left. + \Delta\left[GH^{+}@CB[7]\right]\Delta[Na^{+}]\right) \quad \text{(A 8)}$$

Assuming the following inequalities and considering that the perturbations are small,

$$[Na^{+}]_{eq} \gg \Delta[Na^{+}] \quad \text{(A 9)}$$

$$\left[CB[7]\right]_{eq}\Delta[G] + [G]_{eq}\Delta\left[CB[7]\right] \gg \Delta[G]\Delta\left[CB[7]\right] \quad \text{(A 10)}$$

$$[G]_{eq}\,\Delta[CB[7]{\bullet}Na^{+}] + [CB[7]{\bullet}Na^{+}]_{eq}\Delta[G] \gg \Delta[G]\Delta[CB[7]{\bullet}Na^{+}] \quad \text{(A 11)}$$

$$\left[GH^{+}@CB[7]\right]_{eq}\Delta[Na^{+}] + \Delta\left[GH^{+}@CB[7]\right]\Delta[Na^{+}]$$

$$\ll [Na^{+}]_{eq}\Delta\left[GH^{+}@CB[7]\right] \quad \text{(A 12)}$$

Equation A8 can be re-written as:

$$\frac{d\Delta\left[GH^{+}@CB[7]\right]}{dt} = k_{01}^{+}\left(\left[CB[7]\right]_{eq}\Delta[G] + [G]_{eq}\Delta\left[CB[7]\right]\right)$$

$$-k_{01}^{-}\Delta\left[GH^{+}@CB[7]\right] + k_{11}^{+}\left([G]_{eq}\Delta[CB[7]{\bullet}Na^{+}] + [CB[7]{\bullet}Na^{+}]_{eq}\Delta[G]\right)$$

$$+ - k_{11}^{-}[Na^{+}]_{eq}\Delta\left[GH^{+}@CB[7]\right] \quad \text{(A 13)}$$

The mass balance equation for the guest and CB[7] can be written as:

$$\Delta[G] + \Delta\left[GH^{+}@CB[7]\right] = 0 \quad \text{(A 14)}$$

$$\Delta\left[CB[7]\right] + \Delta[CB[7]{\bullet}Na^{+}] + \Delta[Na^{+}{\bullet}CB[7]{\bullet}Na^{+}] + \Delta\left[GH^{+}@CB[7]\right] = 0 \quad \text{(A 15)}$$

From equation A2,

$$K_2[CB[7]{\bullet}Na^{+}][Na^{+}] = [Na^{+}{\bullet}CB[7]{\bullet}Na^{+}] \quad \text{(A 16)}$$

During perturbation from equilibrium equation A16 can be written as:

$$K_2\left([CB[7]{\bullet}Na^{+}]_{eq} + \Delta[CB[7]{\bullet}Na^{+}]\right)\left([Na^{+}]_{eq} + \Delta[Na^{+}]\right) =$$

$$[Na^{+}{\bullet}CB[7]{\bullet}Na^{+}]_{eq} + \Delta[Na^{+}{\bullet}CB[7]{\bullet}Na^{+}] \quad \text{(A 17)}$$

At equilibrium, equation A18 is valid.

$$K_2[CB[7]{\bullet}Na^{+}]_{eq}[Na^{+}]_{eq} = [Na^{+}{\bullet}CB[7]{\bullet}Na^{+}]_{eq} \quad \text{(A 18)}$$

Combining equations A17 and A18 and assuming inequalities A9 and A19, equation A20 is derived.

$$\Delta[CB[7]{\bullet}Na^{+}]\Delta[Na^{+}] + [CB[7]{\bullet}Na^{+}]_{eq}\Delta[Na^{+}] \ll [Na^{+}]_{eq}\Delta[CB[7]{\bullet}Na^{+}] \quad \text{(A 19)}$$

$$K_2[Na^{+}]_{eq}\Delta[CB[7]{\bullet}Na^{+}] = \Delta[Na^{+}{\bullet}CB[7]{\bullet}Na^{+}] \quad \text{(A 20)}$$

From equation A1,

$$K_1\left[CB[7]\right][Na^{+}] = [CB[7]{\bullet}Na^{+}] \quad \text{(A 21)}$$

During pertirbation from equilibrium and considering inequality A9, equation A21 can be witrren as:

$$K_1\left(\left[CB[7]\right]_{eq}+\Delta\left[CB[7]\right]\right)[Na^+]_{eq}=[CB[7]\bullet Na^+]_{eq}+\Delta[CB[7]\bullet Na^+] \quad \text{(A 22)}$$

At equilibrium,

$$K_1\left[CB[7]\right]_{eq}[Na^+]_{eq}=[CB[7]\bullet Na^+]_{eq} \quad \text{(A 23)}$$

Combining equations A22 and A23, equation A24 can be derived.

$$K_1\Delta\left[CB[7]\right][Na^+]_{eq}=\Delta[CB[7]\bullet Na^+] \quad \text{(A 24)}$$

Combining equations A15, A20 and A24, equation A25 is derived.

$$\frac{\Delta[CB[7]\bullet Na^+]}{K_1[Na^+]_{eq}}+\Delta[CB[7]\bullet Na^+]+K_2[Na^+]_{eq}\Delta[CB[7]\bullet Na^+] = -\Delta\left[GH^+@CB[7]\right] \quad \text{(A 25)}$$

Combining equations A13, A14 and A24 equation A25 is derived.

$$\frac{d\Delta\left[GH^+@CB[7]\right]}{dt}=$$

$$k_{01}^+\left(-\Delta\left[GH^+@CB[7]\right]\left[CB[7]\right]_{eq}+\frac{\Delta[CB[7]\bullet Na^+]}{K_1[Na^+]_{eq}}[G]_{eq}\right)$$

$$+k_{11}^+\left([G]_{eq}\Delta[CB[7]\bullet Na^+]-[CB[7]\bullet Na^+]_{eq}\Delta\left[GH^+@CB[7]\right]\right)$$

$$-\left(k_{01}^-+k_{11}^-[Na^+]_{eq}\right)\Delta\left[GH^+@CB[7]\right] \quad \text{(A 26)}$$

Combining equations A25 and A26, the following equation (A27) is derived.

$$\frac{d\Delta\left[GH^{+}@CB[7]\right]}{dt} =$$

$$k_{01}^{+}\left(-\left[CB[7]\right]_{eq} - \frac{[G]_{eq}}{\left(1 + K_1[Na^{+}]_{eq} + K_1[Na^{+}]_{eq}K_2[Na^{+}]_{eq}\right)}\right)$$

$$\Delta\left[GH^{+}@CB[7]\right] + k_{11}^{+}\left(-[CB[7]\bullet Na^{+}]_{eq} - \frac{[G]_{eq}}{1 + \frac{1}{K_1[Na^{+}]_{eq}} + K_2[Na^{+}]_{eq}}\right)$$

$$\Delta\left[GH^{+}@CB[7]\right] - \left(k_{01}^{-} + k_{11}^{-}[Na^{+}]_{eq}\right)\Delta\left[GH^{+}@CB[7]\right] \qquad \text{(A 27)}$$

The observed rate constant (k_{obs}) is now defined as:

$$\begin{aligned} k_{obs} = k_{01}^{+}&\left(\left[CB[7]\right]_{eq} + \frac{[G]_{eq}}{\left(1 + K_1[Na^{+}]_{eq} + K_1[Na^{+}]_{eq}K_2[Na^{+}]_{eq}\right)}\right) \\ &+ k_{11}^{+}\left([CB[7]\bullet Na^{+}]_{eq} + \frac{[G]_{eq}}{1 + \frac{1}{K_1[Na^{+}]_{eq}} + K_2[Na^{+}]_{eq}}\right) \\ &+ \left(k_{01}^{-} + k_{11}^{-}[Na^{+}]_{eq}\right) \end{aligned} \qquad \text{(A 28)}$$

Combining equations A28 and A23 equation A29 is derived.

$$k_{obs} = k_{01}^{+}\left(\frac{[CB[7]\bullet Na^{+}]_{eq}}{K_1[Na^{+}]_{eq}} + \frac{[G]_{eq}}{\left(1 + K_1[Na^{+}]_{eq} + K_1[Na^{+}]_{eq}K_2[Na^{+}]_{eq}\right)}\right) + k_{11}^{+}\left([CB[7]\bullet Na^{+}]_{eq} + \frac{[G]_{eq}}{1 + \frac{1}{K_1[Na^{+}]_{eq}} + K_2[Na^{+}]_{eq}}\right) + \left(k_{01}^{-} + k_{11}^{-}[Na^{+}]_{eq}\right) \quad \text{(A 29)}$$

Under the experimental conditions, the following inequality can be assumed and equation A31 can be derived.

$$[CB[7]\bullet Na^{+}]_{eq} \gg [G]_{eq} \quad \text{(A 30)}$$

$$k_{obs} = k_{01}^{+}\frac{[CB[7]\bullet Na^{+}]_{eq}}{K_1[Na^{+}]_{eq}} + k_{11}^{+}[CB[7]\bullet Na^{+}]_{eq} + \left(k_{01}^{-} + k_{11}^{-}[Na^{+}]_{eq}\right) \quad \text{(A 31)}$$

At experimental conditions where the total CB[7] concnetration, $\left[CB[7]\right]_T \gg [G]_T$, the following equation holds.

$$\left[CB[7]\right]_T = \left[CB[7]\right]_{eq} + [CB[7]\bullet Na^{+}]_{eq} + [Na^{+}\bullet CB[7]\bullet Na^{+}]_{eq} \quad \text{(A 32)}$$

At sodium ion concentrations of 2-5 mM where the experiments were performed,

$$[Na^{+}\bullet CB[7]\bullet Na^{+}]_{eq} \ll \left[CB[7]\right]_{eq} + [CB[7]\bullet Na^{+}]_{eq} \quad \text{(A 33)}$$

Thus combining equation A23 and A32, equation A34 is derived.

$$[CB[7]\bullet Na^{+}]_{eq} = \left[CB[7]\right]_T\left(\frac{K_1[Na^{+}]_{eq}}{1 + K_1[Na^{+}]_{eq}}\right) \quad \text{(A 34)}$$

Combining equations A31 and A34, equation A35 is derived

$$k_{obs} = \left(\frac{1}{1 + K_1[Na^+]_{eq}}\right)\left(k_{01}^+ + k_{11}^+ K_1[Na^+]_{eq}\right)\left[CB[7]\right]_T + \left(k_{01}^- + k_{11}^-[Na^+]_{eq}\right) \quad \text{(A 35)}$$

Equation A35 can be written as:

$$k_{obs} = k_{app}^+\left[CB[7]\right]_T + k_{app}^- \quad \text{(A 36)}$$

where,

$$k_{app}^+ = \left(\frac{1}{1 + K_1[Na^+]_{eq}}\right)\left(k_{01}^+ + k_{11}^+ K_1[Na^+]_{eq}\right) \quad \text{(A 37)}$$

$$k_{app}^- = k_{11}^-[Na^+]_{eq} + k_{01}^- \quad \text{(A 38)}$$

A. 2. Residuals for the global fits performed on the stopped-flow traces for the mixing of MePy with OA to the model shown in Scheme 4.4.

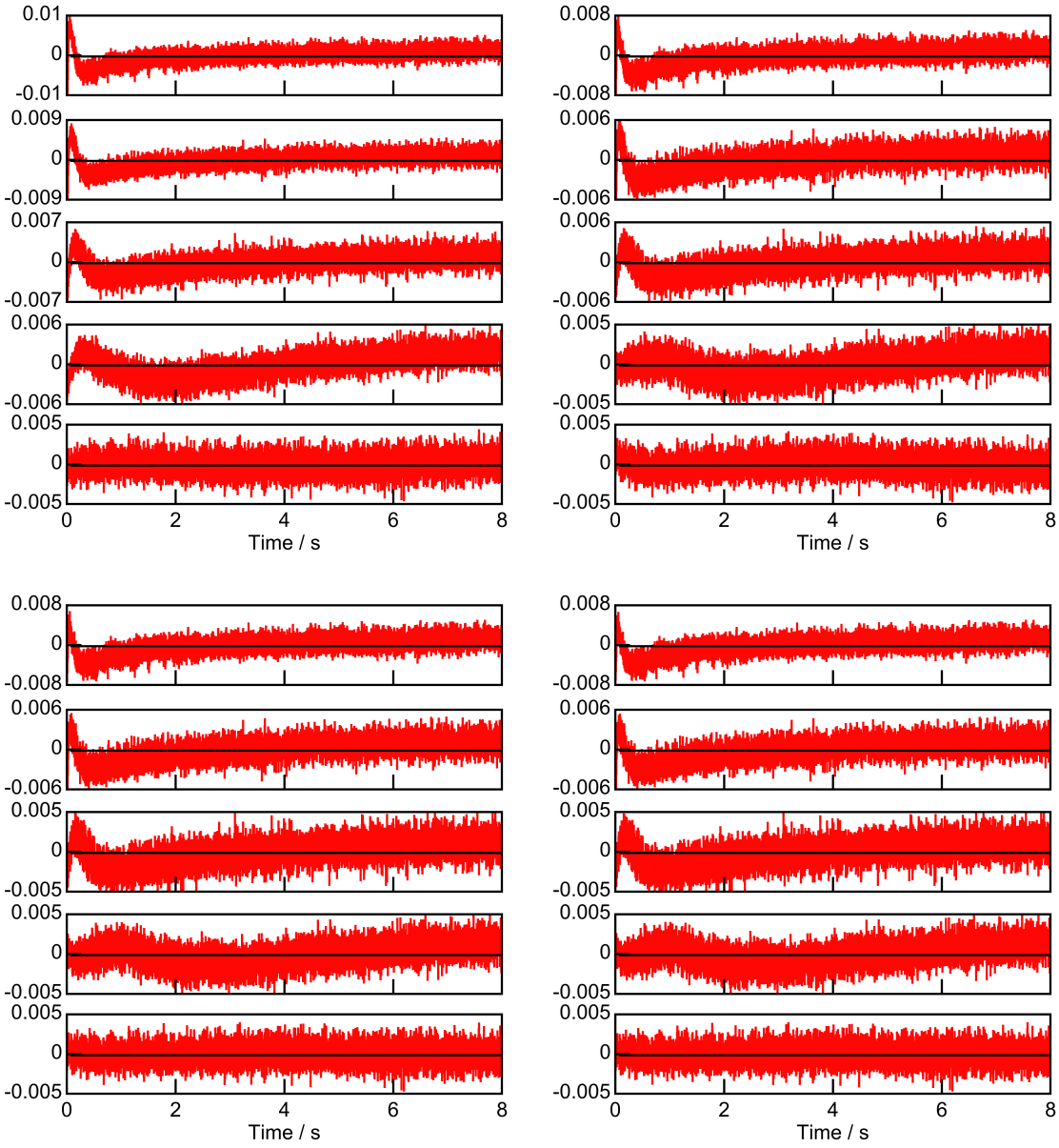

Figure A. 1. Residuals for the global fits performed on the stopped-flow traces for the mixing of MePy with OA to the model shown in Scheme 4.4. In all the figures the concentration of OA increases from 1 to 5 μM from bottom to top panel. The value for K_{11}^{MePy} fixed in the fits were 1.6×10^6 (top left), 1.3×10^5 (top right), 1.0×10^4 (bottom left) and 1.0×10^3 M^{-1} (bottom right).

A. 3. Different models were used in global fits of the stopped-flow traces for MePy and OA. The fits to all the following models were inadequate either due to large systematic deviations in the residuals or dissociation rate constants larger than the time resolution of the equipment recovered from the fits.

Model A1:

$$MePy + OA \overset{{}^{1}K_{11}^{MePy}}{\rightleftharpoons} {}^{1}MePy@OA \tag{A 39}$$

$$MePy + OA \underset{{}^{2}k_{11}^{-}}{\overset{{}^{2}k_{11}^{+}}{\rightleftharpoons}} {}^{2}MePy@OA \tag{A 40}$$

$${}^{2}MePy@OA + OA \underset{k_{21}^{-}}{\overset{k_{21}^{+}}{\rightleftharpoons}} OA@MePy@OA \tag{A 41}$$

Model A2:

$$MePy + OA \underset{k_{11}^{-}}{\overset{k_{11}^{+}}{\rightleftharpoons}} MePy@OA \tag{A 42}$$

$$MePy@OA + OA \underset{k_{21}^{-}}{\overset{k_{21}^{+}}{\rightleftharpoons}} OA@MePy@OA \tag{A 43}$$

Model A3:

$$MePy + OA \underset{k_{11}^{-}}{\overset{k_{11}^{+}}{\rightleftharpoons}} MePy@OA \tag{A 44}$$

$$MePy@OA + OA \xrightarrow{k_{21}^{+}} OA@MePy@OA \tag{A 45}$$

Model A4:

$$MePy + OA \xrightarrow{k_{11}^{+}} MePy@OA \quad \text{(A 46)}$$

$$MePy@OA + OA \xrightarrow{k_{21}^{+}} OA@MePy@OA \quad \text{(A 47)}$$

Model A5:

$$MePy + OA \underset{}{\overset{K_{11}^{MePy}}{\rightleftharpoons}} MePy@OA \quad \text{(A 48)}$$

$$MePy@OA + OA \underset{k_{21}^{-}}{\overset{k_{21}^{+}}{\rightleftharpoons}} OA@MePy@OA \quad \text{(A 49)}$$